# Early Onset Scoliosis in FGFR3-/- Mice

Michael B. Sullivan

Department of Experimental Surgery

McGill University, Montreal

December 2014

A thesis submitted to McGill University in partial fulfillment of the requirements of the degree of Master of Science in Experimental Surgery

I	able of Co	ontents			
A	bstract		4		
Résumé					
Acknowledgements and Contributions					
List of Abbreviations					
Ŀ		les and Figures			
1	Introduction				
	1.1 Pur	pose	12		
		oliosis			
	1.2.1	Idiopathic Scoliosis			
	1.2.2	Other Types of Scoliosis			
	1.2.3	Curve Classification.			
	1.2.4	Natural History of Idiopathic Scoliosis			
	1.2.5	Aetiology			
	1.2.6	Treatment of Scoliosis			
	1.3 Animal Models				
	1.3.1	Kyphoscoliosis Ky/Ky Mice	21		
	1.3.2	Melatonin Models			
	1.3.3	Surgical Tethering	26		
	1.3.4	Epiphysiodesis			
	1.4 Bone Development				
	1.4.1	Endochondral Ossification			
	1.4.2	Signaling Molecules			
	1.4.3	Fibroblast Growth Factors			
		FR3-/- Phenotype			
	1.6 Hu	man Spine Development	42		
2		S			
		ganization and Study Design			
	2.2 Pla	in Radiography	46		
	2.2.1	Posterior-Anterior Spine and Pelvis	46		
	2.2.2	Lateral View			
	2.2.3	Scoliosis Cobb Angle	47		
	2.2.4	Curve Location	47		
	2.2.5	Lateral Cobb Angle	48		
	2.3 <i>Spi</i>	ne Extraction	48		
	2.4 <i>Mid</i>	cro Computed Tomography	49		
	2.4.1	Vertebral Micro-Architecture	50		
	2.4.2	Vertebral Rotation	51		
	2.5 <i>His</i>	tology	52		
	2.5.1	Embedding			
	2.5.2	Staining	53		
	2.5.3	Imaging	54		
	2.6 Sta	tistical Analysis			
	2.6.1	Data Organization			
	2.6.2	Linear Mixed Effects Modeling	55		

	2.6.3	Micro CT Comparisons	57		
3		······			
	3.1 Co	ob Angle	58		
	3.2 An	atomical Measurements	59		
	3.3 Mie	cro Computed Tomography	61		
		Vertebral Rotation			
	3.4 His	tology	62		
4	Discuss	ion	63		
	4.1 Rel	ationship to Humans	63		
	4.1.1	Curve Severity	63		
	4.1.2	Curve Location	64		
	4.1.3	Curve Progression and Relationship to Growth	65		
	4.2 Results		66		
	4.2.1				
	4.2.2	Anatomical Measurements	69		
	4.2.3	Micro Computed Tomography	70		
		ential Mechanisms			
	4.4 Lin	nitations of Model	73		
	4.5 Co	mparison to Other Models	74		
	4.5.1	Kyphoscoliosis	74		
	4.5.2	Melatonin Deficiency	75		
	4.5.3	Surgically Induced	77		
	4.6 Me	thodological Difficulties	82		
	4.7 Fut	ure Directions	84		
5	Conclus	sion	87		
6 Tables and Figures					
7	Appendix 1: Select SPSS Syntax				
8	References10				

### Early Onset Scoliosis in FGFR3-/- Mice

#### **Abstract**

Introduction: Scoliosis can be infantile or juvenile in onset; however, it is more frequently identified in older children, particularly girls as they enter puberty. Untreated scoliosis progresses with age and there are currently few non-operative therapies for severe scoliosis. Early spinal fusion can limit thoracic growth and therefore restrict pulmonary function, which can lead to severe pulmonary morbidity and mortality. Therefore, the ideal treatment will include fusion-less correction of the spinal deformity while maintaining spinal growth and motion. However, testing biological treatments requires an animal model that is practical in the research environment and closely replicates the human disease. We noticed that mice with targeted disruption of Fibroblast Growth Factor Receptor 3 (FGFR3) showed skeletal abnormalities and spontaneously occurring progressive scoliosis. The study will characterize the FGFR3-/- mouse as an improved animal model of early onset scoliosis.

**Methods:** FGFR3-/- and wildtype mice of a C3H background were radiographed between one and nine times with posterior-anterior and lateral views to measure kyphotic and scoliotic Cobb angles. Mice were euthanized at ages ranging from 4 to 25 weeks and processed for histology and imaged with high-resolution micro-computed tomography (micro-CT) to compare parameters such as vertebral and inter-vertebral disc (IVD) morphology, micro architecture, vertebral rotation, and cellular activity. FGFR3-/- mice were paired with an age and gender matched wildtype counterpart for micro-CT and histological analysis to ensure that scoliotic apical vertebrae were compared to the equivalent wild-type vertebrae. Analysis was performed using non-parametric tests, ANOVA and mixed modeling with  $\alpha$ =0.05.

Results: FGFR3-/- mice developed scoliosis by 8 weeks and scoliosis progressed until the end of study, reaching a maximum of 40.9°±18.3. The present model has 98% incidence (≥10°) by skeletal maturity, though location and severity are varied. Micro-CT analysis of FGFR3-/- vertebrae revealed poorer vertebral body micro architecture on the convex aspect of the curve (BV/TV, TbTh, TbSp, TbN, TbPf, SMI, FD, Porosity, and Connectivity). Gross measurements using micro-CT revealed IVD and vertebral wedging, and vertebral body overgrowth. Histological analysis of bone mineralization and cartilage support micro-CT data, and indicates concave IVD compression and convex nucleus pulposus translation.

Conclusion: FGFR3-/- mice developed a high incidence of scoliosis prior to skeletal maturity and comparable in severity to that seen in humans. Both micro-CT and histologic data are consistent with human early onset scoliosis, suggesting a common biomechanical feedback process according to Wolff's Law and the Hueter-Volkmann law of differential growth. This occurs despite different initiating factors between idiopathic scoliosis and the FGFR3-/- model. Because the proposed model features spontaneously occurring scoliosis, we see it as more clinically relevant than surgically induced scoliosis. We propose the FGFR3-/- mouse as an animal model that is inexpensive, easily available, spontaneously occurring and closely reproduces the human disease. This model will be used to test novel biological therapies that serve as non-surgical alternatives in progressive early onset scoliosis.

### Résumé

Introduction: La scoliose peut être infantile ou juvénile. On l'identifie par contre surtout chez les enfants plus âgés, en particulier chez les filles à l'âge de l'adolescence. La scoliose laissée non traitée progresse avec l'âge et il y a présentement peu de thérapies non-opératoires pour la scoliose sévère. La fusion dorsale précoce peut limiter la croissance thoracique et ainsi limiter la fonction pulmonaire, ce qui peut engendrer la morbidité pulmonaire sévère et la mortalité. Ainsi, le traitement idéal serait la correction sans fusion de la difformité lombaire, tout en maintenant la croissance et la motricité. Cependant, pour tester les traitements biologiques, un modèle animal qui est pratique en milieu de recherche et qui reproduit bien la maladie humaine est nécessaire. Nous avons remarqué que les souris dont le gène FGFR3 est interrompu avaient des anomalies squelettiques et une scoliose progressive spontanée. Cette étude a pour but de caractériser la souris FGFR3-/- en tant que modèle animal amélioré pour la scoliose précoce.

**Méthodes:** Les souris FGFR3-/- et le phénotype wildtype de type C3H ont été radiographiés entre une et neuf fois avec les vues postérieures-antérieures et latérales pour mesurer les angles Cobb de scoliose et cyphose. Les souris ont été euthanasiées entre l'âge de 4 et 25 semaines et ont été préparées pour l'histologie et micro CT de haute résolution pour comparer les paramètres tels la morphologie vertébrale et le disque intervertébral, la microarchitecture, la rotation vertébrale et l'activité cellulaire. Les souris FGFR3-/- ont été jumelés avec une souris wildtype de même âge et sexe pour l'analyse micro-CT et histologique pour s'assurer que l'apex vertébrale scoliotique ait été comparée à la vertèbre wildtype équivalente. L'analyse inclus les tests non paramétriques, ANOVA et le modèle mixte avec α=0.05.

Résultats: Les souris FGFR3-/- ont développé la scoliose avant 8 semaines et cette scoliose a progressé jusqu'à la fin de l'étude, atteignant un maximum de 40.9°±18.3 semaines. Le modèle ci-proposé a un taux de 98% (≥10°) par maturité squelettique, tandis que l'emplacement et la sévérité ont varié. L'analyse micro-CT des vertèbres FGFR3-/- a démontré une pire microarchitecture du corps vertébrale à l'aspect convexe de la courbe (BV/TV, TbTh, TbSp, TbN, TbPf, SMI, FD, porosité, et connectivité). Les mesures en utilisant le micro-CT ont révélées la cunéïformisation du corps vertébral et du IVD et la surcroissance du corps vertébral. L'analyse histologique de la minéralisation osseuse et cartilagineuse supportent des données du micro-CT et indiquent la compression concave du IVD et la translation convexe du nucleus pulpeux.

Conclusion: Les souris FGFR3-/- ont développé une haute fréquence de scoliose précédant la maturité squelettique comparable en sévérité à celle des humains. Les analyses micro-CT et histologiques sont en ligne avec la scoliose précoce humaine, suggérant un processus commun de feedback biomécanique selon la loi de Wolff et la loi de croissance différentielle Hueter-Volkmann, malgré des facteurs initiant distincts entre la scoliose idiopathique et le modèle FGFR3-/-. Puisque le modèle proposé inclus la scoliose spontanée, nous la considérons plus valable cliniquement que la scoliose induite par la chirurgie. Nous proposons la souris FGFR3-/- en tant que modèle animal qui n'est pas dispendieux, accessible, non invasif et qui reproduit la réalité humaine. Ce modèle sera utile pour tester de nouvelles thérapies biologiques qui pourront être utiles en tant qu'alternatives non chirurgicales à la scoliose précoce et progressive.

## **Acknowledgements and Contributions**

I would like to thank each lab member and collaborator for his or her involvement in this project. Specifically, I would like to thank Dr. Henderson and Dr. Saran for their ongoing supervision.

Drs. Henderson, Saran, and Ouellet for their integral role in study design and troubleshooting.

Thanks to:

Huifen Wang for breeding all mice used in the study.

Ailian Li for developing histology protocols and aiding in histological processing.

Marco Kneifel for helping with micro-CT processing, radiography, and creating Figure 5.

Ali Esmaeel for helping with study design, radiography, and creating Figure 6a.

Mike and Georgia Sullivan for thesis proofreading.

Sabrina Piedimonte and Melissa Clermont for translation of abstract into French.

Contribution by Self: Study design, radiography of mice, micro-CT processing and analysis, histology (in conjunction with Ailian Li), statistical analysis, data interpretation, and figure generation.

### **List of Abbreviations**

AIS: Adolescent idiopathic scoliosis

ALP: Alkaline Phosphatase

ANOVA: Analysis of variance

Bcl-2: B-Cell Lymphoma 2 Gene

β-Catenin: Beta-cadherin-associated protein

BMP2: Bone Morphogenetic Protein 2

BsBv: specific bone surface

BVTV: Bone volume/total volume, bone volume fraction

Cod: Connectivity Density

FGF: Fibroblast growth factor

FGFR3: Fibroblast growth factor receptor 3

IGF: Insulin-like Growth Factor

Ihh: Indian hedgehog

IVD: Intervertebral disc

Ky/ky: Kyphoscoliosis gene

Lef1: lymphoid enhancing factor 1

Micro-CT: Micro computed tomography

MHC1: Myosin heavy chain 1

MMA: Methyl methacrylate

MMP9: Matrix Metallopeptidase 9

PTH: Parathyroid hormone

PTH1R: Parathyroid hormone receptor 1

PTHrP: Parathyroid hormone related peptide

Runx2: Runt-related transcription factor 2

SMI: Structural model index

Sox5, 6, 9: Transcription Factor SOX-5, 6, 9

SRS: Scoliosis Research Society

TbN: Trabecular number

TbPf: Trabecular pattern factor

TbSp: Trabecular separation

TbTh: Trabecular thickness

TCF2: T-Cell Factor 2

TGF-β: Transforming Growth Factor Beta

TRAP: Tartrate Resistant Acid Phosphatase

## **List of Tables and Figures**

### **Tables**

Table 1. Progression of Kyphosis and Lordosis

Table 2A. Micro-CT analysis of control vertebrae in wildtype mice

Table 2B. Micro-CT analysis of apical vertebrae in FGFR3-/- mice

Table 3C. Comparison of Micro-CT data in wildtype and FGFR3-/- mice

# **Figures**

Figure 1. Curve progression with age

Figure 2. Serial radiographs

Figure 3. Body mass with age

Figure 4. Femur length with age

Figure 5. Micro-CT model showing asymmetrical bone quality in FGFR3-/- mice

Figure 6. Illustration, Micro-CT and Von Kossa staining of apical vertebrae

Figure 7. Histology: Alkaline Phosphatase (ALP) and Tartrate Resistant Acid

Phosphatase (TRAP) of apical vertebrae

### 1 Introduction

### 1.1 Purpose

In order to test potential novel treatments for idiopathic scoliosis, such as drug or biologic therapies, we require an animal model that accurately represents the human disease, and is effective and easily available in the research environment. Many animal models exist, however, as has been expressed previously, the existing animal models have numerous deficiencies (Janssen, de Wilde, Kouwenhoven, & Castelein, 2011) and are unsatisfactory. Whether scoliosis like curvature is induced by mechanical manipulation (as is common in large animal models), or produced by systemic alterations like pinealectomy, each methodology creates curvature that has an inadequate resemblance to the human disease. Therefore, the purpose of this study is to characterize mice with targeted disruption of Fibroblast Growth Factor Receptor 3 (FGFR3-/-) as an animal model for scoliosis that better replicates the human disease than existing animal models.

#### 1.2 Scoliosis

### 1.2.1 Idiopathic Scoliosis

Idiopathic scoliosis is a three dimensional spinal deformity consisting of rotational, angular, and sagittal deformities, though little is known about its aetiology, despite rapid advances in spine radiology and characterization of spine morphology (S. L. Weinstein, Dolan, Cheng, Danielsson, & Morcuende, 2008). Idiopathic scoliosis can develop in healthy children at any stage of growth, but is especially common in girls during puberty. It is classified into three groups based on age of onset: infantile (birth to

age 3), juvenile (age 3 to puberty) and adolescent or late-onset (after puberty)(Lonstein, 1994). Diagnosis is established based on the presence of curvature of at least 10°, measured by the Cobb method, and exclusion of other causes of scoliosis, such as congenital malformation of the vertebrae, degenerative, neuromuscular and other syndromic disorders (Malfair et al., 2010; Murata et al., 2002; S. L. Weinstein, 1999; S. L. Weinstein et al., 2008).

## 1.2.2 Other Types of Scoliosis

### 1.2.2.1 Degenerative Scoliosis

Degenerative scoliosis is a common cause of back pain in elderly individuals and occurs when degenerative changes in the disc and facet joints of the lumbar spine induce lumbar scoliotic curvature. The disorder occurs in elderly individuals with no history of non-degenerative scoliosis (Murata et al., 2002). Curvature is caused by asymmetric biomechanical forces that produce asymmetric disc space collapse and eventual lateral listhesis (Malfair et al., 2010).

### 1.2.2.2 Neuromuscular Scoliosis

Neuromuscular spinal deformity can occur because of disorders of the central and peripheral nervous systems, or a primary muscle abnormality. Asymmetric muscle tone, including spasticity and paralysis is considered the cause of neuromuscular scoliosis, though the process is incompletely understood (Berven & Bradford, 2002).

Neuromuscular scoliosis has a unique presentation, in that the curve is long, C shaped and accompanied by pelvic obliquity (Malfair et al., 2010).

### 1.2.2.3 Neurofibromatosis

Neurofibromatosis is a genetic disorder involving both neuroectodermal and mesenchymal elements and causes scoliosis in one quarter of patients (Malfair et al., 2010). Curves can be classified as either dystrophic or non-dystrophic, with non-dystrophic curves appearing similar to Adolescent Idiopathic Scoliosis (AIS) but occur earlier and more frequently (Crawford & Herrera-Soto, 2007), whereas dystrophic curves have shorter segments, a large degree of apical rotation, and are associated with kyphosis (Hunt & Pugh, 1961).

### 1.2.2.4 Congenital Scoliosis

Congenital scoliosis is caused by vertebral anomalies formed when the anatomical pattern of the spine is formed in mesenchyme (McMaster & Ohtsuka, 1982). It can manifest itself as unilateral failure of formation, leading to wedged vertebra or hemivertebra, unilateral failure of segmentation, and bilateral failure of segmentation. Additionally, pelvic obliquity can be the major deforming factor in severe curves (McMaster & Ohtsuka, 1982).

### 1.2.3 Curve Classification

Curves can be classified into either structural (inflexible) curves, or non-structural compensatory curves (flexible) (Lenke et al., 2001). The latter develop in response to structural curves to maintain truncal balance. However, non-structural curves may become structural over time because of shortening of ligaments, muscle atrophy, and osseous changes (Malfair et al., 2010). A flexible curve will straighten when the patient

bends towards the curve and will often disappear after surgical correction of the primary curve (Malfair et al., 2010). Furthermore, curves are classified as either convex left or right. Adolescent idiopathic scoliosis most commonly features convex right curves, while infantile scoliosis favours convex left curves and juvenile onset scoliosis shows no disposition to either right or left (Janssen, Kouwenhoven, et al., 2011).

### 1.2.4 Natural History of Idiopathic Scoliosis

As with many diseases that are considered idiopathic, idiopathic scoliosis is thought to be a multifactorial disease and a combination of genetic and environmental factors (Burwell, Dangerfield, Moulton, & Grivas, 2011; S. L. Weinstein et al., 2008). Because of this complex relationship, increasing severities of scoliotic curvatures are met with decreasing prevalence. The most severe curves are orders of magnitude less numerous than minor curves. This differs from a disease state that is distinct from the normal population and exists in a bimodal distribution of disease severity. Therefore, the prevalence of scoliosis is highly dependent on curve size cut-off, the variation of which has led to considerable confusion for popular medicine (Kane, 1977). However, using a 10° cut-off, 2.5% of the population qualifies as having scoliosis. Regardless of cut-off, approximately 0.25% of the population will require treatment of scoliosis (Rogala, Drummond, & Gurr, 1978). The female-to-male ratio varies with severity. Overall the ratio is 1.25:1 but curves that potentially require treatment have different ratios. For example, curves greater than 20 degrees have a F:M ratio of 5.4:1 (Kane, 1977; Rogala et al., 1978) and those of greater than 30 degrees have a ratio of 10:1 (Roach, 1999). The

prevalence of curves greater than 40°, often considered for surgery, is approximately 0.1% of the general population (N. H. Miller, 1999).

Progression of scoliosis is highly variable. Many curves stabilize at minor severity, while others rapidly progress to become a serious deformity (Sanders et al., 2007). In one long term follow up study, Weinstein & Ponseti found that curves less than 30 degrees at skeletal maturity rarely progress while those greater than 30 degrees were more likely to progress. Additionally, apical vertebra rotation is associated with curve severity, with more severe curves developing a greater degree of rotation. The progression of lumbar curves is a function of Cobb angle, vertebral rotation, direction of curve, and relationship of the fifth lumbar vertebra to the intercrest line. Greater Cobb angle, greater rotation, a right curve, and an unseated L5 where the intercrest line fails to pass through the L4/L5 intervertebral disk were all associated with more severe curve progression. While in thoracic curves, Cobb angle, rotation, and Mehta angle (rib-vertebra angle) each had prognostic value (S. L. Weinstein & Ponseti, 1983).

### 1.2.4.1 Morbidity and Mortality

Adolescent idiopathic scoliosis does not result in an overall increased mortality rate, however, it has been known to lead to death from cardiopulmonary failure in rare, extremely severe cases with Cobb angle >100° (Asher & Burton, 2006). Severe scoliosis causes case disturbance of pulmonary and cardiac function, leading to grave morbidity and mortality (Collis & Ponseti, 1969; A. Nachemson, 1968; Pehrsson, Larsson, & Nachemson, 1991; S. L. Weinstein, Dolan, Lori A., Spratt, Kevin F., Peterson, Kirk K., Spoonamore, Mark J., Ponseti, Ignacio V., 2003).

Curve characteristics are highly predictive of pulmonary function morbidity severe scoliosis can function as extrathoracic restrictive lung disease. Curves with a thoracic apex and Cobb angle greater than 50° are more highly associated with poorer pulmonary prognosis (S. L. Weinstein, Dolan, Lori A., Spratt, Kevin F., Peterson, Kirk K., Spoonamore, Mark J., Ponseti, Ignacio V., 2003). Pulmonary symptoms occur at Cobb angles greater than 80 degrees. As well, morbid curves tend to have increased rotation, and are single thoracic curves or large double thoracic curves (S. L. Weinstein, Zavala, & Ponseti, 1981).

Patients with scoliosis have an increased prevalence of back pain than control populations. However, it is unclear whether pain severity and duration are (Mayo, Goldberg, Poitras, Scott, & Hanley, 1994) or are not (Ponseti & Friedman, 1950; S. L. Weinstein, Dolan, Lori A., Spratt, Kevin F., Peterson, Kirk K., Spoonamore, Mark J., Ponseti, Ignacio V., 2003) increased with scoliosis. The latter group reports that back pain is an individual experience and can exist regardless of curve location or severity (S. L. Weinstein, Dolan, Lori A., Spratt, Kevin F., Peterson, Kirk K., Spoonamore, Mark J., Ponseti, Ignacio V., 2003). However, other groups suggest that pain changes with curve pattern. Thoracolumbar curves may be the most painful and double curves to be the least painful (ASCANI et al., 1986). Development of arthritis in scoliosis is not associated with increased pain (S. L. Weinstein, Dolan, Lori A., Spratt, Kevin F., Peterson, Kirk K., Spoonamore, Mark J., Ponseti, Ignacio V., 2003), whereas translation of vertebra in the thoracolumbar spine may be associated with increased pain (S. L. Weinstein et al., 1981).

## 1.2.5 Aetiology

The aetiology of idiopathic scoliosis is thought to be a complex interplay between genetic, epigenetic, and environmental factors (Burwell et al., 2011). One meta-analysis of scoliosis in monozygotic and dizygotic twins found a 73% and 36% concordance rates respectively, indicating a genetic aetiology. Interestingly, the curves of monozygotic twins develop and progressed together (Kesling & Reinker, 1997). A complex segregation analysis of 101 families found that idiopathic scoliosis could be attributed to an autosomal dominant, major gene diallele model with incomplete sex-dependent penetrance of the genotypes (Axenovich, Zaidman, Zorkoltseva, Tregubova, & Borodin, 1999). Despite these advances, no single locus can explain the incidence of disease and curve variability of severity and location (Justice, Miller, Marosy, Zhang, & Wilson, 2003; Nancy H. Miller et al., 2005; Salehi et al., 2002; Wise et al., 2000). This indicates that genetic factors are complex and multifactorial, and may include incomplete penetrance, variable expressivity (whether with environmental or other genetic interactions), and phenotypic or genotypic heterogeneity (S. L. Weinstein et al., 2008). A recent review found that the literature is overrepresented by underpowered studies and that more restricted clinical definitions may help confirm or detect aetiological components (Gorman, Julien, & Moreau, 2012).

### 1.2.6 Treatment of Scoliosis

### 1.2.6.1 Surgical Treatment

Until recently (S. L. Weinstein, Dolan, Wright, & Dobbs, 2013), the literature has been conflicting regarding the efficacy of conservative treatment of mild and moderate

scoliosis (Green, 1986; Lenssinck et al., 2005; A. L. Nachemson & Peterson, 1995; S. L. Weinstein et al., 2013). However, surgical treatment is required for severe progressive curves (Carr, Moe, Winter, & Lonstein, 1980; Danielsson, Hasserius, Ohlin, & Nachemson, 2007; Everett & Patel, 2007; Maruyama & Takeshita, 2008; Weiss et al., 2006). Surgical treatment of scoliosis most often involves anterior and posterior spinal fusion, along with posterior spinal instrumentation. Surgical treatment is indicated for curves greater than 45-50 degrees because these curves tend to progress even after skeletal maturity and these curves may cause loss of pulmonary function (Maruyama & Takeshita, 2008). In addition to surgical risks (Reames et al., 2011), surgical correction of the spinal deformity can limit mobility and thoracic growth, thereby limiting pulmonary alveolar growth and creating intrinsic restrictive lung disease (Karol et al., 2008). Although most lung development occurs during infancy, it continues until midadolescence in most individuals (Davies & Reid, 1971). Restriction of lung development and bone growth is an especially important consideration in patients with considerable remaining growth potential. Therefore, the ideal treatment for scoliosis will include fusion-less correction of the spinal deformity while maintaining spinal growth and motion. This is the rationale of developing a suitable animal model of scoliosis: a preclinical model on which to test fusion-less corrections.

### 1.2.6.2 Conservative Treatment

The most common form of conservative therapy in adolescent idiopathic scoliosis is bracing. However, exercise therapy and electrical stimulation have also been investigated to no avail. Until recently, bracing had limited evidence due to poor study

design. Studies that found bracing effect were of poor quality (Lenssinck et al., 2005) and tended to lack randomization (A. L. Nachemson & Peterson, 1995), adequate control groups (El-Sayyad & Conine, 1994; Noonan, Weinstein, Jacobson, & Dolan, 1996), or found no effect (Goldberg, Dowling, Hall, & Emans, 1993).

A recent landmark randomized controlled trial compared bracing to observation, where primary treatment outcomes were progression of the curve to 50° (treatment failure) or reaching skeletal maturity without this degree of curve progression (treatment success)(S. L. Weinstein et al., 2013). One hundred sixteen patients were randomly assigned to bracing or observation, while 126 declined randomization and chose between bracing and observation. These groups had similar baseline characteristics, though a combined analysis used a propensity-score adjusted odds ratio to account for the lack of randomization in the latter group. Additionally, braces contained a heat-sensor to monitor hours of wear.

In a combined analysis of both randomized and preference groups, the rate of treatment success after bracing was 72% compared to 48% after observation (propensity-score adjusted odds ratio 1.93; 95% confidence interval 1.08 to 3.46). In the randomization only group with intention-to-treat analysis, the rate of treatment success was 75% in patients assigned to bracing and 42% in patients assigned to observation (OR 4.11; 95% CI 1.85-9.16). As well, treatment success had a dose response to hours of wear. Patients who wore the brace for an average of at least 12.9 hours per day had treatment success of 90-93%, while patients with less than 6.0 hours of wear had treatment success of 42%, a rate similar to observation only. These results show that bracing significantly

decreased progression of high-risk curves to the threshold for surgery in patients with adolescent idiopathic scoliosis. Therefore, bracing now has evidence as a non-operative method to reduce the progression in idiopathic scoliosis. However, in recalcitrant cases, surgical correction is still required and in addition, many non-idiopathic forms of scoliosis do not respond to brace therapy.

### 1.3 Animal Models

Animal models of scoliosis can be broadly categorized into: genetic mutant models, melatonin deficiency via pinealectomy, and mechanically manipulated large and small animals. Although the models have varying degrees of success producing a disease that appears grossly and radiographically similar to scoliosis, they are imperfect analogues to the human disease and aetiology.

## 1.3.1 Kyphoscoliosis Ky/Ky Mice

A mutant gene causing kyphoscoliosis, designated ky, was first identified in mice by Dickinson & Meikle (Dickinson & Meikle, 1973). Kyphoscoliosis mice suffer from a progressive symmetrical muscular disorder that is characterised by initial muscle necrosis followed by atrophy, and thus develop muscular scoliosis. The disorder has been attributed to a mutation in a novel muscle-specific protein (Blanco et al., 2001). Kyphoscoliosis symptoms are nearly ubiquitous in ky/ky mice and can be identified with 98% accuracy at 4 weeks old. The primary method of detection is the "placing reflex", whereby a healthy mouse held by its tail will stretch its forelegs forward and retroflex its head. Absence of the placing reflex is observed in affected mice. Respiration is impaired, body weight is reduced by up to 30%, and viability is impaired in extremely deformed

mice. Interestingly, the model also displays cardiac abnormalities and has since been used as a model for occult cardiac pathology (Hou, Le Bihan, Vega-Avelaira, & Coulton, 2006). Although placing reflex allows identification of affected mice at a young age, vertebral deformity appeared by 100 days. Light microscopy revealed that at 16 days of age, a variety of axial and appendicular muscles were necrotic, and experienced muscle regeneration and interstitial infiltration by macrophages (Bridges, Coulton, Howard, Moss, & Mason, 1992). By 6 weeks, necrosis was rare but atrophy was common.

In addition to the necrosis and atrophy that occurs through the normal course of life in ky/ky mice, surgical compensatory overload provoked no hypertrophy of the extensor digitorum longus. Furthermore, muscles showed a progressive and eventually complete shift to type 1 fibres only expressing myosin heavy chain 1 (MHC1). Kyphoscoliosis mice also show intervertebral disc degeneration similar to that seen in humans. The discs show a loss of cellularity and loss of the normal division of the disc into annulus fibrosis and nucleus pulposus (Mason & Palfrey, 1984).

The authors suggested that this mouse may be a system for examining neuromuscular and skeletal mechanisms by which scoliosis develops and for testing potential treatments (Bridges et al., 1992). However, they do admit that although proximal muscle weakness is often found in human scoliosis patients, humans do not have any muscle dysfunction similar to that observed in ky/ky mice (Blanco et al., 2001).

### 1.3.2 Melatonin Models

It was originally observed that pinealectomy, removal of the melatonin producing pineal gland, in chickens produced spinal deformities (Thillard, 1959). This led

researchers to believe that melatonin may be involved in the development of adolescent idiopathic scoliosis and provoked the development of similar models. Spinal deformity has been observed in animals ranging from rats (Masafumi Machida et al., 1999) to Atlantic salmon (Fjelldal et al., 2004). Each will be briefly discussed to provide an overview of the literature.

### Pinealectomized Chickens

While the pinealectomized chicken model has been available for over fifty years (Thillard, 1959), it has only been recently that the model has been reproduced and rigorously tested. An initial re-examination of the procedure produced very optimistic results with incidence as high as 100% (Masafumi Machida et al., 1993). However, these results could not be replicated. A repeat experiment found a scoliosis incidence of 75%, versus 38% in a sham operation group and 19% in the control group (Fagan, Kennaway, & Oakley, 2009). Furthermore, numerous animals died from the procedure. The study also showed that the resulting scoliosis was dissimilar from human scoliosis and that deformities contained short angular curves rather than the long curves present in human idiopathic scoliosis. Additionally, while pinealectomy significantly decreased plasma melatonin levels, its relationship with scoliosis was unclear, in that not all chickens with scoliosis had diminished melatonin concentrations (Fagan et al., 2009). Unsurprisingly, this paper cautioned against drawing conclusions regarding the pathogenesis of adolescent idiopathic scoliosis from the pinealectomized chicken model. Furthermore, although chickens are bipedal, their intervertebral joints resemble synovial joints and not intervertebral disks. It lacks both an annulus fibrosus and nucleus pulposus, and is

histologically distinct from mammal discs (Fagan et al., 2009). Through an alternate mode of melatonin reduction, scoliosis developed in 15% of chickens exposed to intense 24h light (Nette et al., 2002). A combination of continuous exposure to light and pinealectomy increased the incidence of scoliosis from 50% to 80%, compared to pinealectomy alone. The authors suggested that melatonin levels may need to drop below a threshold before scoliosis develops (Nette et al., 2002).

An additional reproduction of the pinealectomized chicken experiment used micro computed tomography (Micro-CT) analysis in addition to Cobb angle to evaluate curve severity and characteristics. By post-operative 3 weeks, 90% of chickens had developed curvature of at least 10° (mean 21.1°). Micro-CT examined bone volume fraction (BV/TV), trabecular thickness, trabecular number, and trabecular separation. They found that by the third week post-operative, each of these measures were significantly greater in the concave side than the convex side (Fu et al., 2011). Micro-CT changes mimic those seen in humans (Shea, Ford, Bloebaum, D'Astous, & King, 2004) and indicates that the concave and convex sides are responding to compression and tension forces, respectively, and that micro-architecture changes are secondary to the underlying skeletal deformity.

### Bipedal Rodents

In order to determine whether pinealectomy induced scoliosis in a mammal model and whether bipedalism was important in this model, pinealectomy was performed on Sprague-Dawley rats (Masafumi Machida et al., 1999; M. Machida et al., 2005). Forelegs were amputated at the humeroscapular joint and tail ligated at its base. After amputation, a skull flap was created and the pineal gland removed by suction using a syringe. No

quadruped rats. Although no quantitative data was presented or statistical analysis performed, the authors report that pinealectomy and bipedal operation produced scoliosis ranging in severity from 14° to 55° by 3 months. The authors neglected to report the incidence of scoliosis in the pinealectomized bipedal group. Implantation of a slow release pellet containing melatonin reduced the incidence of scoliosis, further supporting the claim that the pathogenesis of scoliosis in this model is due to melatonin insufficiency (Masafumi Machida et al., 1999). At the same time that Machida et al. examined the effects of bipedalism and melatonin deficiency, another group performed pinealectomies on chickens, hamsters, and rats, arguing that the latter two were more phylogenetically similar to humans than chickens or rabbits (O'Kelly et al., 1999). Scoliosis developed in 10/21 chickens but no hamsters or rats (O'Kelly et al., 1999).

C57BL/6J mice are a natural knock-down model of melatonin synthesis and exhibit depressed plasma melatonin levels in comparison to C3H/HeJ and CBA strains of mice (Oyama, Murai, Kanazawa, & Machida, 2006). To further determine whether low plasma melatonin levels alone were responsible for scoliosis when combined with the bipedal operation, a pinealectomy was combined with a bipedal operation in C3H/HeJ mice. Mice were anaesthetized and bilateral forelegs and the tail were tied and cut at the humeroscapular and basal levels, respectively. The same bipedal operation was performed on C3H/HeJ mice, with a portion of the mice also receiving pinealectomy. Although curve severity was not reported in this study, the bipedal operation produced similar rates of scoliosis in both C57BL/6J mice (64.3%) and pinealectomized C3H/HeJ mice (70.0%). In C3H/HeJ mice bipedalism alone caused scoliosis in far fewer mice

(25.0%) (Oyama et al., 2006). This indicates that plasma melatonin levels are sufficiently low in bipedal non-pinealectomized C57BL/6J mice to produce scoliosis.

Calmodulin has been suggested as the neurotransmitter effective in regulating melatonin release. It is likely that melatonin exerts its effects in preventing scoliosis because it is a calmodulin antagonist. This theory is supported by the ability of tamoxifen, a calmodulin antagonist, to reduce the incidence and magnitude of scoliosis in pinealectomized chickens (Akel, Kocak, et al., 2009) and melatonin deficient bipedal mice (Akel, Demirkiran, et al., 2009).

### 1.3.2.1 Relationship to Humans

Despite the ability to produce scoliosis in chickens and rodents, pinealectomy failed to produce scoliosis in rhesus monkeys (Cheung, Poon, Luk, & Leong, 2005). This suggests that the melatonin related aetiological factors involved in the pathogenesis of scoliosis are different in lower and higher animals. This is reinforced by the observation that there is no difference in melatonin production between human females with and without scoliosis (Hilibrand et al., 1996). Additionally, the incidence of scoliosis is not higher in children with pineal lesions (Day et al., 2007). Based on current evidence, melatonin is not related to the pathogenesis of adolescent idiopathic scoliosis in humans (Grivas & Savvidou, 2007).

### 1.3.3 Surgical Tethering

Early methods to surgically induce scoliosis were based on asymmetric muscle or rib excision and scarring to create spinal imbalance (Bisgard, 1935; Langenskiold &

Michelsson, 1961; Schwartzmann & Miles, 1945; Smith & Dickson, 1987; Thomas & Dave, 1985). However, the most recent literature tends to use unilateral vertebral fusion and spinal tethering to create a structural scoliosis. Unilateral tethering has been employed as a method to surgically induce scoliosis in a variety of large animal models, including calves (Newton, Farnsworth, et al., 2008; Newton et al., 2005; Newton et al., 2002), pigs (Accadbled et al., 2011; Laffosse et al., 2010; Newton, Upasani, et al., 2008; A. Patel, Schwab, Lafage, Lafage, & Farcy, 2011; Ashish Patel et al., 2009; Schwab, Patel, Lafage, & Farcy, 2009) and goats (Braun & Akyuz, 2005; Braun, Hines, Akyuz, Vallera, & Ogilvie, 2006; Braun, Hoffman, et al., 2006; Braun, Ogilvie, Akyuz, Brodke, & Bachus, 2006; Braun et al., 2003; Y. G. Zhang, G. Q. Zheng, X. S. Zhang, & Y. Wang, 2009). In several of these studies, tethering has been employed to investigate the effect of unilateral growth modulation as a potential for fusion-less surgery for scoliosis.

### 1.3.3.1 Goats

Braun et al (2003) produced scoliosis in young goats using posterior asymmetric tethering and rib resection. Hemilaminotomy was performed at the T4-T5 and L1-L2 levels for placement of inferiorly directed and superiorly directed sublaminar hooks, respectively. The hooks were then connected with a submuscular rod. Eighty-two percent of surviving goats (68% of total) developed a progressive idiopathic-type scoliosis with a lordotic component, and apical wedging of the vertebral bodies and intervertebral discs. The curves progressed from an initial post-operative severity of 42° to a maximal Cobb of 60° over 6 to 15 weeks. The authors report that pilot studies using only concave rib tethering and convex rib resection, intervention limited to the thorax, failed to produce

scoliosis. In contrast, posterior asymmetric tethering alone produced a non-progressive deformity, while the complimentary effect of the rib procedures allowed for progression. Additionally, histologic analysis of the apical vertebrae demonstrated vertebral and disc wedging, as well as cortical and trabecular thickening of the concave side (Braun et al., 2003), each of which are consistent with human literature (Adam & Askin, 2009; Shea et al., 2004)

### 1.3.3.2 Calves

Using an alternative tethering method in calves and shorter spanned distance,
Newton et al. tethered two adjacent vertebrae, either T6-T7 or T8-T9. Right facing
laterally directed screws positioned in the anterior vertebral body were connected with a
flexible steel cable with controlled tension and calves were left to grow for 12 weeks.
This produced an average Cobb angle of 11.6° with accompanied kyphosis and disc space
wedging (Newton et al., 2002). Subsequent studies tethered T6-T9 to produce more
severe scoliosis (Newton, Farnsworth, et al., 2008; Newton et al., 2005).

### 1.3.3.3 Pigs

Similar to the surgery previously performed in calves, Newton et al. used a staple-screw construct connected with a polyethylene tether between T8 and T11 on 7-month-old pigs (Newton, Upasani, et al., 2008). This produced a coronal deformity of 14°±4 by 6 months and 30°±13 by 12 months. However, contrary to that seen in humans and other animal models, the tethered side of the vertebral body was larger than the untethered side and the nucleus pulposus had shifted towards the side of tethering. Magnetic Resonance Imaging revealed no evidence of disc degeneration (Newton, Upasani, et al., 2008). A

subsequent study by the same group using MRI and histological evaluation found no signs of disc degeneration, however, differences in annulus fibrosus water and glycosaminoglycan content may reflect metabolic responses to disc compression (Upasani et al., 2011).

A longer spanning tether using a steel cable was made between T5/T6 and L1/L2 of 4 week-old pigs, which were left to grow for 2 months (Accadbled et al., 2011; Laffosse et al., 2010). This procedure produced scoliosis of Cobb angle of 44° (15°-58°) and rotation of 40° (23°-50°) (Laffosse et al., 2010). In another experiment, the procedure produced scoliosis with a Cobb angle of 42° (21-55), lordosis of 44° (15°-58°) and rotation of 21° (18°-26°) (Accadbled et al., 2011). Micro-CT analysis indicated that the concave side had increased bone volume fraction (BV/TV), decreased specific bone surface (BS/BV), decreased connectivity density index (Cod), increased trabecular thickness (TbTh), decreased trabecular separation (TbTp), and increased structural model index (SMI). Each of these parameters indicates improved bone strength, except SMI (T. Hildebrand, Laib, Muller, Dequeker, & Ruegsegger, 1999; Parkinson, Forbes, Sutton-Smith, & Fazzalari, 2010). This micro-CT analysis represents important reference material for analysis of FGFR3-/-, as it is, to our knowledge, one of only two micro-CT studies on animal models of scoliosis (Fu et al., 2011; Laffosse et al., 2010).

#### 1.3.3.4 Rabbits

Carpintero et al. theorized that unilateral muscular dominance of the paraspinal muscles produced asymmetrical lordosis and is a prerequisite for scoliosis in the rabbit, as was postulated by previous studies (Poussa, Schlenzka, & Ritsila, 1991; Somerville,

1952). They aimed to produce scoliosis in rabbits by tethering, using silk string, three consecutive spinous processes of the thoracic vertebrae to the left or right transverse process of the most inferior of these three vertebrae. This attempted to mimic asymmetric paraspinal muscles and produced curvature of 29.1°±5.8 and apical rotation of 16.4°±3.6. The authors noted that every rabbit developed C shaped curvature with no compensatory curve (Carpintero, Mesa, Garcia, & Carpintero, 1997). Dickson & Smith produced severe scoliosis by tethering the thoracic spine into asymmetric lordosis, accompanied by localized spinal cord damage. The authors tethered T4 to T10, followed by contralateral "release" of the paraspinal muscles using an electric soldering iron (Smith & Dickson, 1987). With this procedure, 6/18 animals died shortly post-operatively. The remaining rabbits developed severe curvature with a mean Cobb angle of over 100°, four of which underwent severe respiratory failure. Histology revealed that cauterization caused local spinal cord damage and added a paralytic component to the instability of lordosis.

Using an alternative method, the scapulae of 7-week-old rabbits were tethered to the contralateral pelvis (Kallemeier et al., 2006). Rabbits were divided into two groups, one with a sham control tethering suture that spontaneously released, while the other had a robust tether and pelvic fixation. Experimental animals initially developed a Cobb angle of 59° (29-90°) and control animals' 23° (6-39°). Sham control curves resolved following spontaneous release. The experimental group Cobb angle peaked at 62° and, following scheduled release, decreased to 43°. However, only 11/17 rabbits survived throughout the study (Kallemeier et al., 2006).

#### 1.3.3.5 Rats

In rats, the scapula was tethered to the ipsilateral pelvis and tightened to instantaneously produce curvature (Sarwark et al., 1988). The tether was surgically released between 1 and 12 weeks postoperatively and found that 6 weeks of tethering was the minimum length of time to cause permanent curvature, while 8 weeks produced more stable curvature upon release. A second group of rats was tethered for between 2 and 8 weeks and grouped based on severity for morphologic and histological assessment. This revealed apical wedging, deviation of the apical spinous process, pelvic asymmetry, rib hump deformity, vertebral rotation, disc compression and displacement of the nucleus pulposus, disorganised epiphyseal growth plate, and increased number of type 1 muscle fibers on the convex paraspinal musculature. Of note, however, the direction of vertebral rotation varied and therefore does not mimic the human condition (Sarwark et al., 1988).

### 1.3.4 Epiphysiodesis

Scoliosis was produced in pigs by epiphysiodesis (Beguiristain, De Salis, Oriaifo, & Canadell, 1980; Coillard, Rhalmi, & Rivard, 1999; Zhang & Sucato, 2008, 2011). A screw was inserted into the pedicle through the neurocentral cartilage towards the anterior portion of the vertebral body. Screws were placed in four or five successive thoracic vertebrae and animals were euthanized variably between 4 and 12 months postoperatively. Surgery consistently produced scoliosis of varying severities, between 10° 5 months postoperative and 80° 12 months postoperative. Curvature included rotation and wedging, with convexity on the side of screw fixation. The authors note that the neurocentral cartilage usually disappears in the juvenile stage and that its role in scoliosis is

controversial. Additionally, they find the mechanism of production of this scoliosis to be difficult to explain, especially because the convexity lies on the operated side (Beguiristain et al., 1980). In similar studies, double pedicle screws increased the effect of epiphysiodesis and caused greater curvature than that created by only a single screw (Zhang & Sucato, 2008). They also found that contralateral double pedicle screws inserted 6 weeks after the initial surgery produced a 41% correction of the deformity (Zhang & Sucato, 2011). However, one study found that sham operation that violated the neurocentral cartilage but did not compress it caused the same growth disturbances as a pedicle screw, raising a question to the cause of scoliosis in previous studies and whether appropriate controls were used (Cil et al., 2005).

## 1.4 Bone Development

The formation of the skeleton, as in other tissues, is a complex process that involves patterning during pre-natal development, bone growth during post-natal development, and remodeling throughout life (P. Marie, 2003; Yu & Ornitz, 2007). These processes, and more, are governed by 22 distinct polypeptide members of the fibroblast growth factor (FGF) family of growth factors, and constitute one of the largest families of growth and differentiation factors for cells of mesenchymal and neuroectodermal origin (Eswarakumar, Lax, & Schlessinger, 2005; Givol & Yayon, 1992; Ornitz & Itoh, 2001). Because the targeted mutation of Fibroblast Growth Factor Receptor 3, a receptor for FGFs, causes the unique skeletal phenotype that forms the basis for the current research, the following section will provide a brief overview of skeletal growth and development, and discuss FGFs and FGFR3 within this context. In particular, FGF18 has been shown

to signal through FGFR3 to promote chondrocyte growth during endochondral ossification (Davidson et al., 2005). In addition to FGFs, the maturation of mesenchymal stromal cells into chondrocytic and osteoblastic lineages are directed by secreted polypeptides of the Hedgehog, Wnt, and TGF-β families, as well as transcription factors of the Pax, Hox, homeodomain-containing, BHLH, and Forkhead families (Nakashima et al., 2002).

### 1.4.1 Endochondral Ossification

Skeletal development and repair proceed by two distinct mechanisms: intramembranous ossification and endochondral ossification. Intramembranous ossification features mesenchymal precursor cells condensing to convert directly into bone producing osteoblasts that produce extracellular matrix. Intramembranous ossification is responsible for producing the flat bones of the skull and clavicle. Endochondral ossification is responsible for the remainder of the skeleton, including the vertebrae and longbones. The stages of endochondral ossification are characterised by changes in the synthesis, deposition, and degradation of extracellular matrix (Henderson et al., 2000), whereby chondrocytes lay a scaffold, or anlagen, for osteoblast secretion of bone. The process of endochondral ossification is composed of three cell types from two lineages, osteoblasts and chondrocytes derived from a mesenchymal lineage and osteoclasts derived from a hematopoietic lineage (Karsenty & Wagner, 2002; Kobayashi & Kronenberg, 2005).

Endochondral bone formation begins with the aggregation of mesenchymal cells.

Cells in the core of the aggregation differentiate into chondrocytes, whereas spindle-

shaped cells at the periphery form the perichondrium (Ohbayashi et al., 2002; B. R. Olsen, Reginato, & Wang, 2000; Vortkamp et al., 1996). Central chondrocytes express specific molecular markers, such as aggrecan and collagen α1(II), that distinguish them from undifferentiated mesenchymal cells and those of the perichondrium (Karsenty & Wagner, 2002; Shukunami et al., 1996). Shortly after the condensations form, chondrocytes cease proliferating, become hypertrophic and alter their extracellular matrix in such a way to allow blood vessels to invade from the perichondrium, a process which is closely followed by appearance of bone marrow cells and osteoblasts (Vortkamp et al., 1996). The perichondrial cells differentiate into osteoblasts and express Runx2, then mineralize and form the bone collar (Karsenty & Wagner, 2002). The matrix surrounding hypertrophic chondrocytes, the most mature cells of the growth plate, begins to calcify and forms a scaffold for osteoblasts (Vortkamp et al., 1996). This calcified cartilage is removed by chondroclasts to make room for bone secreting osteoblasts (Engsig et al., 2000; Mundlos & Olsen, 1997). Chondroclasts differ from osteoclasts in that they express more MMP9 but less Tartrate Resistant Acid phosphatase (TRAP) than osteoclasts (Engsig et al., 2000; Henriksen, Bollerslev, Everts, & Karsdal, 2011). The zone of hypertrophic cartilage and the ossified region expand towards the ends of the bone, leaving the shaft of the bone mostly mineralized (Vortkamp et al., 1996). Growth plates are the remaining narrow bands of proliferative chondrocytes and transitional hypertrophic chondrocytes at the ends of each bone, and are the source of elongation during skeletal growth (Hartmann & Tabin, 2000; Vortkamp et al., 1996). Careful control of the rate of chondrocyte proliferation and differentiation into hypertrophic chondrocytes is vital in the regulation of endochondral ossification and bone

morphogenesis. Therefore, disruptions in this control, as is the case in FGFR3-/- mice, can cause unique skeletal phenotypes (Valverde-Franco et al., 2004).

## 1.4.2 Signaling Molecules

In order to better gain a holistic understanding of Fibroblast Growth Factors (FGFs) and their receptors, it is first necessary to review the interaction between FGFs and other signaling molecules governing skeletal development. In both mechanisms of skeletal development, endochondral and intramembranous ossification, the process is coordinated by a variety of signaling molecule families, including FGF, TGF-β, IGF, Wnt, Runx2, and hedgehog. Cells of chondrocytic and osteoblastic lineage are both derived from osteoprogenitor cells, which, in addition to adipocytes, are derived from mesenchymal stromal cells. Of greatest importance at the osteoprogenitor stage, Runx2 is necessary and sufficient to direct multipotent mesenchymal cells into an osteoblastic lineage and inhibits them from entering the chondrocytic and adipocytic lineages (Karsenty & Wagner, 2002; Komori, 2006). Sox 5, 6, and 9 direct osteoprogenitor cells into chondrocytic lineage while Runx2, osterix, and β-Catenin direct towards osteoblastic lineage (P. J. Marie, 2008). Osterix is an essential transcription factor for osteoblast differentiation that acts downstream of Runx2 and acts to differentiate pre-osteoblasts into functional osteoblasts (Nakashima et al., 2002).

Although the integration of these signaling molecules with FGFs is not entirely clear (Kim, Kim, Bae, Choi, & Ryoo, 2003), they may converge at the FGF18 promoter. Recent evidence shows that FGF18 is a target of the canonical Wnt signaling pathway, which directs development in a variety of tissues. Of particular interest to the osteogenic

lineage, they also regulate protein levels of β-catenin and stabilizes the protein for its migration into the nucleus. β-Catenin acts as a binding partner to Lef/TCF transcription factors to activate or repress a variety of target genes (Glass II & Karsenty, 2006). Canonical Wnt signaling has also been shown to promote Runx2 expression, as β-catenin promotes Runx2 and its activity, and can also induce osterix expression (Bodine et al., 2004; Gaur et al., 2005). Runx2 forms a complex with either Lef1 or TCF2 and this complex binds to the composite binding site of the FGF18 promoter. This suggests that Runx2 and cWnt signaling are required for FGF18 expression (Reinhold & Naski, 2007). Canonical Wnt signaling also regulates osteoclast differentiation by regulating osteoprotegerin expression, and was further found to induce the expression of Runx2 and osterix (Reinhold & Naski, 2007). This is self-regulating, as Runx2 positively regulates osteoprotegerin, which is itself a potent inhibitor of osteoclast differentiation and bone resorption (Thirunavukkarasu et al., 2000). BMP2 is incorporated into this pathway by promoting Runx2 expression in mesenchymal osteoprogenitors and osteoblastic cells (K.-S. Lee et al., 2000; M.-H. Lee et al., 2003), and by promoting osterix and homeobox protein DLX5 (M.-H. Lee et al., 2003; M. H. Lee, Kwon, Park, Wozney, & Ryoo, 2003; Miyama et al., 1999).

Parathyroid hormone related peptide (PTHrP) is a paracrine mediator of endochondral bone growth, in which it regulates cell proliferation, differentiation, and apoptosis (Amizuka et al., 2004; K. Lee et al., 1996). It can act either by interacting with the cell surface PTH1R to activate signal transduction pathways and regulate chondrocyte differentiation (Guo et al., 2001; Shukunami et al., 1996) or directly translocate to the nucleus (L. Okoumassoun, Averill-Bates, Denizeau, & Henderson, 2007; L. E.

Okoumassoun, Russo, Denizeau, Averill-Bates, & Henderson, 2007). Experiments based on the disruption of either PTHrP or PTH1R cause osteochondrodysplasia due to reduced proliferation and increased apoptosis of immature chondrocytes. The primary influence of PTHrP is to stimulate the proliferation of chondrogenic cells and to inhibit differentiation into hypertrophic chondrocytes (Amizuka et al., 2004). PTHrP expression is partially mediated by FGFR3. Cells with a constitutively activated mutation of FGFR3, as is seen in achondroplasia and thanatophoric dysplasia (Michael C. Naski, Wang, Xu, & Ornitz, 1996; Wang et al., 1999), have decreased production of PTHrP and the antiapoptotic protein Bcl-2 (Yamanaka, Tanaka, Koike, Nishimura, & Seino, 2003). Furthermore, parathyroid hormone (PTH), the systemically released counterpart to PTHrP, has been shown to alter the expression of FGF2 and the FGFRs (Hurley et al., 1999).

#### 1.4.3 Fibroblast Growth Factors

Fibroblast growth factors control embryonic development by regulating cell proliferation, differentiation, and cell migration. In the post-natal and adult organism, FGFs help control tissue repair, wound healing, and the nervous system (Eswarakumar et al., 2005). In vivo and in vitro studies on growth plate cartilage and endochondral bones identify FGF2 and FGF18 signalling through FGFR3 as the primary cause of the FGFR3-/- phenotype (Davidson et al., 2005; Liu, Xu, Colvin, & Ornitz, 2002; Ohbayashi et al., 2002; Valverde-Franco et al., 2006). In vitro studies found that FGF2 signaling through FGFR2 blocked ALP accumulation and inhibited nodule mineralization in primary cultures of calvarial osteoblasts (Mansukhani, Bellosta, Sahni, & Basilico, 2000). Current

literature proposes that FGF18 is an endogenous ligand for FGFR3 in growth plate chondrocytes, where FGFR3 is expressed in resting and proliferating chondrocytes (Valverde-Franco et al., 2004). Because FGF18 null mice do not survive past birth while FGFR3-/- mice survive with skeletal dysplasias and growth plate abnormalities, FGF18 must signal through other FGF receptors. FGF18 is thought to act through FGFR2 in osteoblasts and their precursors to promote their proliferation, where FGFR2 is expressed in the perichondrium, periosteum, and the metaphysis. Additionally, FGF2 signalling may activate FGFR1 to promote early differentiation of osteoprogenitor cells (Valverde-Franco et al., 2004). FGFR1 and FGFR2 are up-regulated in FGFR3-/- mice, so signaling through these receptors may promote early differentiation and proliferation of osteoprogenitor cells, respectively. Therefore, it is consistent that FGFR3-/- mice have increased number and activity of osteoblasts, further supporting the hypothesis that FGFR1 and FGFR2 control osteoblast function and FGFR3 regulates chondrocyte activity (Valverde-Franco et al., 2004).

FGFs mediate their responses by binding to a family of four receptor tyrosine kinases, designated as FGF receptors 1-4 (Eswarakumar et al., 2005; P. L. Lee, Johnson, Cousens, Fried, & Williams, 1989). A common feature of all members of the FGF family is their affinity for extracellular matrix heparin sulphate and glycosaminoglycan heparin (Givol & Yayon, 1992; P. L. Lee et al., 1989). Cell surface heparin sulphate proteoglycans act as a reservoir for heparin-binding growth factors and protect the FGF from proteolysis ("Fibroblast growth factors: time to take note," 1990), but also play an essential role in the FGF signaling pathway (Givol & Yayon, 1992). FGFs bind to heparin or heparin sulphate proteoglycans in a low affinity receptor and allow the FGF to

bind to its high affinity FGFR. Heparin or heparin-like immobilized molecules, heparin sulphate proteoglycans, interchangeably confer a stable, receptor compatible conformational change upon FGFs, allowing them to bind to the FGFR (Yayon, Klagsbrun, Esko, Leder, & Ornitz, 1991). FGFRs, like all receptor tyrosine kinases, are composed of an extracellular ligand binding domain to which the FGF binds, a single transmembrane domain, and a cytoplasmic domain that contains the catalytic protein tyrosine kinase core that is autophosphorylated during activation, as well as additional regulatory sequences (Schlessinger, 2000).

FGFR3 is the primary concern for this project, as its absence is the cause of the unique phenotype that includes scoliosis. However, before discussing the phenotype of FGFR3-/- mice, it is important to review its expression, involvement in cellular pathways, and interaction with fibroblast growth factors. A number of bone disorders are a result of mutations in FGFR3. Activating mutations cause achondroplasia, the most common dwarfism in humans, and related conditions such as hypochondroplasia, thanatophoric dysplasia, and Crouzon syndrome with acanthosis nigricans. These activating mutations, supported by in vitro experiments, indicate that FGFR3 mediates the inhibitory influence on chondrocytes proliferation and Ihh expression (Henderson et al., 2000; B. R. Olsen et al., 2000). Conversely, targeted deletion of FGFR3 in mice leads to skeletal overgrowth, deafness, kyphoscoliosis, and a number of other skeletal deformities (Colvin, Bohne, Harding, McEwen, & Ornitz, 1996; Deng, Wynshaw-Boris, Zhou, Kuo, & Leder, 1996; Valverde-Franco et al., 2004; Yu & Ornitz, 2007).

In addition to the four variants of FGFR (1-4), FGFR1, FGFR2, and FGFR3 each have two isoforms, designated b and c. The "b" isoform is expressed in the epithelium while the "c" isoform is expressed in the mesenchyme (Miki et al., 1992) and differ in their affinity for various FGFs. These isoforms are generated by alternative splicing of FGFR transcripts, whereby a single gene may encode multiple proteins by reconnecting exons in multiple combinations to produce a variety of mRNAs (Black, 2003). The alternative splicing of FGFR mRNA is the main mechanism by which the different FGF-ligand binding profiles are generated. During development the differential expression of the two isoforms allow for directional epithelial-mesenchymal signaling (S. K. Olsen, 2006).

Despite the overlap between FGFR2 and FGFR3, FGFR1 and FGFR3 maintain very distinct domains of expression with very little overlap (Yu & Ornitz, 2007). FGFR3 is expressed in proliferating chondrocytes, whereas FGFR1 is expressed in prehypertrophic and hypertrophic chondrocytes. FGFR3 is expressed in the reserve and proliferating zones of the growth plate and further supports that FGFR3 plays a role in chondrocyte proliferation and differentiation (Peters, Ornitz, Werner, & Williams, 1993; Yu & Ornitz, 2007). Additionally, FGFR3 is expressed in mature osteoblasts and osteocytes (Xiao et al., 2004).

In addition to the careful control of chondrocyte proliferation, FGFR3 signaling regulates the expression of Ihh, PTHrP and BMP signaling pathways, each of which are important regulators of chondrogenesis (Kronenberg, 2003; Minina, Kreschel, Naski, Ornitz, & Vortkamp, 2002; M.C. Naski, Colvin, Coffin, & Ornitz, 1998; Vortkamp et al.,

1996). As well, FGFR3 signalling via a STAT1 dependent pathway mediates chondrocyte survival and apoptosis (L'Hôte & Knowles, 2005; Su et al., 1997). Limb explant experiments suggest that FGF signaling regulates chondrocyte differentiation upstream of PTHrP and Ihh signaling, while BMP and FGF act in an antagonistic relationship regulating chondrocyte proliferation, Ihh expression, and hypertrophic differentiation (Minina et al., 2002; M.C. Naski et al., 1998). Explant experiments also showed that PTHrP forms a negative feedback loop with Ihh to regulate the rate of chondrocyte differentiation (Vortkamp et al., 1996). Therefore, disruption to FGFR3 signalling will disrupt the balance between chondrocyte proliferation and differentiation in growth plates.

# 1.5 FGFR3-/- Phenotype

Targeted disruption of FGFR3 was achieved by replacing a 3kb portion of the genomic locus with a neomycin resistance cassette. Following homologous recombination, this resulted in a deletion in the gene's exon and prevented receptor expression on the cell surface (Colvin et al., 1996). Mice with targeted inactivation of FGFR3 (FGFR3-/-) have skeletal overgrowth attributed to increased chondrocyte proliferation, delayed differentiation, and reduced transition of mature cartilage to bone at the chondro-osseous junction (Amizuka et al., 2004). Bones formed by endochondral ossification featured widened physeal proliferative zones, and exhibited longer and bowed long bones. Young adult mice were osteopenic due to reduced cortical thickness and defective trabecular bone mineralization. Additionally, long bones had decreased mineralization with an increased proportion of osteoid. Because of these skeletal

dysplasias and growth plate abnormalities, FGFR3-/- mice were deaf, and had kinked tails and severe kyphoscoliosis. This final feature was what raised our curiosity about its potential as an animal model for idiopathic scoliosis.

# 1.6 Human Spine Development

To better understand the abnormal growth of the spine in scoliosis, it is necessary to provide a brief review of normal human spine growth and development. The embryonic development of the spine can be separated into 6 phases: gastrulation, and formation of the somitic mesoderm and notochord, condensation of the somitic mesoderm to form somites, reorganization of the somites to form dermomyotome and sclerotome, membranous phase of somitic development and re-segmentation of the somites to form the definitive vertebrae, vertebral chondrification, and vertebral ossification (Dias, 2007).

Within the phase of gastrulation and formation of somites and the notochord, during the second week after fertilization, the embryo has developed craniocaudal orientation and a midline primitive streak develops at the caudal end of the embryo and elongates cranially. As this process progresses, the embryo converts from two layers (epiblast and hypoblast) into the more familiar ectoderm, mesoderm and endoderm. As the primitive streak regresses, the remaining epiblast cells migrate through the primitive groove to form neuroectoderm and cutaneous ectoderm. At the cranial end of the primitive streak is Hensen's node, the cells of which invaginate through a structure called the primitive pit to form the midline notochord. The notochord elongates and is surrounded by the somitic mesoderm bilaterally, which together form the axial skeleton.

Somitic mesoderm aggregates to form discrete blocks of tissue called somites, which are adjacent to the notochord and neural tube. In humans, 38 or 39 somites form (Dias, 2007), and are precursors to the axial skeleton. The number of somites are specific to the vertebrate, with mice requiring 65 somites to account for the tail (Gilbert, 2000). The patterning of the somites is determined by the expression of homeobox genes. In the next phase, the somite becomes reorganized dorsoventrally to form the sclerotome, which will form the axial skeleton, and the dermomyotome, which will form the dorsal trunk musculature (Dias, 2007). The sclerotome form the vertebral column and undergo subsequent changes, including membranous phase, chondrification, and ossification.

During the membranous phase, the somites migrate ventrally to surround the notochord and dorsally to surround the neural tube. There is ongoing research on the formation of the vertebral body. It is unknown whether the body is derived from a single sclerotome or from the fusion of the cranial and caudal halves of adjacent sclerotomes, with the hypocellular fissure of von Ebner contributing to the intervertebral disc (Dias, 2007). Experimental evidence supports the concept of fusion, a theory known as resegmentation (Ewan & Everett, 1992).

In humans, the chondrification phase starts at the sixth embryonic week. Three paired chondrification centers appear for each vertebra: within the vertebral body, dorsolaterally within the posterior vertebral arches and spinous process, and a third pair between the first two chondrification centres and within the transverse processes (Dias, 2007). During the chondrification phase, cells of the notochord form the nucleus pulposus while perinotochordal cells from the somites form the annulus fibrosis. As well, the

anterior and posterior longitudinal ligaments are formed from the surrounding mesenchymal cells.

The ossification stage begins at the eighth week and continues after birth. The number of ossification centers is debated, however, most authors describe three: one for the vertebral body and one for each side of the dorsal vertebral arch. However, these lateral centers probably contain three ossification zones: pedicles, lamina, and transverse processes. Disordered vertebral formation or malalignment of the column leads to congenital abnormalities.

#### 2 Methods

# 2.1 Organization and Study Design

The study included male and female mice from a C3H background. Sixty three FGR3-/- mice and 58 FGFR3 Wildtype mice, both +/+ and +/- (functional FGFR3 is a dominant allele so homozygotes and heterozygotes have the same phenotype, were monitored variably at ages ranging from birth to 25 weeks between one and nine time-points to evaluate the severity and progression of scoliosis and various gross anatomical measurements, each with respect to age, gender, and genotype. The mice were euthanized at the end of the study, most commonly at 25 weeks. The spines were then extracted, and processed for Micro Computed Tomography (Micro-CT) and histology. Thirty-four mice were chosen for Micro-CT analysis of vertebral micro-architecture and dimensions. FGFR3-/- mice were age and sex matched with wild-type counterparts so that the curve characteristics present in the FGFR3-/- mice could be compared to the equivalent vertebrae on wild-type mice.

Anaesthesia: Mice were anaesthetized with an injectable anaesthesia prior to plain radiography and anatomical measurements. In order to guarantee that the mice were anaesthetized for a sufficient length of time and depth of anaesthesia, an injectable rodent cocktail designed by McGill Animal Resource Centre was used. The rodent cocktail consisted of ketamine (0.25mL<sub>ketamine</sub>/10mL<sub>cocktail</sub>) acepromazine (0.05mL<sub>acepromazine</sub>/10mL<sub>cocktail</sub>), and xylazine (0.125mL<sub>xylazine</sub>/10mL<sub>cocktail</sub>) in 9.575mL of sterile saline and delivered intraperitoneally at 5μL/g. Mice were weighed on an electronic scale to determine the appropriate dosage, bodies inverted and rodent cocktail delivered into the lower abdomen with a slight lateral offset. After mice were sufficiently anaesthetized, anatomical measurements and X-Rays could be performed.

Anatomical Measurements: Because the aim of the study was to characterize scoliosis in FGFR3-/- mice, gross anatomical measurements were made to ascertain additional characteristics, covariates, and predictors of scoliosis. Body mass was recorded by electronic scale. Body length was determined by laying the mouse prone and measuring the distance between the nose and base of the tail with the body in neutral position. Likewise, tail length was measured from the base to the tip of the tail. However, tail length cannot be used for statistical analysis beyond generalizations because the tail tips of many mice were removed during genotyping, limiting the validity of measurements. Finally, the presence of a tail kink was recorded. A tail kink was deemed present if visible or palpable.

# 2.2 Plain Radiography

A Kubtek XPERT 80 (Milford, CT, USA) was used for all plain radiography. Prior to placement in the X-Ray machine, the machine was automatically calibrated in accordance with manufacturer specifications and a file created for each mouse. Additionally, mouse characteristics and age were appended to each X-Ray for record integrity. A typical X-Ray intensity was 750μA and 25kV. Using a dosimeter, Kubtek found that these settings would result in 3.1mGy of radiation per radiograph. Because 3 images were taken for each mouse at each age, X-rays for a single time-point resulted in approximately 9.3mGy of radiation.

## 2.2.1 Posterior-Anterior Spine and Pelvis

Mice were laid prone in a Kubtek XPERT 80 in neutral position with the body above the detector to create a posterior-anterior X-Ray with a field of view spanning from the neck to the pelvis. The resulting film included thoracic and lumbar vertebrae. This film was used to measure scoliosis Cobb angles. In the same body position, the mouse was moved so that its pelvis and femurs were visible. Using the Kubtek controller software measurement tool, femur lengths were recorded by measuring between the base of the femoral neck where it meets the proximal femoral metaphysis and the most distal aspect of the femoral condyles.

### 2.2.2 Lateral View

The mouse was laid on its side in a neutral position with limbs outstretched to obtain a lateral film. As with the posterior-anterior view, the lateral field of view included the pelvis, lumbar, thoracic, and a portion of cervical vertebrae. The length of lumbar

vertebrae L1-L5 and of L1 itself were determined using the measurement tool. These were measured using the lateral view because the natural kyphosis of the mouse limits the validity of lengths measured posterior-anterior.

# 2.2.3 Scoliosis Cobb Angle

Scoliosis was measured using the Cobb Method (Cobb, 1948) were performed in a manner identical to that used in humans, using Gingko CADx 2.4.1. The end vertebrae were identified as the vertebrae tilted maximally towards the concavity of the curve, based on American College of Radiology guidelines. Using Ginkgo CADx, parallel lines were drawn from the superior endplate of superior end vertebrae and the inferior endplate of the inferior end vertebrae. If endplates were not visible or indistinct, equivalent points of the pedicles were used. Perpendicular lines were constructed and the angle subtended by these lines is the Cobb angle. Many spines contained several scoliosis curves. All curves were measured and recorded, however, only the largest curve was used for analysis and is considered the primary curve. Furthermore, the apical vertebra was defined as the most laterally deviated vertebra of the primary curve.

#### 2.2.4 Curve Location

Location of the primary curve was divided into four categories: Proximal thoracic (T1-T7), Distal Thoracic (T8-T12), Thoracolumbar (T13 and L1) and Lumbar (L2-L6). This is a modification of the Scoliosis Research Society (SRS) and Lenke classification systems (Lenke et al., 2001), with SRS's Thoracic curves being subdivided into proximal and distal thoracic curves, and with vertebrae cut-offs being adjusted for the additional

thoracic and lumbar vertebrae in mice. Primary curves were also categorized as being either concave left or concave right.

### 2.2.5 *Lateral Cobb Angle*

Angles to quantify kyphosis and lordosis from lateral views were found using the Cobb method. To measure the angle of lordosis was made using the Cobb method, where the superior endpoint was defined as T1 and the inferior endpoint was the vertebra most maximally tilted towards the concavity of the curve (approximately T8). Likewise, the kyphosis Cobb angle used the superior endplate of the maximally tilted vertebra, the vertebra inferior to the inferior endpoint of the lordosis curve, and the next maximally tilted vertebra, usually in the lumbar vertebrae.

## 2.3 Spine Extraction

Mice were euthanized at approximately 25 weeks of age by CO<sub>2</sub> asphyxiation and cervical dislocation in accordance with McGill ethical guidelines. Immediately after euthanization, spines were extracted and fixed in 4% paraformaldehyde for 72 hours. In brief, an incision was made from the base of the neck to the pelvis along the mid-sagittal line. Connective fascia was disrupted by blunt dissection. After using a scalpel blade to locate the pelvis and lumbar vertebrae, bone scissors were used to sever the spine between L6 and the sacrum, within the cervical vertebrae, and to cut through the posterior rib cage. Short sections of the ribs were retained for reference during micro-CT and histology. Excess paraspinal muscles were removed and the spine was immediately placed in 4% paraformaldehyde and refrigerated for 72 hours. Although typical protocol specifies 24 hour fixation for a long bone with open medulla, 72 hours was chosen

because of residual musculature and limited diffusion through the cortex into the vertebral medulla. After fixation spines were placed in changes of 1x Phosphate Buffered Saline.

# 2.4 Micro Computed Tomography

A SkyScan 1172 high resolution Micro Computed Tomography (Micro-CT) Scanner (Kontich, Belgium) was used to assess the 3-Dimensional structure of spines and their micro-architecture. The scanner is equipped with an 11MP Camera. Each spine underwent two Micro-CT scans at different resolutions. A higher resolution scan with a spatial resolution of 11.0µm targeted the apical vertebra of the primary curve and included the adjacent vertebrae. This scan was used to assess the vertebral microarchitecture, vertebral body dimensions, and the intervertebral disks adjacent to the apical vertebra. A configuration file specifying several aspects of the scan was created to optimize results and guarantee high quality images with maximum contrast. The scan used a 2000 x 1000 pixel camera and filtered the X-rays using a 0.5mm aluminum filter. The X-Ray source had a configured power of 10W, at 50kV and 200µA. A second scan with a large field of view was used to capture the 3D structure of the entire spine and evaluate the rotation of vertebrae in the curve. This used a lower resolution 27µm pixel size in conjunction with a multi-section oversize scan, whereby the sample is adjusted vertically to capture an image of the entire spine. Because resolution was not a critical factor, a 1000 x 500 pixel camera was used to reduce scan time.

The resulting series of images were reconstructed and processed using SkyScan proprietary software. 3-Dimensional models were reconstructed using NRecon (1.6.3.3).

A volume of interest containing the appropriate vertebrae was specified to eliminate dead space and used a dynamic range of 0.000 to 0.100. In order to improve the quality of images and reduce artefacts, images were reconstructed using a ring artefact reduction of 4x and beam hardening correction of 30%.

Prior to analysis, vertebrae were manipulated along the three dimensional planes using Dataviewer (1.4.3). Images were saved in a coronal view (ventral/dorsal view) for analysis of vertebral dimensions and assessment of intervertebral disk thickness. Images were saved in an axial view for the evaluation of vertebral body micro-architecture.

Lastly, CTVox (2.0.0) was used to model the spine in three dimensions to aide in visualization.

#### 2.4.1 Vertebral Micro-Architecture

Bone volume/total volume (BV/TV or Bone Volume Fraction) acted as the primary measure of bone quality and was determined for both the concave and convex aspects of the apical vertebrae using CTAn (1.6.3.3). Higher bone volume fraction indicates improved bone quality. In an axial view, the vertebral body was divided along the mid sagittal line and a cylindrical volume of interest with a 0.55mm diameter was made between the superior and inferior endplates, bilaterally on both sides of the midsagittal line. Each cylinder was placed an equal distance from the mid-sagittal line to the lateral aspect of the vertebral body. The grey-scale threshold of bone had a radio-opacity of 55-255, while 0-54 was considered empty space. After defining the cylindrical volume of interest, the volume occupied by bone was compared to the total volume of the cylinder to measure micro architecture. Parameters included bone volume fraction,

trabecular number and thickness, anisotropy, structural model index, connectivity, porosity and trabecular pattern factor.

Measurement of the vertebral height and an approximation of the thickness of intervertebral disks were made using a coronal series of images in CTAn. A coronal image at approximately the midpoint between the anterior and posterior aspects of the vertebral body was used for vertebral height and intervertebral disk thickness. In this image, the midpoints between the mid-sagittal line and the lateral aspects of the vertebral body were approximated. Using the measurement tool, a line was drawn from the superior midpoint to its ipsilateral inferior midpoint and recorded as the concave or convex vertebral height. Likewise, a line was drawn from the superior midpoint of the apical vertebrae to the equivalent midpoint on the inferior endplate of the superior vertebrae. These methods produced vertebral heights for the left and right sides, and two intervertebral disk thicknesses for each side. Although these distances are not a direct measure of intervertebral disk thickness, it is accurate and reliable.

#### 2.4.2 Vertebral Rotation

Dataviewer was used to orient the low-resolution full spine reconstructions vertically and saved in an axial/transverse series. After visualizing the spine in CTVox, the axial series was loaded into CTAn to determine the rotation of vertebrae throughout the spinal curve. A line is drawn from standard mid-sagittal line on the anterior aspect of the vertebral body to the most posterior point of the visible vertebrae, along the same line. This point is often the spinous process. The first vertebra forms a reference line by which the second and subsequent vertebrae are compared. When the line of interest and the

reference line are superimposed, an angle is formed that measures the rotation of that vertebra with respect to the first vertebra. This method was adapted from Ho's method using different landmarks (Ho, Upadalyay, Chan, Hsu, & Leong, 1993).

In order to form these lines, an axial image that displays the necessary anatomical structures was chosen and the specific vertebra noted. Two reference points, indicating the endpoints of the previously mentioned line, were saved and exported to a custom excel program. These reference points create a vector that can be compared to other vectors to form the angle of interest and measure of rotation.

# 2.5 Histology

## 2.5.1 Embedding

In preparation for undecalcified embedding in poly-methylmethacrylate, the vertebrae of interest in the scoliosis curve, namely the apical vertebra and four adjacent vertebrae, were separated from the rest of the spine. The spine was laid supine under a dissection microscope and scalpel was used to remove fascia from the anterior aspect of the vertebrae and to allow for precise further dissection. Care was taken to not penetrate the thin cortex or penetrate the intervertebral disks. After fascia removal and accurate visualization of the anterior vertebral bodies, a scalpel was used to cut through the intervertebral disk between the vertebrae two places above and below the apical vertebrae. Therefore, the remaining tissue consisted of five vertebrae and four intact intervertebral disks. If the vertebrae of interest were thoracic, ribs were trimmed to an extent that they were flush with the anterior vertebral body and could lie flat for histology.

Dissected vertebrae were fixed in 70% ethanol for 24 hours and were embedded undecalcified in polymethylmethacrylate. In contrast to previous methods, the addition of methylbenzoate to the infiltration and polymerization improved the antigenicity of the tissue and allowed for demonstration of alkaline phosphatase (ALP) and tartrate-resistant acid phosphatase (TRAP). Samples were placed in an initial MMA1 solution containing 60mL of methylmethacrylate, 35 mL of butylmethacrylate, 5 mL of methylbenzoate and 1.2mL of polyethylene glycol. Solution 2 consisted of 100mL of MMA1 and 0.4g of dry benzoyl peroxide while Solution 3 added 0.8g of dry benzoyl peroxide. The embedding plastic consisted of MMA 3 with the addition of 400µL of N,N-dimethyl-p-toluidine. Samples were placed prone, anterior down, in a 10mL plastic embedding sample holder and filled with embedding medium. Sufficient medium was added to guarantee air was excluded and that the holder cap could be closed, as oxygen prevents plastic polymerization. Polymerization was carried out in a -20°C freezer for 3 days. Embedded plastic samples were trimmed using a band saw to form a block approximately 2cm<sup>3</sup>.

#### 2.5.2 Staining

Sections for Von Kossa were individually isolated using a liquid blocker pen and stained with 5% silver nitrate for 60 minutes under UV light and counterstained with 0.2% toluidine blue for 1 minute to identify phosphate mineralization, and osteoid, marrow, or IVD, respectively. Slides were washed in distilled water 3 times and left to air dry for 60 minutes, after which cover slips were mounted using permount (Thermo Fisher Scientific, Waltham MA)

For either Alkaline Phosphatase (ALP) or Tartrate Resistant Acid Phosphatase (TRAP) staining, slides were incubated in 20% sucrose solution for 60 minutes, rinsed, and further processed. For TRAP staining, slides were incubated for 30 minutes in an aluminum foil wrapped coplin jar in a dark, 37°C water bath in a solution containing 2.0mL of 4% sodium nitrite, 2.0mL of 4% pararosaniline hydrochloride, 46mL of 0.2M acetate buffer, 16mg of naphthol AS-TR phosphate disodium salt, 115mg sodium tartrate, at pH 5.0. For ALP Staining, slides were incubated with a solution containing 200mM Tris-maleate buffer, 3mg Naphthol AS-TR phosphate, 150μL N,N-dimethyl formamide, 200μL NBT/BCIP. Tissues were isolated using liquid blocker and staining solution individually pipetted onto slides, covered, and placed in a 37°C water bath for 60 minutes incubation. ALP and TRAP stained sections were rinsed three times for 10 minutes each with distilled water before being counterstained (0.018% methyl green, 0.01% fast green) and mounted with permount (Thermo Fisher Scientific, Waltham MA).

#### 2.5.3 Imaging

Histology slides were visualized using a Zeiss Axioskop 40 microscope with 2.5x and 10x objectives. Images were captured using an attached Zeiss AxioCamMRc. For each slide with serial sections, the tissue section with fewer artefacts was selected for imaging. A 2.5x image captured up to three vertebrae in its field of view while a 10x image captured one half a vertebral endplate. A single 2.5x images was taken for the tissue section, whereas one each of a left and right 10x images were taken of the endplate of the apical vertebra in FGFR3-/- mice and a single 10x image was taken of the endplate of the associated wildtype vertebra.

# 2.6 Statistical Analysis

# 2.6.1 Data Organization

All data was transcribed into a unified database using SPSS 20.0 and arranged by case, where each case is an age of X-Ray. Cases included variables such as mouse number, gender, genotype, age, body mass, body and tail lengths, presence of a tail kink, left and right femur lengths, L1-L5 length, L1 height, Cobb angle of each curve with their superior and inferior endpoints, the sum of Cobb angles, primary curve Cobb angle and location of apex vertebra, primary curve direction (Concave left or right), computed average femur length, kyphosis and lordosis Cobb angles, and age at euthanization. In addition, a number of artificial dummy variables were created for statistical purposes.

Data was organized differently, in a so-called "wide orientation", for micro-CT comparisons so information on microarchitecture, vertebral height, and intervertebral disk thickness were stored in a separate SPSS Database. Because each apical vertebra had a superior and inferior intervertebral disk space, thicknesses were averaged to decrease measurement error while not inflating sample size.

## 2.6.2 Linear Mixed Effects Modeling

The nature of the data is such that a number of mice with certain fixed characteristics were radiographed an unequal number of times at inconsistent ages. Furthermore, age was taken to be a continuous variable. All data that was recorded with respect to mouse age, such as Cobb angle and body mass, were analyzed using Linear Mixed-Effects Modeling (mixed model) in SPSS. Mixed modeling was chosen because it is capable of handling correlated data and unequal variances. Mixed modeling is a

special case of the general linear model (GLM), which also includes ANOVA, ANCOVA, MANOVA, MANCOVA, linear regression, F test and T test. In fact, mixed modeling is similar to repeated-measures ANOVA except that subjects have an unequal number of observations and that independent variables such as age may be continuous. Because of the unequal number of observations, the data is considered unbalanced. Linear Mixed-Effects Model is also a specific case of the Generalized Linear Mixed-Effects Model in which the random effect (u) is normally distributed, and that measurement parameter given the random effect (Y|u) is normally distributed (Klinker, 2011). One of the advantages of the mixed model is that it can handle missing data, an essential characteristic in unbalanced data.

Mixed modeling is such named because it combined random effects, such as the FGFR3-/- gene expressivity and individual characteristics of the mouse, and fixed effects, such as genotype or gender. Variables are considered fixed if they affect the population mean whereas effects associated with sampling procedure, such as the subject, are considered random effects. In this model, data are thought to be the sum of the fixed and random effects (SPSS, 2005). Therefore, the mixed model can be described as:

$$Y = X\beta + Zu + e$$

X and  $\beta$  are the fixed effect parameter estimate and presence of fixed effect, respectively, Z and u are the random effects parameter estimate and presence of random effect, respectively, and e is the error (Klinker, 2011; Taylor). Random effects like subject effects contribute to the covariance structure and will introduce correlations

between cases. More simply, each subject has certain undefined characteristics that affect variables such as scoliosis severity or body mass.

The mixed model was chosen because it is able to account for these characteristics and reveal the effects of fixed effects like age, gender, and genotype. The mixed model is able to not only distinguish the relationship between two variables, such as the effect of age on scoliosis severity (main effect of age on primary curve), but also on the interaction of multiple characteristics on the variable in question, such as wildtype mice growing body mass more quickly than FGFR3-/- mice (interaction between age and genotype on body mass). Main effects are considered linear explanatory factors, whereas interaction effects are joint effects different than the component main effects (Yaffee). Despite these advantages, a limitation of the mixed model is that it assumes there is a linear relationship between the independent and dependent variables.

It is also important to note that an initial analysis found no difference in curve severity between male and female mice. Therefore, for all subsequent analyses the two sexes were combined. Of additional note, discussion of the age at which FGFR3-/- mice developed statistically significant scoliosis is based upon independent T-tests performed for each 4-week age bin (0-3.9 weeks = 1 month, 4.0-7.9 weeks = 2 months, etc). For all analyses, significance was considered  $\alpha$ =0.05.

## 2.6.3 Micro CT Comparisons

Because Micro-CT uses data that is based only on one time point, and because FGFR3-/- and wild-type mice were age and gender matched, comparisons could be made using a variant of the student's T-Test. The Mann Whitney U Test is a non-parametric

variant of the Student's T-Test and was chosen because of the relatively low sample size for Micro-CT, with only 17 samples in each group. As in mixed modelling, significance was considered  $\alpha$ =0.05.

#### 3 Results

# 3.1 Cobb Angle

Cobb angle of the primary curve was equal between FGFR3-/- and wildtype during the first month but was significantly greater in FGFR3-/- by 8 weeks (p<0.001) and rapidly progresses by 12 weeks. By 6 months the curve reached 41±17°. Meanwhile, wildtype mice had no change in spine shape (p=0.659) and maintained a straight spine with measured Cobb angle of 5.1±3.4, a value indicative of random observational error (Figure 1) due to positional changes between X-rays. However, between subject variance within FGFR3-/- was high, with a number of mice displaying severe (>80°) and others maintaining minor (<20°) scoliosis (Figure 1). The most severe curve found in the present study reached 105.5° at a young age of 9 weeks. Meanwhile, a 19-week-old mouse was found to have only a 7.0° curve.

Mouse sex had neither main (p=0.280) nor interaction effect (p=0.999) on curve severity, so the sexes were pooled for all subsequent analyses. As expected, average femur length had a significant effect on primary curve severity (p<0.001), as both variables are related to age. However, femur length holds little predictive value for primary curve severity in mutant mice (r=0.336).

Similar to scoliotic Cobb Angle, kyphosis progressed with age in FGFR3-/- from a baseline of 87.0±16.5° to 109.1±11.7° at 6 months (p<0.001), whereas wildtype mice

maintained approximately 80° of thoracolumbar kyphosis (p=0.945) (Table 1). Likewise, thoracic and cervical lordosis increased with age in mutant mice (p=0.005) but not in wildtype mice (0.485). There was an unexpected significant main effect of kyphosis on scoliotic Cobb angle for both genotypes (Wildtype p=0.005; FGFR3-/- p<0.001).

Because the control group was used to monitor observational error and these mice did not have scoliotic curvature at any age, we expected a non-significant relationship between "scoliotic curvature" and kyphosis. Because the control group showed significance, it is invalid to draw any conclusions with regards to a relationship between kyphosis and primary curve severity versus genotype. Future studies should re-evaluate the modified use of the Cobb angle method to measure kyphosis in mice. Figure 2 shows curve progression through serial radiographs in an FGFR3-/- mouse with average curve severity, along with the growth of an age and sex matched wildtype mouse.

As was common in most mice, Figure 2 shows that FGFR3-/- mice initially appear identical to their wildtype counterparts but that developing curvature is visible by 8 weeks (p<0.001) and clearly defined by skeletal maturity at 16 weeks. Wildtype mice maintain straight spines in which the only "curvature" is due to random positional changes between x-rays and not indicative of any underlying changes.

#### 3.2 Anatomical Measurements

Whereas there were no sex differences with regards to curve severity, typical anatomical differences were present. Male mice are consistently heavier than females in both genotypes by approximately 5g. Due to rapid growth and thus high standard deviation at a very young age, this sex difference is significant only if mice 4 weeks and

under are excluded (WT p<0.001, KO p<0.01). Additionally, wildtype mice acquire body mass more quickly (p<0.001), though the genotype main effect is insignificant (Figure 3). This indicates that while the rates of growth are statistically significant, an overall comparison between the body masses of wildtype and FGFR3-/- mice is not significantly different.

As previously identified (Valverde-Franco et al., 2004), by 6 months FGFR3-/-mice have skeletal overgrowth of femurs (KO=1.6832±0.0989cm, WT=1.3209±0.08449cm). FGFR3-/- mice have longer femurs at all ages (p<0.001) (Figure 4), which grow faster (p<0.001), though both genotypes have ceased growth by 5 months. As another measure of endochondral bone growth, the length of lumbar vertebra 1 (L1) is greater in FGFR3-/- mice at all ages (p=0.025). By 6 months, FGFR3-/- L1 vertebrae are noticeably longer (KO=0.3825±0.0261cm, WT=0.3518±0.0204cm). However, potentially due to confounding factors such as lumbar curvature, total lumbar length is no greater in FGFR3-/- mice (p=0.180).

An easily identifying factor of FGFR3-/- mice by gross anatomy is the presence of a kinked tail. In the vast majority of cases a kink was visible, and in all other cases a vertebral column misalignment was easily palpable. In contrast, no wildtype mice displayed any caudal abnormalities.

Body length did not vary by genotype, whether by main effect (p=0.824) or by interaction with age (p=0.210). Additionally, tail length was longer in FGFR3-/- mice (p<0.001) by approximately 2cm and their tails grew faster (p=0.001). Wildtype male mice had longer body lengths than females (p=0.007), though they grew at equal rates

(0.286). On the other hand, between the sexes FGFR3-/- mice had equal body lengths (p=0.649) and body length growth rates (p=0.194).

# 3.3 Micro Computed Tomography

Three-dimensional analysis of vertebral body architecture revealed a number of parameters that indicate poorer bone quality on the convex aspect of the curve (Figure 5). There is less bone (BV/TV, porosity), trabeculae are thinner and less numerous (Trabecular thickness, trabecular separation, trabecular number, Structural Model Index (SMI) (Fields, Eswaran, Jekir, & Keaveny, 2009; Tor Hildebrand & Ruegsegger, 1997)), and have diminished connectivity (as measured by Trabecular Pattern Factor (Hahn, Vogel, Pompesius-Kempa, & Delling, 1992), Fractal Dimension (Chappard et al., 2001), connectivity, and connectivity density) (Table 2A, 2B, 2C).

The concave side of FGFR3-/- curve has normal micro-architectural values, as compared to the symmetry seen in wild type mice. However, the exceptions to this statement are greater fractal dimension, a measure of connectivity, being greater in the concave side of the scoliotic curve, SMI greater in the wild-type mouse, and measures of porosity more severe in the FGFR3-/- mouse (Table 2A, 2B, 2C).

FGFR3-/- mice display vertebral overgrowth where both the concave and convex sides have greater vertebral body height than their wild type counterparts. However, scoliotic curves showed vertebral body and IVD wedging, in that concave vertebral body height and IVD thickness were diminished. The convex aspect of the FGFR3-/- IVD was uncompressed and of equal thickness to the wildtype IVD (Table 2A, 2B, 2C).

#### 3.3.1 Vertebral Rotation

Because of measurement difficulties, as will be expressed later, quantitative data could not be compiled for vertebral rotation. However, rotations greater than 15° from neutral were commonly observed. Furthermore, large degrees of rotation appeared to be more common in mice with very severe scoliosis.

# 3.4 Histology

Micro-CT results of altered microarchitecture and vertebral body/IVD wedging are further supported by histology visualization of mineralization and the IVD using Von Kossa/toluidine blue stain (Figure 6). Mineralization stained black provided a qualitative support for the conclusions drawn from quantitative micro-CT data. Notably, the concave aspect of the curve was more highly mineralized than the convex side. Toluidine blue staining of the IVD allows for the differentiation of nucleus pulposus and annulus fibrosis. The nucleus pulposus has shifted towards the convexity of the curve, further indicating IVD compression.

As was previously described, osteoblast and osteoclast activity were increased in the endplates of FGFR3-/- mice, as represented by ALP and TRAP stains (Valverde-Franco et al., 2004). However, no conclusions could be drawn based on concave/convex asymmetries of ALP and TRAP because if any qualitative difference existed it was too small to detect visually (Figure 7).

#### **Curve Location**

The large proportion of skeletally mature mice, whose curves have been firmly established, had curve apexes in the distal thoracic region (42.6%) while a minority had proximal thoracic (16.3%), thoracolumbar (17.1%) and lumbar apexes (24.0%). The direction of the primary curve in FGFR3-/- mice was equally distributed towards the left and right (p=0.56).

## 4 Discussion

# 4.1 Relationship to Humans

## 4.1.1 Curve Severity

Idiopathic scoliosis in humans is thought to be a multifactorial disease, comprised of a complex interaction of genetic, epigenetic, and environmental factors (Burwell et al., 2011). Whereas a single locus mutation would result in a bimodal distribution of curve severity distinct from the normal population, the complex interaction that exists in idiopathic scoliosis results in decreasing prevalence with increasing severity (N. H. Miller, 1999; Rogala et al., 1978). Because the shape of the prevalence severity curve, scoliosis is defined by an arbitrarily defined cut-off of  $10^{o \text{ (Kane, 1977)}}$  and so there is no average severity of human scoliosis by which to compare FGFR3-/- mice. Rather, the model should be compared to clinically significant severities of scoliosis. Although patient preference and individual functionality are important in clinical and surgical decision making, primary curve Cobb angles of 45-50° can be used as a guideline for consideration of surgical treatment (Maruyama & Takeshita, 2008). FGFR3-/- mice achieved a mean primary curve Cobb angle of  $41\pm17^{o}$  by 6 months (Figure 1), putting the

model in line with human surgical indications. This similarity would allow FGFR3-/mice to act as a model for non-surgical treatment for curves that, under the status quo,
would normally be treated surgically. Therefore, the adequate severity of this model
increases its suitability as a model on which to test non-surgical treatments for scoliosis.

An additional aspect of curve severity similarity is that both humans and FGFR3-/- mice, in extreme cases, develop primary curves in excess of 80°. In humans these are associated with increased morbidity and, in case reports, mortality, particularly due to pulmonary function. Although our study did not investigate functional impairments due to scoliosis, it is important that for surgically managed severities an adequate mouse model can replicate the full range of the disease spectrum.

However, while the variance in curve severity serves as an advantage for its similarity to the human disease, it is important to note that such a high standard deviation complicates its use as a model on which to test non-surgical treatments. An inherently larger standard deviation within the control population, FGFR3-/- mice with no corrective intervention, will require that sample sizes be larger to elucidate a given effect size of a treatment, compared to a narrow curve distribution.

#### 4.1.2 Curve Location

Because the existing literature primarily uses Lenke classification for curve type and location, a system not utilized in this study, it is difficult to compare curve type and location of this model to idiopathic scoliosis in humans. However, there is a predominance of thoracic and thoracolumbar apexes, and are commonly accompanied by

lumbar curves, whether structural or compensatory. This data suggests that curve location of this model is relevant to the human disease.

FGFR3-/- mice curve directions are equally left and right, while human adolescent idiopathic scoliosis favours right convex thoracic curves (Janssen, Kouwenhoven, et al., 2011). Infantile idiopathic scoliosis featured primarily convex left curves and occurred more commonly in boys. Juvenile idiopathic scoliosis is equally prevalent in either direction. Janssen et al. hypothesized that this is due to slight rotation in healthy, non-pathological spines that varies with age. The authors found tendency towards leftward rotation in infants, equal prevalence between the ages of 4 and 9, and tendency towards rightward deviation in adolescents. Therefore, the authors conclude that patterns of scoliosis directionality can be explained by the observed patterns of vertebral rotation that pre-exist at the corresponding age of scoliosis onset (Janssen, Kouwenhoven, et al., 2011). However, the determinants of curve directionality in humans are by no means clearly defined. Likewise, it is unknown what factors determine the directionality of scoliosis in FGFR3-/- mice.

#### 4.1.3 Curve Progression and Relationship to Growth

An advantage of the proposed FGFR3-/- mice model over existing animal models is that it is spontaneous, is non-congenital, and progresses with age. In the same way that children who go on to develop scoliosis cannot initially be differentiated from other children, this model begins with spines phenotypically identical to wildtype mice. By 8 weeks, spinal curvature is statistically significant and visible in the majority of mice (p<0.001). Curvature quickly worsens between 8 and 12 weeks and is associated with a

phase of rapid growth. Although the purpose of the study was not to follow mutant mice well into adulthood, Cobb angle patterns appear to show that curve progression ceases or slows once mice reach skeletal maturity (Figure 1). This timeline suggests that curve progression is related to overall skeletal growth, as measured by femur length (Figure 4). This correlation with the adolescent growth period indicates that FGFR3-/- mice are not a model of congenital or degenerative scoliosis.

## 4.2 Results

#### 4.2.1 Cobb Angle

Scoliosis in FGFR3-/- mice was not present at birth, nor statistically significant at 4 weeks. However, between four and twelve weeks scoliosis rapidly developed and reached a plateau by skeletal maturity and a primary curve Cobb angle of 41±17° by 6 months (Figure 1)(Figure 2). Several characteristics of this progression warrant discussion. As was previously discussed, the absence of spinal curvature at birth and young ages is an important characteristic of similarity to early onset scoliosis and helps differentiate the model from congenital scoliosis. Unfortunately, insufficient mice were followed from birth to skeletal maturity to determine whether there was a relationship between age of onset of scoliosis and severity at skeletal maturity.

Although it was not within the scope of this study to measure the age at which FGFR3-/- mice go through puberty, the phase of rapid progression of spinal curvature between 4 and 12 weeks corresponds to a phase of rapid development, as measured by both femur length (Figure 4) and body mass (Figure 3). Furthermore, the literature suggests that mice begin early puberty at 4 weeks (Callewaert et al., 2010; Zhou et al.,

2007). This correlates well with the human disease, in which adolescent idiopathic scoliosis often presents at or slightly before puberty.

As previously mentioned, there is a high standard deviation of primary curve severity. Although curves from 30-60 degrees are very common, there are also outliers that have curves ranging from 7.0°-105.5°. Given that all mice included in the study have common ancestry, this variability can only be explained by a so-far un-identified mechanism of variable expressivity. Potential explanatory factors include environmental and epigenetic influences. However, if these influences solely modified the FGFR3 mutation, a mutation that we know mediates skeletal development via endochondral bone growth, we would expect similar variance in femur length and vertebral length. Similarly, we would expect a high degree of within-subject correlation between scoliosis severity and endochondral bone growth as indicated by femur length (Figure 4). Because neither of these relationships exist, there must be factors that influence the severity of scoliosis without affecting long bone growth.

An important difference between the proposed model and the human disease is the lack of scoliosis sexual dimorphism in mice, whereas in humans there is a much higher prevalence of scoliosis in females. This is attributable to the unknown aetiology of human scoliosis, while curvature in the proposed model is related to the FGFR3 mutation, which is a mutation not mediated by sexual differences.

The progression of kyphosis and lordosis of both genotypes are represented in Table 1. As expected, thoracolumbar kyphosis increased in mutant mice (p<0.001) but remained unchanged in wildtype mice (p=0.945). Likewise, thoracic and cervical lordosis

increased with age in mutant mice (p=0.005) but not in wildtype mice (p=0.485). Although we cannot conclude whether lordosis was merely compensating for an increase in kyphosis or vice versa, it would be essential for both to increase in tandem for mice to maintain head position and so these results are expected. Table 1 showed kyphosis and lordosis at 2 months (4.0-8.0 weeks) and 6 months (20.0-24.0 weeks). One-month views were not included because it was not possible to obtain consistent lateral views on newborn and young mice due to positioning difficulties. Two and 6 month cross sectional time points were used for ease of representation but do not reflect a statistical comparison. The statistical modelling (mixed model) to determine the relationship between kyphosis or lordosis and age used all mice for all measurement points and accounted for the unbalanced nature of the data.

Because scoliosis in humans often coexists with kyphosis, kyphosis and scoliosis are thought to be etiologically related and interact. Therefore, we would expect a correlation between the severity of kyphosis and scoliosis in mutant mice as both increase with age. Meanwhile, in wildtype mice we would expect no correlation, as kyphosis is maintained throughout the mouse's lifespan at approximately 80° and "scoliotic Cobb angle" simply indicates measurement error, as the true value should be approximately 0°. Strangely, there is a significant main effect of kyphosis on primary curve for both wildtype (p=0.005) and mutant mice (p<0.001). This cannot be explained and is probably due to a statistical modeling error or systematic error in kyphosis measurement. Because both the control group and mutant group show a significant relationship between kyphosis and primary curve severity (indicating a methodological flaw), we cannot comment on the significance of any correlation or relationship between scoliosis and

kyphosis aetiologies. Future studies should re-evaluate the use of the modified Cobb angle method to measure kyphosis in mice.

#### 4.2.2 Anatomical Measurements

Body mass was greater in males of both genotypes by approximately 5 grams and was expected as normal sexual dimorphism (Figure 3). Wildtype mice acquired body mass more quickly than mutant mice, though when compared as a whole there was no significant difference between wildtype and FGFR3-/- body mass. It is unclear whether the growth rate difference is due to an intrinsic effect of FGFR3 or a functional impairment that inhibits feeding.

Body length had no relationship to genotype (p=0.824) or by genotype age interaction (p=0.210). Given that the individual vertebra L1 is longer in mutant mice (p=0.025), it is interesting that the genotype main effect was insignificant. Vertebrae were expected to be longer in FGFR3-/- mice because, like long bones, vertebrae are formed by endochondral ossification. The non-significant body length difference is probably due to a combination of thoracolumbar kyphosis and cervicothoracic lordosis, and large inter-subject differences. However, tail length was longer in FGFR3-/- mice (p<0.001) by approximately 2cm and their tails grew faster (p=0.001). This finding is despite the practice used at the beginning of the study of removing the tips of tails for genotyping, prior to the use of kinked tails for the same purpose. The tips of tails were sampled for genotyping of mice, prior to the realization that FGFR3+/+ and +/- mice have the same phenotype and that the presence of a kinked tail is a sensitive and specific identifier of FGFR3-/- mutation. Wildtype male mice had longer body lengths than

females (p=0.007), though they grew at equal rates (p=0.286). On the other hand, by sex comparison FGFR3-/- mice had equal body lengths (p=0.649) and body length growth rates (p=0.194). Probably neither of these relationships are relevant, except that sexual dimorphism of skeletal size is more pronounced in wildtype mice.

Mutant mice have a ubiquitous kink in the tail. In the vast majority of cases, this kink is present from a very young age and is visible. In the remaining few cases, the kink is easily palpable. There were no kinks in any wildtype tails. Although no histology, CT, or radiographic measurements were performed on the kinks, we suspect that both the kinks and scoliosis progress by the same mechanism of irregularity in the vertebral growth plates. Deformity in the tail may be more distinct than deformities in the thoracic and lumbar spine due to the relative absence of stabilizing musculature. Because visual or palpable tail kinks are specific to FGFR3-/- mice, they act as a useful proxy in the place of genotyping when separating mutant and wildtype mice for study.

## 4.2.3 Micro Computed Tomography

Although the link between the FGFR3 mutation and the resultant scoliosis is unknown, a component of its progression is thought to be altered biomechanics leading to differential growth of the concave and convex aspects of the vertebrae. The Hueter-Volkmann law of differential growth states that compression of a bone limits growth, while tension promotes growth. In this manner, compression of the concave side inhibits growth, which leads to a positive feedback loop of curve progression (Aronsson, Stokes, & McBride, 2010; Stokes, Burwell, & Dangerfield, 2006). The hypothesis of altered biomechanics is supported by Micro-CT analysis of vertebral micro-architecture that

reveals poor bone quality in the convex aspect of the curve (Table 2A, B, C) (Figure 5) (Figure 6). In accordance with Wolff's law, this suggests that asymmetric force distribution causes a similar asymmetry in the trabecular structures required to bear these forces, just as is seen in human cases of idiopathic scoliosis (Adam & Askin, 2009; Shea et al., 2004), and chicken (Fu et al., 2011) and porcine (Laffosse et al., 2010) tethered animal models. Additionally, there is a trend towards improved bone micro-architecture in the concave side compared to control mice. A trend, rather than significance, may exist because of the known osteomalacic phenotype of FGFR3-/- (Valverde-Franco et al., 2004), partially compensating for biomechanically induced concave bone formation.

In the literature, additional modalities have been used to support the theory of asymmetric loading leading to skeletal architectural changes. Modic changes are pathological changes in the vertebral body, endplates, and intervertebral discs. In an analysis of magnetic resonance imaging, patients with degenerative lumbar scoliosis have a higher incidence (60%) of Modic changes than patients with lumbar degeneration alone (23%) (Wu et al., 2012). These changes occur asymmetrically and are most pronounced at the apex, with signs of trabecular changes and microfracture more common on the concave side (Wu et al., 2012).

#### 4.3 Potential Mechanisms

Although the initiating factors for adolescent idiopathic scoliosis and that of the FGFR3-/- model proposed in this paper are currently unknown, evidence suggests that both progress by a biomechanical feedback mechanism described above. Asymmetrical forces may cause micro architectural compensation in which bone quality adapts to the

increased forces placed upon the concave side and resorbs convex trabeculae following its unloading. The Hueter-Volkmann law of differential growth, stating that compression of a growth plate slows longitudinal growth while tension promotes growth, is a pervasive phenomenon in orthopaedics and is thought to be the driving biomechanical mechanism behind idiopathic scoliosis. Its implications range from epiphysiodesis of long bones, repeated physeal compression causing premature closure in young athletes, progression of skeletal dysplasias, and the correction of which forms the basis for bracing correction of scoliosis. In both human and FGFR3-/- scoliosis, an initiating irregularity could trigger a cascade in which unilateral growth plate compression leads to further vertebral body dysplasia and so on.

Biomechanical feedback may not be limited to the vertebral bodies. Our histology demonstrating concave compression of the intervertebral discs resemble their human counterparts. In humans the concave side of scoliotic intervertebral discs features proteolytic degradation of chondroadherin: a protein that may provide a mechanism for regulation of extracellular matrix and cell metabolism within the intervertebral disc. Degradation by aggrecanase and metalloproteinases induced by biomechanical changes may provide a pathological basis for intervertebral disc degeneration in scoliosis (Haglund, Ouellet, & Roughley, 2009).

Given the known growth plate abnormalities of the FGFR3-/- genotype, one may speculate that the initiating factor for its scoliosis arises from abnormalities or intrinsic asymmetries in newborn FGFR3-/- vertebral growth plates. Unusual growth factor signaling stemming from an inactivated FGFR3 leads to dysregulation of chondrocyte

Although it is also possible that widened, weak physes make vertebrae especially susceptible to asymmetry in muscular tone that precipitates a biomechanical cascade, the presence of other skeletal dysplasias and asymmetries suggest a problem intrinsic to the growth plate. Notably, kinked tails are not weight bearing or subject to considerable muscular tone so must be caused by growth plate dysregulation or another feature of the FGFR3-/- phenotype, such as their neurological abnormalities.

#### 4.4 Limitations of Model

A limitation of the study is that the aetiology of scoliosis in FGFR3-/- mice is currently unknown. Additionally, although human FGFR3-/- exist in the form of CATSHL syndrome (Toydemir et al., 2006), this mutation is not a characteristic of idiopathic scoliosis. Therefore, because the mechanism of development in both FGFR3-/-mice and idiopathic scoliosis are unknown, it is likely that they are initiated by different mechanisms. Because of the different aetiology, for this model to be used as a basis for testing drug and biologic therapies the therapy must target the scoliosis deformity itself rather than direct involvement of FGFR3-/-. That FGFR3 has been extensively researched is important when developing a treatment for scoliosis using the FGFR3-/-model. If the therapy's mechanism of action is known to not involve FGFR3, it is more likely to be efficacious in human scoliosis.

Methodological limitations of the study include inadequate measurement of newborn mice, and the lack of quantitative histomorphometry to examine osteoblast and osteoclast activity, and provide insight into the scoliosis aetiology. Additionally, the significant 3-dimensional component of kyphoscoliosis handicaps 2-dimensional plain radiography with measurement error. For example, a femur length captured at an oblique angle will always underestimate its true length.

Finally, humans are unique in the animal kingdom in that they are the only truly bipedal mammals. Therefore, mice, along with all other quadrupeds, have necessarily different ambulation and spinal biomechanics, and may affect scoliosis progression.

Although this aspect is important to take into consideration when assessing the validity of the model, it is important to note that micro-CT and gross features indicate that FGFR3-/- and human scoliotic spines have similar biomechanics. Therefore, the quadruped nature of a model should not impair its usefulness.

An important difference between the proposed model and the human disease is the lack of scoliosis sexual dimorphism in mice, whereas in humans there is a much higher prevalence of scoliosis in females. Although FGFR3-/- mice are different from humans in this respect, this difference should not interfere with the validity of the mouse model. Human scoliosis has a so-far unknown sex related factor that modifies scoliosis, whereas mice do not have this sexual dimorphism and mouse sex can be ignored.

## 4.5 Comparison to Other Models

## 4.5.1 Kyphoscoliosis

The kyphoscoliosis (ky/ky) genotype is the only mammalian animal model, other than the proposed FGFR3-/- mice, that exhibits a spontaneously developing scoliosis. However, the curve progresses via neuromuscular abnormalities, involving the necrosis and atrophy of skeletal muscle with the complete shift towards type-1 muscle fibres

expressing exclusively MHC1. Although the authors suggest that the model can be used to study the neuromuscular and skeletal mechanisms by which adolescent idiopathic scoliosis progresses, they recognize that a similar muscle dysfunction does not occur in humans. Intervertebral discs of ky/ky mice do show degeneration and collapse of the nucleus pulposus. As well, there is degradation of the endplate cartilages, manifesting as cavitation and cell loss. Human idiopathic scoliosis IVDs contain calcification and display degeneration, including loss of cell viability, and proteoglycan and water loss (Hristova et al., 2011)

## 4.5.2 Melatonin Deficiency

The abundance of pinealectomized and melatonin deficient bipedal animals displaying scoliosis suggests that melatonin plays a role in normal spine development in these animals and that its absence is pathological. However, its role in humans is elusive and is unlikely to play a role in the development of human idiopathic scoliosis. This notion is supported by the observation that the incidence of scoliosis is not higher in children with pineal lesions (Day et al., 2007). Additionally, pinealectomy failed to produce scoliosis in rhesus monkeys, suggesting that melatonin may not play an aetiological factor in the development of scoliosis in primates (Cheung et al., 2005).

Like melatonin deficiency based models, FGFR3 is unlikely to play a role in the pathogenesis of human idiopathic scoliosis. Rather, the advantage of FGFR3-/- mice over the melatonin deficiency models is its ease of production in the research environment. Besides pinealectomized chickens, animals that contain spinous synovial joints rather than intervertebral discs, melatonin deficient animals must be made bipedal by removing

forelimbs and tails prior to developing scoliosis. This complicates the models by requiring surgical time and expertise, anaesthesia, and potentially lengthening the research ethics committee process. Pinealectomy in Sprague-Dawley rats (Masafumi Machida et al., 1999) and C3H/HeJ mice (Oyama et al., 2006) further require surgical time and expertise, anaesthesia, and ethics approval, though pinealectomy is not required in C57BL/6J mice (Oyama et al., 2006). An additional benefit of FGFR3-/- mice over melatonin deficient counterparts is that much is known about the FGFR3 pathway, whereas little is known about melatonin's involvement in skeletal growth and development, nor why melatonin deficiency leads to scoliosis in these models but not primates.

Furthermore, melatonin deficiency based models produce inconsistent incidence of scoliosis, often with curves less severe than in FGFR3-/- mice and human idiopathic scoliosis. The incidence of scoliosis in Sprague-Dawley was not reported in either of Machida et al's nearly identical studies (Masafumi Machida et al., 1999; M. Machida et al., 2005) but severity is reported to have reached 37.5°± 6.5°. The group states "The deformities, with the long thoracic curve, were similar to those found in human idiopathic scoliosis, particularly vertebral rotation and rib humps". While vertebral rotation and rib humps bear similarity to scoliosis, the both the descriptor of "long thoracic curve" and radiography figure highlighted in their 1999 paper (Masafumi Machida et al., 1999) are dissimilar to human idiopathic scoliosis and do not display the variety of curves in the Lenke Classification (Lenke et al., 2001).

## 4.5.3 Surgically Induced

### 4.5.3.1 Surgical Tethering

Unilateral vertebral tethering in early development produces a scoliosis like spinal deformity in a number of large animal models, including calves (Newton, Farnsworth, et al., 2008; Newton et al., 2005; Newton et al., 2002), pigs (Accadbled et al., 2011; Laffosse et al., 2010; Newton, Upasani, et al., 2008; A. Patel et al., 2011; A. Patel, Schwab, Lafage, Obeidat, & Farcy, 2010; Ashish Patel et al., 2009; Schwab et al., 2009) and goats (Braun & Akyuz, 2005; Braun, Hines, et al., 2006; Braun, Hoffman, et al., 2006; Braun, Ogilvie, et al., 2006; Braun et al., 2003; Y.-G. Zhang, G.-Q. Zheng, X.-S. Zhang, & Y. Wang, 2009)

In goats, sublaminar hooks with hemilaminectomy produces scoliotic curves that progressed from an initial post-operative severity of 42° to a maximal Cobb angle of 60° over 6 to 15 weeks. The incidence of scoliosis in surviving goats was 82%, however, 17% of goats died as a result of the procedure. Histologic analysis showed disc wedging, and trabecular and cortical thickening of the concave side (Braun et al., 2003). This data is consistent with FGFR3-/- mice and human literature (Adam & Askin, 2009; Shea et al., 2004). Given that this goat model has a purely biomechanical aetiology, these characteristics likewise must be due to biomechanical factors in animal models and humans. A similar method in calves tethering vertebral body screws over a single intervertebral disc produced a minimally severe curve while tethers spanning T6-T9 produced a more severe scoliosis (Newton et al., 2005; Newton et al., 2002).

A similar surgery was performed in pigs using a staple-screw construct connected with a polyethylene tether between T8 and T11 on 7-month-old pigs (Newton, Upasani, et al., 2008). The surgery produced a moderately progressive coronal deformity of 14°±4 by 6 months and 30°±13 by 12 months. Strangely, the height of the tethered side of the vertebral body was greater than the untethered side, and similarly the nucleus pulposus had shifted towards the site of tethering. Neither of these results reflects the human disease, nor are they consistent with other animal models. Other similar experiments produced more severe curves with vertebral rotation (Accadbled et al., 2011; Laffosse et al., 2010; Schwab et al., 2009).

A micro-CT analysis of one porcine surgical tethering model (Laffosse et al., 2010) indicated improved bone quality on the concave side. This micro-CT analysis and another performed on chickens (Fu et al., 2011), to our knowledge the only two micro-CT studies on animal models of scoliosis, help verify the results obtained in FGFR3-/-mice. However, the measurements reported in these two papers were not as extensive as those performed in the present research. The improved bone quality of the concave side suggests that the vertebral body micro-architecture is adapting to the external forces placed upon it by the surgical tethering. That these results are consistent throughout pigs (Laffosse et al., 2010), chickens (Fu et al., 2011), FGFR3-/- mice and humans (Shea et al., 2004) suggest that micro-architecture remodeling is consistent with Wolff's law and secondary to the altered biomechanics of scoliosis.

Rabbits have long been used as models for surgically induced scoliosis (Somerville, 1952). Similar to what was later done in large animal models, silk string was

used to tether the spinous and transverse processes of rabbits in an attempt to reproduce asymmetric paraspinal muscle tone. However, the authors noted that every rabbit developed C shaped curvature with no compensatory curve (Carpintero et al., 1997). As in other models (Masafumi Machida et al., 1999; M. Machida et al., 2005), this variety of spinal curve is not representative of the human disease. Smith & Dickson produced a severe scoliosis (>100°) by tethering the thoracic spine into asymmetric lordosis with localized spinal cord damage using tethering and an electric soldering iron, respectively (Smith & Dickson, 1987). 6/18 animals died shortly post-operatively and 4 of the surviving rabbits died from respiratory failure. Histology revealed that cauterization caused local spinal cord damage and added a paralytic component to the instability of lordosis. Local spinal cord damage does not occur in human scoliosis, while the high mortality rate makes this method unusable as a consistent animal model.

Kallemeier et al. tethered rabbits scapulae to the contralateral pelvis. This produced a moderately severe scoliosis (mean 59°), with control animals becoming untethered via spontaneous release. However, like the other rabbit models, mortality was high with only 11/17 rabbits surviving throughout the study (Kallemeier et al., 2006).

## 4.5.3.2 Epiphysiodesis

Epiphysiodesis through the pedicles into the neurocentral cartilage towards the anterior portion of the vertebral bodies was used to produce scoliosis in pigs (Beguiristain et al., 1980; Coillard et al., 1999; Zhang & Sucato, 2008, 2011). This produced scoliosis varying between 10° 5 months post-operatively to 80° at 12 months post-operatively. Curvature included rotation and wedging, with convexity on the side of the screw fixation.

However, the authors admitted that neurocentral cartilage usually appeared prior to the usual onset of adolescent idiopathic scoliosis and that its role in the human disease is controversial. Additionally, they find the mechanism of production of this scoliosis to be difficult to explain, especially because the convexity lies on the operated side (Beguiristain et al., 1980). Cil et al. found that a sham operation that violated the neurocentral cartilage but did not compress it caused the same growth disturbances as a pedicle screw (Cil et al., 2005), raising a question to the cause of scoliosis in previous studies and whether appropriate controls were used.

Surgically induced scoliosis holds a variety of disadvantages compared to FGFR3-/- mice as models for non-surgical treatment of scoliosis, including their ease of use in the research environment and validity of comparison to the human disease. Although some surgeries produced low mortality, other studies in goats and rabbits (Braun et al., 2003; Smith & Dickson, 1987) had a high mortality rate. Because the death was unintended and presumably painful, animal ethics approval for these surgeries would be exceedingly difficult. High mortality increases the cost of the study and potentially biases the results if death is concentrated in a certain type or severity of scoliosis.

Large animal models such as goats, pigs and calves have the practical disadvantage of slow growth and large size; both of these factors increase the cost and accessibility. Large animals are more difficult to keep in a controlled environment and require more space than can often be provided in healthcare research settings at academic centres. This combination of factors usually necessitates a smaller sample size. Because large animal models with surgically induced scoliosis have standard deviations as equally

high as FGFR3-/- mice or any of the small animal models previously discussed, small sample size may not provide enough statistical power to reject the null. Especially in initial phases of development, non-surgical treatments are likely to have small or variable effect sizes so would require considerable statistical power.

Surgery on large animal models requires surgical time, expertise, and anaesthesia. Anaesthetic itself can add hundreds of dollars to the cost of a human surgery and would be similar when performing an extensive spine surgery on a large animal. Although these studies reported how long the surgery took to perform or whether an orthopaedic surgeon performed the surgery, the inconvenience of time and expertise is greater than in a model with spontaneously occurring scoliosis. Each of the complicating factors of large animal models would be acceptable if the intention were to develop new surgical techniques for treating scoliosis, as surgical techniques would be nearly impossible on rodents. However, because the intention of the current line of research is to develop non-surgical or fusionless correction, these disadvantages are unnecessary.

Even though no animal model will be able to perfectly replicate human idiopathic scoliosis in terms of aetiology, it is important that the spinal deformity resembles those seen in humans. Long C shaped curves with no compensatory curve in rabbits are dissimilar to humans and should be met with scepticism as an animal model of human scoliosis (Carpintero et al., 1997). Some models showed structural abnormalities that could not be explained biomechanically, such as nucleus pulposus migration towards the concavity of a curve and vertebral body height being greater in the concavity (Newton, Upasani, et al., 2008). These models should be re-evaluated prior to any comparison to

the human disease. Other surgically induced models had well documented curve patterns that appeared similar to human idiopathic scoliosis (Laffosse et al., 2010).

Regardless of the structural similarity to the human disease, scoliosis produced by tethering, paraspinal ablation, or epiphysiodesis are unlikely to bear resemblance to the pathogenesis of human idiopathic scoliosis. For example, the involvement of paraspinal muscles with asymmetrical biomechanics of spinal soft tissues may have secondary involvement, if any, rather than primary involvement in human scoliosis. Authors also admitted that the involvement of neurocentral cartilage is controversial in human scoliosis (Beguiristain et al., 1980).

Surgery is generally performed in young animals to maximize deformity with growth but human idiopathic scoliosis most often occurs before or during puberty. A more valid animal would show a temporal relationship to the pubertal growth period. As well, like other animal models, epiphysiodesis has unknown relevance to human scoliosis due to the likely different pathophysiology.

## 4.6 Methodological Difficulties

Critical analysis of this paper's methods is important for subsequent research in the field. In terms of study design, insufficient mice were followed from birth, both from study design error and because of difficulty in anaesthetizing safely and X-ray positioning difficulty in young mice. The acepromazine/xylazine/ketamine cocktail was delivered into the peritoneal space and was difficult in young mice. Even if sufficiently and safely anaesthetized, young mice did not have adequate body mass to be reliably laid prone. Ideally, mice followed from birth would form a cohort with uniformly distributed

measurement dates until an endpoint at 6 months (such as monthly). The non-uniform X-ray dates increased the difficulty of statistical analysis and interpretation. This also led to the paucity of easily interpretable figures tracking genotype characteristics such as curve severity or femur length versus time.

Mice have a natural thoracolumbar kyphosis, a characteristic amplified in the FGFR3-/- mutation. Given that this study measured three-dimensional characteristics using a two-dimensional x-ray, mid-thoracic vertebrae were superimposed upon one another. This obstructed bony structures used for measurement and masked spinal orientation. This makes measuring curve severity and pinpointing curvature apex more imprecise. The same difficulty applied to measuring vertebral rotation along the length of the spinal column. Within the CT manipulation and analysis software, Dataviewer and CTAn, respectively, the axial, sagittal, and coronal planes must be defined and dataset saved into a series of axial images. However, the 3D nature of the spine, with both the scoliosis and natural thoracolumbar kyphosis, makes it impossible to define planes that are anatomically consistent for every vertebra. For example, if T1 is taken to be the neutral vertebra (index vertebra), every other vertebra is necessarily oblique to T1. Because T1 was defined as neutral for the axial dataset, subsequent axial images may be oblique or even coronal to the anatomical orientation of the vertebra. It was common for vertebrae to be rotated up to 90 degrees in the sagittal plane with respect to one another.

This characteristic made it impossible to measure vertebral rotation using the conventional methods. Even when using CT to measure rotation in humans, spines with

less kyphosis and lordosis than mice, previous literature noted the difficulty and problems associated with vertebral tilt.(Lam, Hill, Le, Raso, & Lou, 2008)

Histology was performed on un-decalcified sections. Despite standard protocols, vertebral body growth plates were softer than the surrounding bone so tended to compress and wrinkle during sectioning. Consistently high quality sections that included the growth plates would have improved alkaline phosphatase (ALP) and tartrate resistant acid phosphatase (TRAP), staining for osteoblast and osteoclast activity, respectively. More definitive results regarding osteoblast and osteoclast activity would provide better insight into the cellular responses to altered biomechanics in scoliosis and are an important correlate to micro-CT data. Improved histology sectioning, along with greater sample size and histomorphometry may have made it possible to reveal asymmetry in osteoblast and osteoclast activity, and thus insight into the aetiology of FGFR3-/-scoliosis.

#### 4.7 Future Directions

This mouse model of early onset scoliosis may be a platform on which to design treatments for the human disease. However, potential treatments should target the biomechanical processes in scoliosis development, rather than gene therapy for the FGFR3-/- defect. Compression of the intervertebral disc and vertebral body, which necessarily occur in the concave side of a scoliotic curve, causes up-regulation of tumor necrosis factor- $\alpha$  (TNF- $\alpha$ ). TNF- $\alpha$  is a pro-apoptotic signalling molecule that induces apoptosis via the mitochondrial pathway. It is possible that TNF- $\alpha$  induced by concave compression mediates cell death in response to the biomechanical forces described in

Wolff's Law and the Hueter-Volkmann laws. Therefore, we hypothesize that the inhibition of TNF- $\alpha$  mediated apoptosis may prevent curve progression in scoliosis.

As previously discussed, parathyroid hormone related protein (PTHrP) is a multifunctional cytokine that is expressed in fetal and adult tissues to help regulate cell proliferation, differentiation, and apoptosis (L. Okoumassoun et al., 2007). In vitro studies have shown that PTHrP 87-107, the nuclear targeting sequence (NTS), inhibits TNF-α induced apoptosis through a variety of related mechanisms. In vitro studies have shown that PTHrP 87-107 promotes events that maintain mitochondrial membrane integrity (internal pathway of apoptosis). PTHrP inhibited pro-apoptotic proteins and increased the anti-apoptotic protein Bcl-2 (L. Okoumassoun et al., 2007). Therefore, PTHrP protected cells from in vitro TNF-α induced apoptosis by regulating the trafficking of pro-apoptotic proteins to the mitochondria and maintaining mitochondrial membrane integrity. As well, PTHrP partially inhibited the activation of the caspase cascade of proteolytic enzymes and apoptosis (extrinsic pathway of apoptosis). However, this inhibition may not be unique to the NTS sequence but rather on a sequence external to NTS (L. Okoumassoun et al., 2007). A further supporting experiment showed that cells from mice deficient in PTHrP (PTHrP -/- and PTHrP +/-) had decreased survival compared to PTHrP sufficient cells, with accompanying upregulation of the caspase cascade (extrinsic pathway), and increased pro-apoptotic proteins and decreased amounts of the anti-apoptotic protein Bcl-2 (intrinsic, mitochondrial pathway of apoptosis) (L. Okoumassoun et al., 2007). An additional previous experiment showed that PTHrP NTS protected chondrogenic cells from apoptosis by promoting cell quiescence in a hostile cellular environment. Previous experiments suggest that protection of chondrogenic cells

from apoptosis is mediated by PTHrP 87-107 to promote cell quiescence in an unfavourable environment (Aarts et al., 2001). Taken together, these in vitro results suggest that PTHrP, in particular the NTS 87-107, is an effective inhibitor of TNF- $\alpha$  induced apoptosis. We hypothesize that application of exogenous PTHrP to the scoliotic spines of FGFR3-/- mice will prevent the progression of scoliosis.

We designed an experiment to appraise PTHrP (NTS) as a non-operative therapy to limit curve progression in FGFR3-/- scoliosis. Fifty FGFR3-/- mice will be radiographed posterior-anterior at 8 weeks, the approximate age of initial scoliosis development, to determine the location and baseline severity of scoliosis. A 3mm pellet containing 0.5mg of PTHrP (NTS) or placebo will be inserted subcutaneously at the level of the scoliotic apical vertebra. The pellet will release PTHrP with zero-order kinetics for 60 days. After the course of release, the mouse will have reached skeletal maturity and accurately depicts the time frame during which human therapy would be initiated. Curve status will be monitored bi-weekly using plain radiography and spines harvested for micro-CT and histological evaluation at euthanization. Histologic evaluation will be based on the methods previously described in this thesis; however, five spines of each group will be embedded in paraffin to identify apoptosis using terminal deoxynucleotidyltransferase (TdT)-mediated deoxy-UTP nick end labelling (TUNEL) assay. Statistical analysis will use two-way ANOVA with repeated measures to compare the treatment and placebo groups at each bi-weekly x-ray and independent T-test for micro-CT and histologic comparison. We hypothesize that administration of the antiapoptotic agent PTHrP will reduce curve progression, reduce microarchitectural asymmetry of the apical vertebra, reduce apoptosis, and limit histologic asymmetry of

vertebral mineralization, osteoblast and osteoclast activity. These results would indicate that PTHrP (NTS) is able to reduce apoptosis induced by biomechanical asymmetry and therefore be a candidate for non-surgical treatment of human early onset scoliosis.

#### 5 Conclusion

FGFR3-/- mice developed a high incidence of scoliosis prior to skeletal maturity and comparable in severity and shape to those seen in humans. Plain radiography, histology, and micro-CT demonstrated that the model bears considerable resemblance to the human disease in terms of curve appearance, severity, disc and microarchitectural adaptations. Although variable in location and severity, mice developed curves of 41±17° by 6 months, most often in thoracic or thoracolumbar locations. In humans these curve severities may warrant surgical correction. Therefore, this model is of sufficient severity to test therapies in curves that would normally be treated surgically. Micro-CT demonstrated improved trabecular quality in the concave side of apical vertebrae, resorption of convex vertebral body trabeculae, and asymmetrical vertebral body heights. These results are adherent to the Wolff and Hueter-Volkmann laws that govern a bone's growth in response to biomechanical forces, with bone quality and growth plates modified, respectively.

Given that human scoliosis is not caused by an FGFR3 mutation, non-surgical treatments tested on FGFR3-/- mice should target cellular responses to biomechanical stimuli and pathways not directly involving FGFR3. The model has the additional advantage that, unlike melatonin, FGFR3's role in skeletal growth and development has

been extensively researched so is easier to avoid targeting the FGFR3 mutation in a novel therapy.

Spontaneously occurring scoliosis is more clinically relevant than the surgically induced scoliosis produced in large and small animal models. Additionally, FGFR3-/-mice do not require the surgical time and expertise necessary to generate curvature, an asset that makes the model more economically feasible in the research environment. FGFR3-/- mice are an improved animal model of early onset scoliosis that is inexpensive, easily available, is not produced by invasive methods, and closely reproduces the human disease. Therefore, FGFR3-/- mice should be used for future development of non-surgical treatments of scoliosis.

# **6** Tables and Figures

	Kyphosis (Degrees)		Lordosis	(Degrees)
Months	2	6	2	6
FGFR3-/-	91.1±17.2	109.1±11.7*	53.7±16.6	70.8±11.8
Wildtype	82.9±9.5	78.5±10.2	45.3±3.6	56.4±6.8

Table 1. Progression of kyphosis and lordosis

Note: Statistics were calculated using mixed modeling, rather than a paired T-test.

FGFR3-/- kyphosis (p<0.001) Wildtype kyphosis (p=0.945)

	Wildtype			
Measure	Concave (mean)	Standard Deviation	Convex (mean)	Standard Deviation
Bone Volume Fraction	15.219	3.409	15.315	3.001
Trabecular Thickness	0.062	0.007	0.062	0.007
Trabecular Separation	0.237	0.039	0.249	0.027
Trabecular Number	2.443	0.467	2.462	0.344
Trabecular Pattern	16.043	2.390	16.408	2.459
Factor Structural Model Index	1.755	0.155	1.781	0.129
Degree of Anisotropy	8.936	9.860	14.165	17.359
Fractal Dimension	2.051	0.047	2.039	0.051
Total Volumetric	0.278	0.125	0.279	0.128
Porosity Total Porosity	84.781	3.409	84.685	3.001
Euler Number	-23.412	16.685	-23.824	18.541
Connectivity	37.118	21.980	38.235	23.682
Connectivity Density	111.456	40.962	112.832	33.248
Vertebral Height	2.064	0.745	2.058	0.762
IVD Thickness	0.290	0.079	0.291	0.080

Table 2A. Micro-CT analysis of wildtype vertebrae corresponding to age and sex matched FGFR3-/- mice.

	FGFR3-/-				
Measure	Concave (mean)	Standard Deviation	Convex (mean)	Standard Deviation	
Bone Volume Fraction	17.107	5.016	11.728	4.736	
Trabecular Thickness	0.062	0.006	0.058	0.005	
Trabecular Separation	0.226	0.053	0.279	0.068	
Trabecular Number	2.711	0.677	1.987	0.697	
Trabecular Pattern Factor	13.447	5.560	18.322	5.203	
Structural Model Index	1.509	0.324	1.782	0.261	
Degree of Anisotropy	18.503	17.787	24.662	36.376	
Fractal Dimension	2.109	0.086	2.009	0.105	
Total Volumetric	0.314	0.080	0.331	0.074	
Porosity Total Porosity	82.893	5.016	88.272	4.736	
Euler Number	-31.824	17.597	-18.235	17.437	
Connectivity	48.824	17.008	32.529	19.587	
Connectivity Density	128.345	36.187	84.938	44.799	
Vertebral Height	2.340	0.487	2.467	0.525	
IVD Thickness	0.232	0.076	0.260	0.069	

Table 2B. Micro-CT analysis of apical vertebrae in FGFR3-/- mice.

	Concave Convex Comparison (a)		Wildtype/FGFR3-/- Comparison (b)	
Measure	Wildtype	FGFR3-/-	Concave	Convex
Bone Volume Fraction	0.946	0.005*	0.131	0.016*
Trabecular Thickness	0.973	0.029*	0.946	0.099
Trabecular Separation	0.306	0.016*	0.160	0.274
Trabecular Number	0.586	0.004*	0.106	0.018*
Trabecular Pattern Factor	0.658	0.024*	0.085	0.399
Structural Model Index	0.496	0.016*	0.024*	0.760
Degree of Anisotropy	0.322	0.734	0.005*	0.079
Fractal Dimension	0.658	0.005*	0.041*	0.496
Total Volumetric Porosity	0.973	0.245	0.014*	0.009*
Total Porosity	0.946	0.005*	0.131	0.016*
Euler Number	1.000	0.045*	0.131	0.586
Connectivity	0.786	0.012*	0.057	0.610
Connectivity Density	0.865	0.005*	0.231	0.038*
Vertebral Height	0.865	0.375	0.013*	0.004*
IVD Thickness	0.533	0.026*	0.011*	0.179

<sup>(</sup>a) Related samples wilcoxon signed ranks test

Table 2C. Comparison of micro-CT analyses in wildtype (Table 2A) and FGFR3-/-(Table 2B) mice.

<sup>(</sup>b) Independent samples Mann-Whitney U Test \* indicates p<0.05

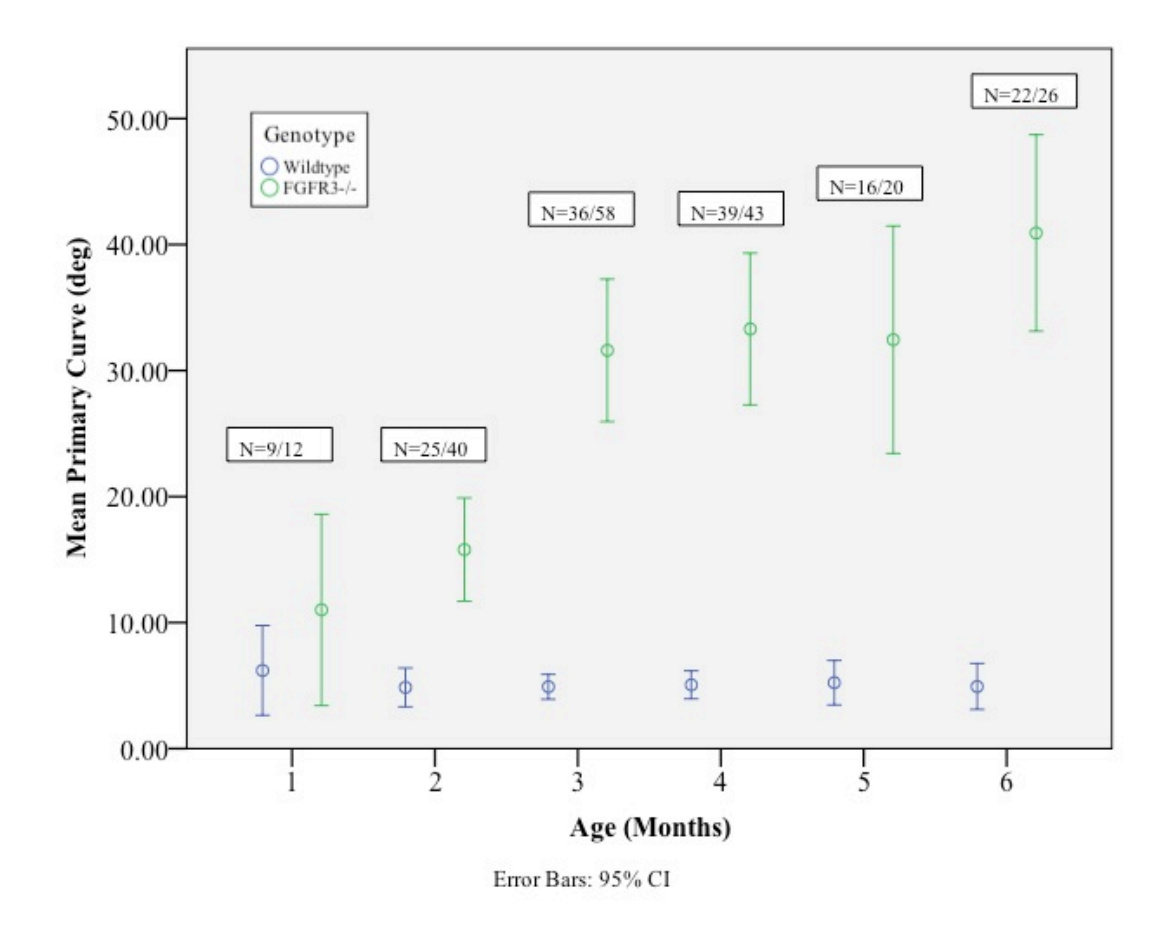


Figure 1. Curve progression with age Cobb angles are equal at 1 month, are different by 2 months, and reach an average severity of 41° by 6 months. (N=WT/KO)

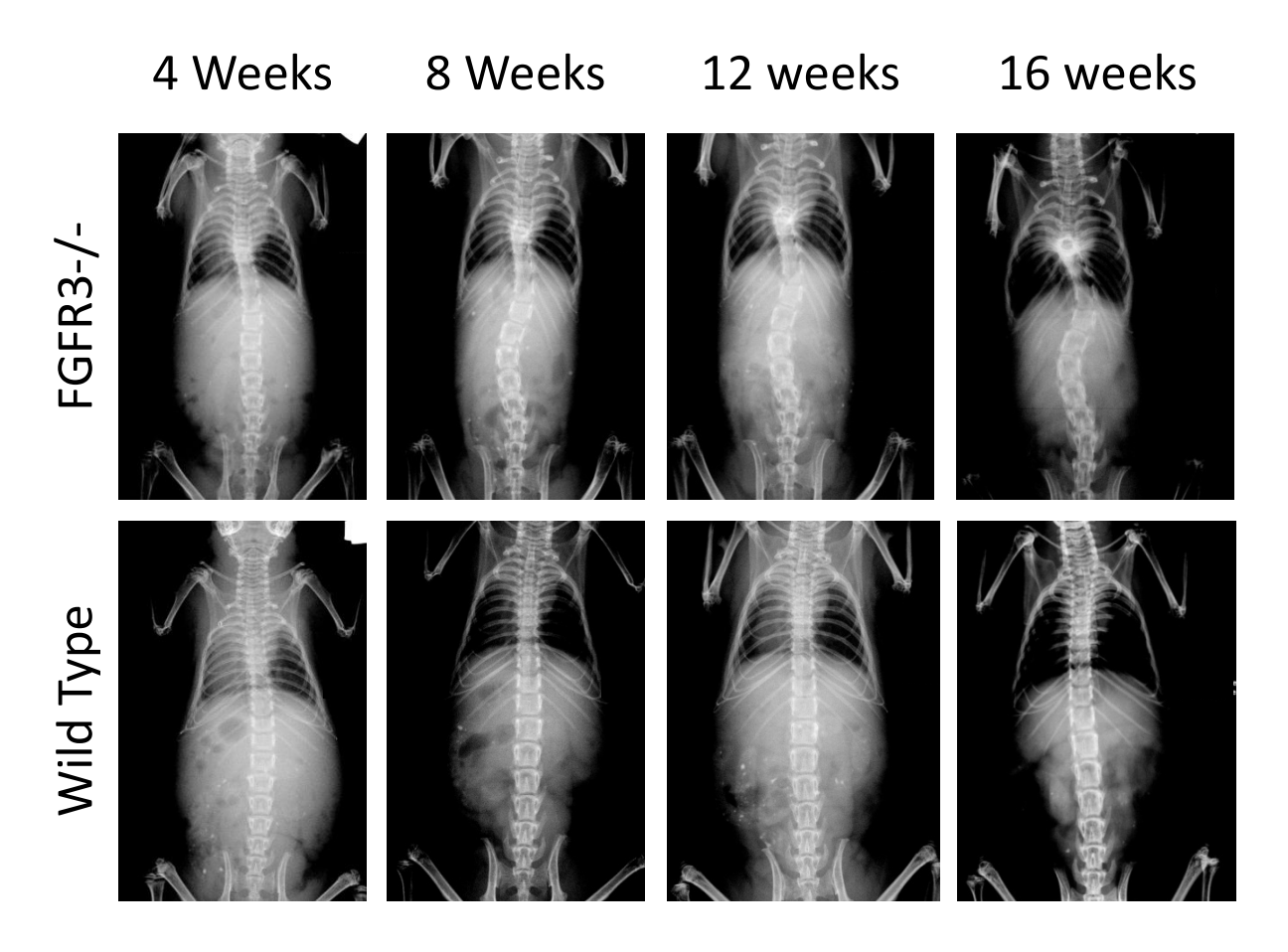


Figure 2. Serial radiographs of FGFR3-/- and Wildtype mice, showing the FGFR3-/- curve progression from an equal baseline to a thoracolumbar curve of 41°.

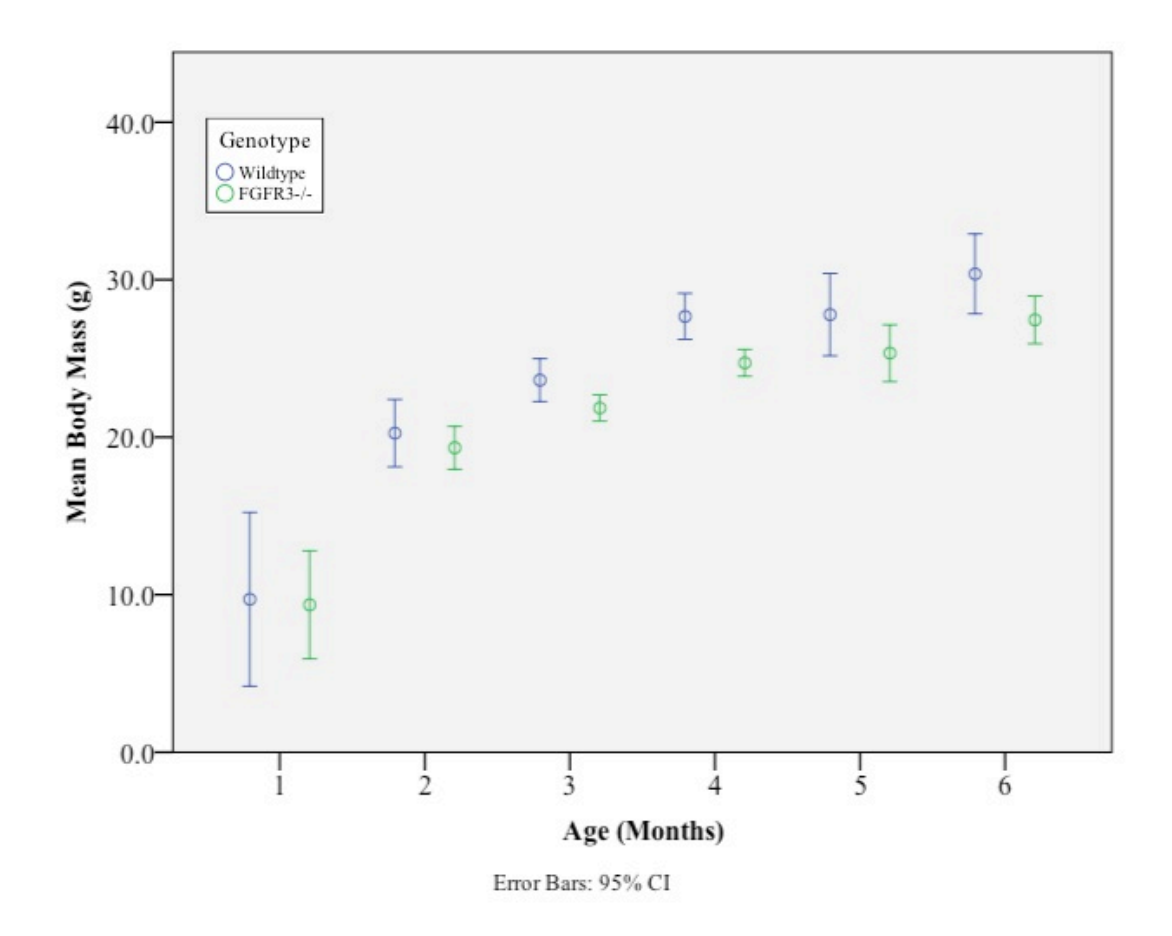


Figure 3. Mean body mass in grams throughout the growth of both male and female, FGFR3-/- and wildtype mice.

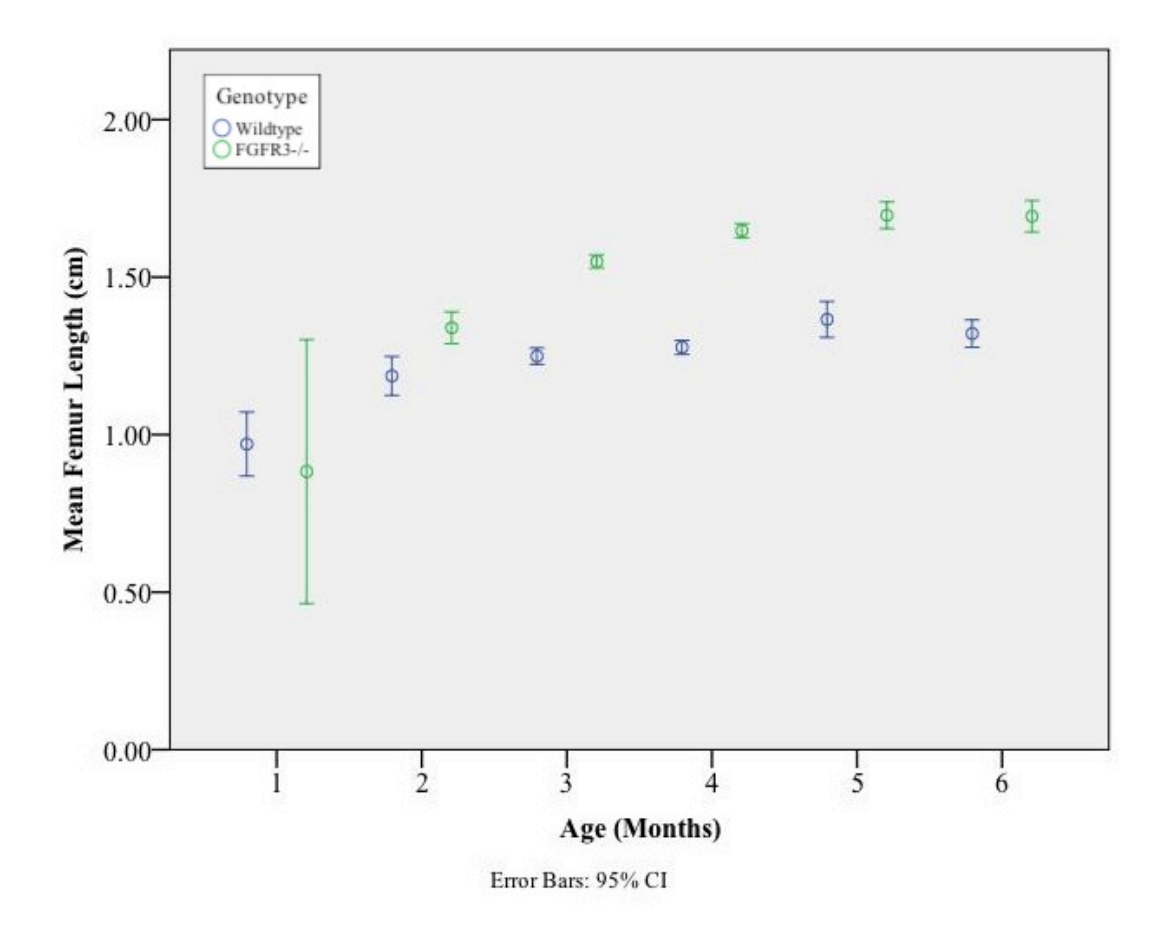


Figure 4. Mean femur lengths FGFR3-/- and wildtype mice grouped by age in months. With femur length used as a proxy for growth and skeletal maturity, mice have a rapid phase of growth at 2 months, corresponding to an adolescent growth spurt. Mice have reached skeletal maturity by 4-5 months.

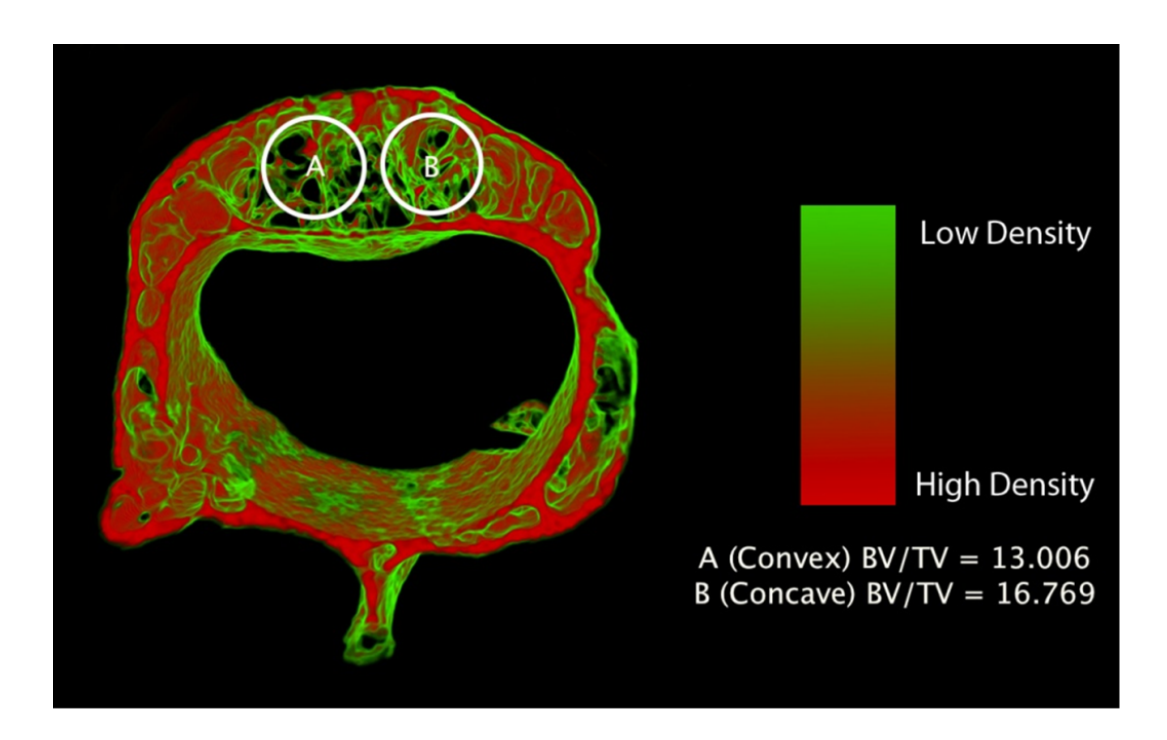


Figure 5. Micro-CT generated sample model of micro-architectural changes in the apical vertebrae of FGFR3-/- mice. The figure indicates higher bone quality (bone volume fraction) on the concave side of the apical vertebra.

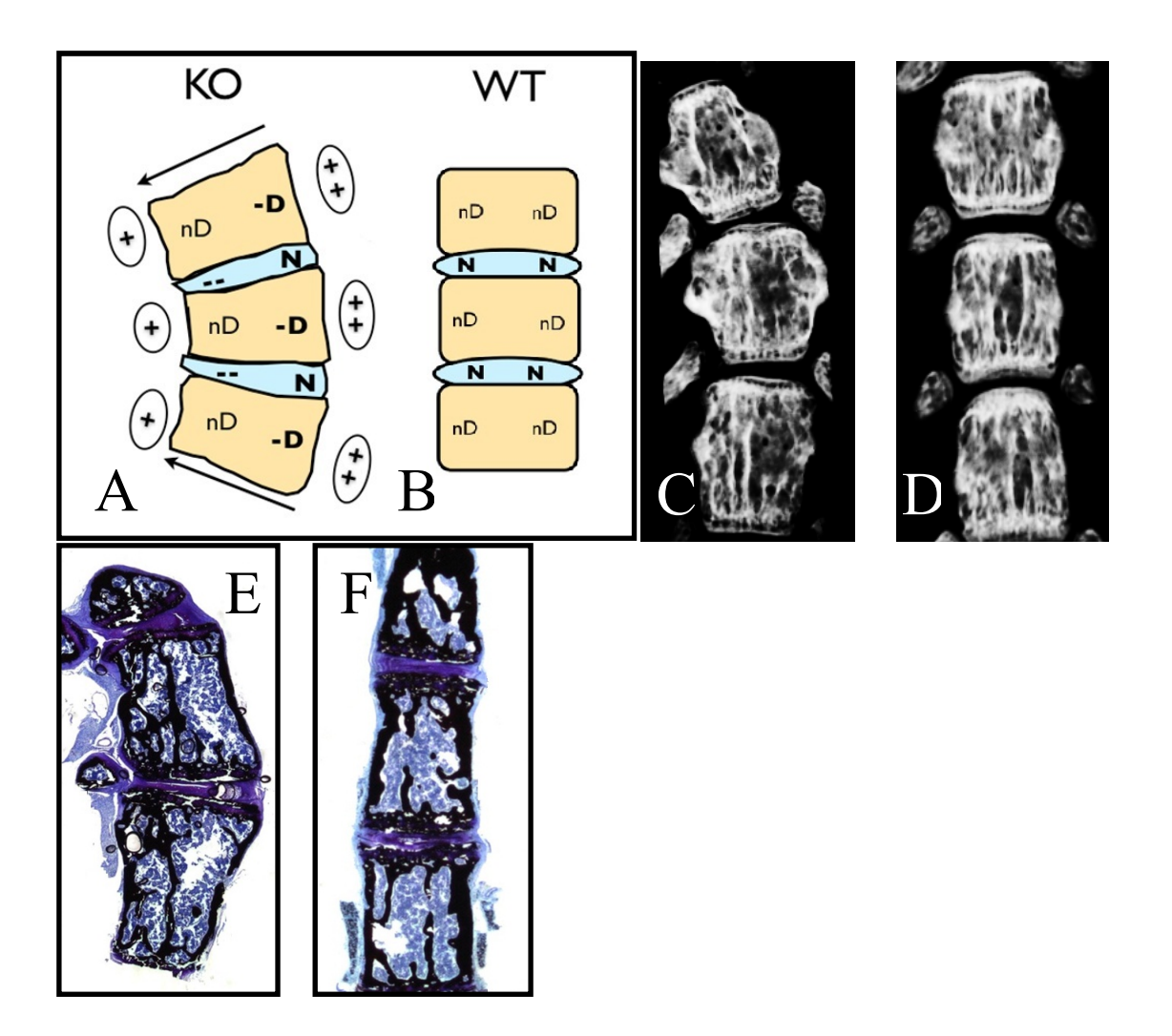


Figure 6. **(A,B)** Illustrated **(C,D)** μCT, and **(E,F)** histological coronal images depicting the data found in Table 2 (A, B, C). The concave (left) side of FGFR3-/- (KO) scoliosis **(A,C,E)** has intervertebral disk wedging with translation of the nucleus pulposus to the convexity and a relative smaller vertebral height. The convex side shows low bone volume fraction and decreased mineralization, stained black with von Kossa. Wildtype (WT)**(B,D,F)** show symmetry in each parameter.

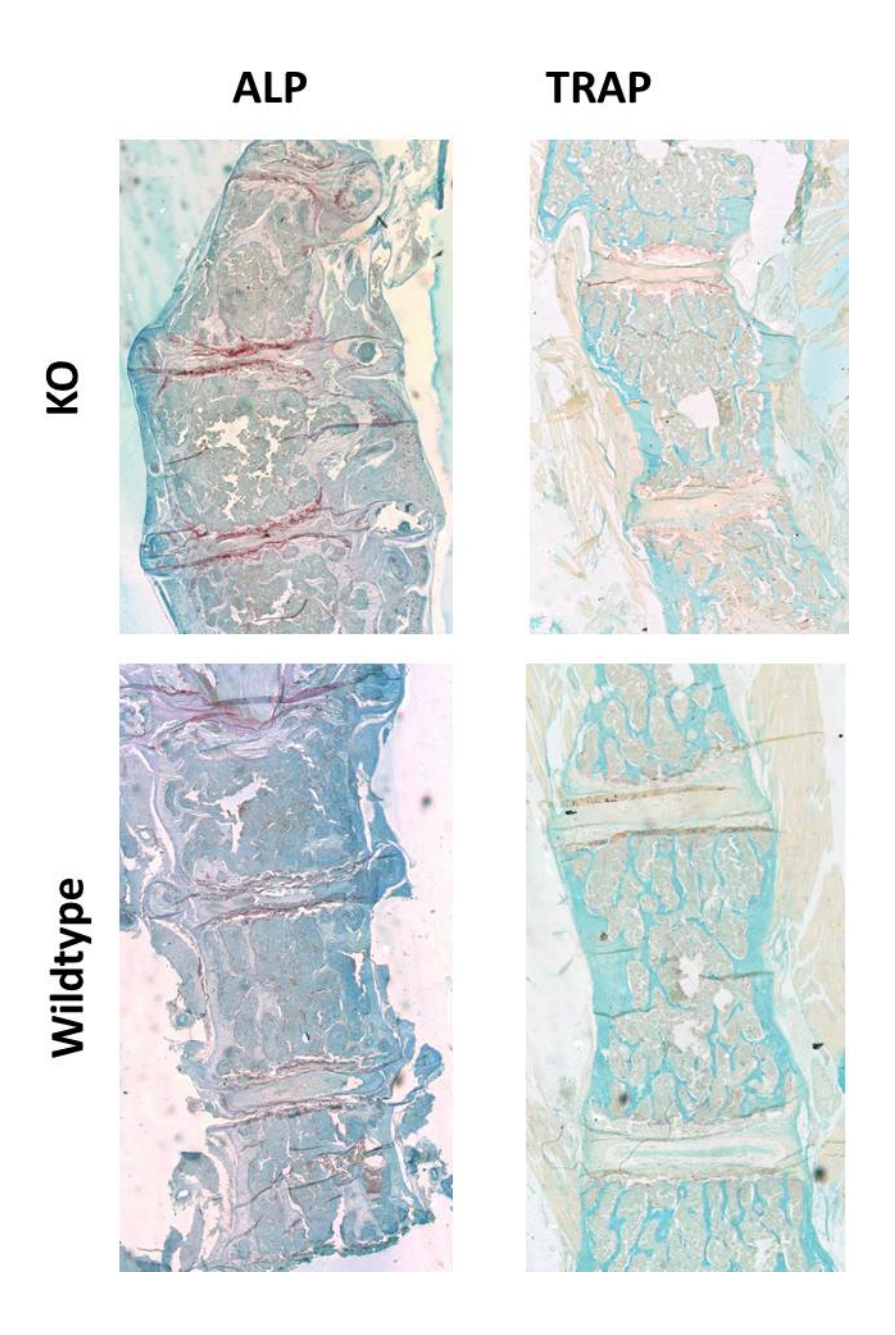


Figure 7. Comparison between FGFR3-/- (KO) and wildtype vertebrae using a stain for Alkaline Phosphatase (ALP) and Tartrate Resistant Acid Phosphatase (TRAP) to examine osteoblast and osteoclast activity, respectively. Activity stains red in both ALP and TRAP.

# 7 Appendix 1: Select SPSS Syntax

**Linear mixed effects model:** The following syntax was used to compare scoliosis severity in FGFR3-/- and wildtype mice controlling for age. Similar syntax was used for all other mixed model comparisons such as for body mass, femur length, vertebra height, body length, kyphosis, etc.

MIXED primarycurve BY genotype WITH age

/FIXED=genotype age genotype\*age | SSTYPE(3)

/METHOD=ML

/RANDOM=INTERCEPT | SUBJECT(mouseid) COVTYPE(id).

#### 8 References

- Aarts, M. M., Davidson, D., Corluka, A., Petroulakis, E., Guo, J., Bringhurst, F. R., . . . Henderson, J. E. (2001). Parathyroid Hormone-related Protein Promotes Quiescence and Survival of Serum-deprived Chondrocytes by Inhibiting rRNA Synthesis. *Journal of Biological Chemistry*, 276, 37934-37943.
- Accadbled, F., Laffosse, J. M., Odent, T., Gomez-Brouchet, A., Sales de Gauzy, J., & Swider, P. (2011). Influence of growth modulation on the effective permeability of the vertebral end plate. A porcine experimental scoliosis model. *Clin Biomech (Bristol, Avon)*, 26(4), 337-342. doi: 10.1016/j.clinbiomech.2010.11.007
- Adam, C. J., & Askin, G. N. (2009). Lateral bone density variations in the scoliotic spine. *Bone*, 45(4), 799-807. doi: 10.1016/j.bone.2009.06.023
- Akel, I., Demirkiran, G., Alanay, A., Karahan, S., Marcucio, R., & Acaroglu, E. (2009). The effect of calmodulin antagonists on scoliosis: bipedal C57BL/6 mice model. *Eur Spine J*, 18(4), 499-505. doi: 10.1007/s00586-009-0912-1
- Akel, I., Kocak, O., Bozkurt, G., Alanay, A., Marcucio, R., & Acaroglu, E. (2009). The effect of calmodulin antagonists on experimental scoliosis: a pinealectomized chicken model. *Spine (Phila Pa 1976), 34*(6), 533-538. doi: 10.1097/BRS.0b013e31818be0b1
- Amizuka, N., Davidson, D., Liu, H., Valverde-Franco, G., Chai, S., Maeda, T., . . . Henderson, J. E. (2004). Signalling by fibroblast growth factor receptor 3 and parathyroid hormone-related peptide coordinate cartilage and bone development. *Bone, 34*(1), 13-25. doi: 10.1016/j.bone.2003.08.009
- Aronsson, D. D., Stokes, I. A., & McBride, C. (2010). The role of remodeling and asymmetric growth in vertebral wedging. *Stud Health Technol Inform*, 158, 11-15.
- ASCANI, E., BARTOLOZZI, P., LOGROSCINO, C. A., MARCHETTI, P. G., PONTE, A., SAVINI, R., . . . SILVESTRE, M. D. (1986). Natural History of Untreated Idiopathic Scoliosis After Skeletal Maturity. *Spine (Phila Pa 1976)*, 11(8), 784-789.
- Asher, M. A., & Burton, D. C. (2006). Adolescent idiopathic scoliosis: natural history and long term treatment effects. *Scoliosis*, *1*(1), 2. doi: 10.1186/1748-7161-1-2
- Axenovich, T. I., Zaidman, A. M., Zorkoltseva, I. V., Tregubova, I. L., & Borodin, P. M. (1999). Segregation analysis of idiopathic scoliosis: Demonstration of a major gene effect. *American Journal of Medical Genetics*, 86(4), 389-394. doi: 10.1002/(sici)1096-8628(19991008)86:4<389::aid-ajmg15>3.0.co;2-d
- Beguiristain, J. L., De Salis, J., Oriaifo, A., & Canadell, J. (1980). Experimental scoliosis by epiphysiodesis in pigs. *Int Orthop*, *3*(4), 317-321.
- Berven, S. H., & Bradford, D. S. (2002). Neuromuscular Scoliosis: Causes of Deformity and Principles for Evaluation and Management. *Seminars in Neurology*, 22(2), 167-178.
- Bisgard, J. D. (1935). Experimental Thoracogenic Scoliosis. *Journal of Thoracic Surgery*, 4, 435-442.
- Black, D. L. (2003). Mechanisms of alternative pre-messenger RNA splicing. *Annu Rev Biochem*, 72, 291-336. doi: 10.1146/annurev.biochem.72.121801.161720

- Blanco, G., Coulton, G. R., Biggin, A., Grainge, C., Moss, J., Barrett, M., . . . Brown, S. D. M. (2001). The kyphoscoliosis (ky) mouse is deficient in hypertrophic responses and is caused by a mutation in a novel muscle-specific protein. *Hum Mol Genet*, 10(1), 9-16.
- Bodine, P. V. N., Zhao, W., Kharode, Y. P., Bex, F. J., Lambert, A.-J., Goad, M. B., . . . Komm, B. S. (2004). The Wnt Antagonist Secreted Frizzled-Related Protein-1 Is a Negative Regulator of Trabecular Bone Formation in Adult Mice. *Molecular Endocrinology*, 18(5), 1222-1237. doi: 10.1210/me.2003-0498
- Braun, J. T., & Akyuz, E. (2005). Prediction of curve progression in a goat scoliosis model. *J Spinal Disord Tech*, 18(3), 272-276.
- Braun, J. T., Hines, J. L., Akyuz, E., Vallera, C., & Ogilvie, J. W. (2006). Relative versus absolute modulation of growth in the fusionless treatment of experimental scoliosis. *Spine (Phila Pa 1976)*, *31*(16), 1776-1782. doi: 10.1097/01.brs.0000227263.43060.50
- Braun, J. T., Hoffman, M., Akyuz, E., Ogilvie, J. W., Brodke, D. S., & Bachus, K. N. (2006). Mechanical modulation of vertebral growth in the fusionless treatment of progressive scoliosis in an experimental model. *Spine (Phila Pa 1976)*, *31*(12), 1314-1320. doi: 10.1097/01.brs.0000218662.78165.b1
- Braun, J. T., Ogilvie, J. W., Akyuz, E., Brodke, D. S., & Bachus, K. N. (2006). Creation of an experimental idiopathic-type scoliosis in an immature goat model using a flexible posterior asymmetric tether. *Spine (Phila Pa 1976)*, *31*(13), 1410-1414. doi: 10.1097/01.brs.0000219869.01599.6b
- Braun, J. T., Ogilvie, J. W., Akyuz, E., Brodke, D. S., Bachus, K. N., & Stefko, R. M. (2003). Experimental scoliosis in an immature goat model: a method that creates idiopathic-type deformity with minimal violation of the spinal elements along the curve. *Spine (Phila Pa 1976)*, 28(19), 2198-2203. doi: 10.1097/01.brs.0000085095.37311.46
- Bridges, L. R., Coulton, G. R., Howard, G., Moss, J., & Mason, R. M. (1992). The Neuromuscular Basis of Hereditary Kyphoscoliosis in the Mouse. *Muscle and Nerve*, *14*, 172-179.
- Burwell, R. G., Dangerfield, P. H., Moulton, A., & Grivas, T. B. (2011). Adolescent idiopathic scoliosis (AIS), environment, exposome and epigenetics: a molecular perspective of postnatal normal spinal growth and the etiopathogenesis of AIS with consideration of a network approach and possible implications for medical therapy. *Scoliosis*, 6(1), 26. doi: 10.1186/1748-7161-6-26
- Callewaert, F., Venken, K., Kopchick, J. J., Torcasio, A., Lenthe, G. H. v., Boonen, S., & Vanderschueren, D. (2010). Sexual Dimorphism in Cortical Bone Size and Strength But Not Density Is Determined by Independent and Time-Specific Actions of Sex Steroids and IGF-1: Evidence From Pubertal Mouse Models. *Journal of Bone and Mineral Research*, 25(3), 617-626.
- Carpintero, P., Mesa, M., Garcia, J., & Carpintero, A. (1997). Scoliosis induced by asymmetric lordosis and rotation: an experimental study. *Spine (Phila Pa 1976)*, 22(19), 2202-2206.

- Carr, W. A., Moe, J. H., Winter, R. B., & Lonstein, J. E. (1980). Treatment of Idiopathic Scoliosis in the Milwaukee Brace. *Journal of Bone and Joint Surgery*, 62-A(4), 599-612.
- Chappard, D., Legrand, E., Haettich, B., Chales, G., Auvinet, B., Eschard, J.-P., . . . Audran, M. (2001). Fractal dimension of trabecular bone: comparison of three histomorphometric computed techniques for measuring the architectural two-dimensional complexity. *Journal of Pathology*, 195, 515-521.
- Cheung, K. M. C., Poon, A. M. S., Luk, K. D. K., & Leong, J. C. Y. (2005). The Effect of Pinealectomy on Scoliosis Development in Young Nonhuman Primates. *Spine* (*Phila Pa 1976*), 30(18), 2009-2013.
- Cil, A., Yazici, M., Daglioglu, K., Aydingoz, U., Alany, A., Acaroglu, E., . . . Surat, A. (2005). The Effect of Pedicle Screw Placement With or Without Application of Compression Across the Neurocentral Cartilage on the Morphology of the Spinal Canal and Pedicle in Immature Pigs. *Spine (Phila Pa 1976)*, 30(11), 1287-1293.
- Coillard, C., Rhalmi, S., & Rivard, C. H. (1999). Experimental scoliosis in the minipig: study of vertebral deformations. *Ann Chir*, *53*(8), 773-780.
- Collis, D. K., & Ponseti, I. V. (1969). Long-Term Follow-up of Patients with Idiopathic Scoliosis Not Treated Surgically. *Journal of Bone and Joint Surgery*, 51-A(3), 425-445.
- Colvin, J. S., Bohne, B. A., Harding, G. W., McEwen, D. G., & Ornitz, D. M. (1996). Skeletal overgrowth and deafness in mice lacking fibroblast growth factor receptor 3. *Nature Genetics*, *12*, 390-397.
- Crawford, A. H., & Herrera-Soto, J. (2007). Scoliosis Associated with Neurofibromatosis. *The Orthopedic clinics of North America*, 38(4), 553-562.
- Danielsson, A. J., Hasserius, R., Ohlin, A., & Nachemson, A. L. (2007). A Prospective Study of Brace Treatment Versus Observation Alone in Adolescent Idiopathic Scoliosis. *Spine (Phila Pa 1976)*, 32(20), 2198-2207.
- Davidson, D., Blanc, A., Filion, D., Wang, H., Plut, P., Pfeffer, G., . . . Henderson, J. E. (2005). Fibroblast growth factor (FGF) 18 signals through FGF receptor 3 to promote chondrogenesis. *J Biol Chem*, 280(21), 20509-20515. doi: 10.1074/jbc.M410148200
- Davies, G., & Reid, L. (1971). Effect of scoliosis on growth of alveoli and pulmonary arteries and on right ventricle. *Archives of Disease in Childhood*, 46(249), 623-632. doi: 10.1136/adc.46.249.623
- Day, G., McPhee, I., Tuffley, J., Tomlinson, F., Chaseling, R., Kellie, S., . . . Brankoff, B. (2007). Idiopathic scoliosis and pineal lesions in Australian children. *Journal of Orthopaedic Surgery*, 15(3), 327-333.
- Deng, C.-X., Wynshaw-Boris, A., Zhou, F., Kuo, A., & Leder, P. (1996). Fibroblast Growth Factor Receptor 3 Is a Negative Regulator of Bone Growth. *Cell*, 84, 911-921.
- Dias, M. S. (2007). Normal and abnormal development of the spine. *Neurosurg Clin N Am*, 18(3), 415-429. doi: 10.1016/j.nec.2007.05.003
- Dickinson, A., & Meikle, V. M. H. (1973). Genetic Kyphoscoliosis in Mice. *The Lancet*, 1186.

- El-Sayyad, M., & Conine, T. A. (1994). Effect of exercise, bracing, and electrical surface stimulation on idiopathic scoliosis: a preliminary study. *International Journal of Rehabilitation Research*, 17(1), 70-74.
- Engsig, M. T., Chen, Q.-J., Vu, T. H., Pedersen, A.-C., Therkidsen, B., Lund, L. R., . . . Delaisse, J.-M. (2000). Matrix Metalloproteinase 9 and Vascular Endothelial Growth Factor Are Essential for Osteoclast Recruitment into Developing Long Bones. *Journal of Cell Biology*, 154(4), 879-890.
- Eswarakumar, V. P., Lax, I., & Schlessinger, J. (2005). Cellular signaling by fibroblast growth factor receptors. *Cytokine Growth Factor Rev, 16*(2), 139-149. doi: 10.1016/j.cytogfr.2005.01.001
- Everett, C. R., & Patel, R. K. (2007). A Systemic Literature Review of Nonsurgical Treatment in Adult Scoliosis. *Spine (Phila Pa 1976), 32*(19S), S130-S134.
- Ewan, K. B. R., & Everett, A. W. (1992). Evidence for Resegmentation in the Formation of the Vertebral Column Using the Novel Approach of Retroviral-Mediated Gene Transfer. *Experimental Cell Research*, 198, 315-320.
- Fagan, A. B., Kennaway, D. J., & Oakley, A. P. (2009). Pinealectomy in the chicken: a good model of scoliosis? *Eur Spine J, 18*(8), 1154-1159. doi: 10.1007/s00586-009-0927-7
- Fibroblast growth factors: time to take note. (1990). The Lancet, 336, 777-778.
- Fields, A. J., Eswaran, S. K., Jekir, M. G., & Keaveny, T. M. (2009). Role of trabecular microarchitecture in whole-vertebral body biomechanical behavior. *J Bone Miner Res*, 24(9), 1523-1530. doi: 10.1359/jbmr.090317
- Fjelldal, P. G., Grotmol, S., Kryvi, H., Gjerdet, N. R., Hansen, T., Porter, M. J. R., & Totland, G. K. (2004). Pinealectomy induces malformation in the spine and reduces the mechanical strength of the vertebrae in Atlantic salmon, Salmo salar. *Journal of Pineal Research*, *36*, 132-139.
- Fu, G., Yoshihara, H., Kawakami, N., Goto, M., Tsuji, T., Ohara, T., & Imagama, S. (2011). Microcomputed tomographic evaluation of vertebral microarchitecture in pinealectomized scoliosis chickens. *J Pediatr Orthop B, 20*(6), 382-388. doi: 10.1097/BPB.0b013e3283474c6e
- Gaur, T., Lengner, C. J., Hovhannisyan, H., Bhat, R. A., Bodine, P. V. N., Komm, B. S., . . . Lian, J. B. (2005). Canonical WNT Signaling Promotes Osteogenesis by Directly Stimulating Runx2 Gene Expression. *Journal of Biological Chemistry*, 280(39), 33132-33140. doi: 10.1074/jbc.M500608200
- Gilbert, S. F. (2000). *Developmental Biology, 6th Edition*. Swarthmore College: Sinauer Associates.
- Givol, D., & Yayon, A. (1992). Complexity of FGF receptors: genetic basis for structural diversity and functional specificity. *FASEB Journal*, *6*, 3362-3369.
- Glass II, D. A., & Karsenty, G. (2006). Molecular Bases of the Regulation of Bone Remodeling by the Canonical Wnt Signaling Pathway. In P. S. Gerald (Ed.), *Current Topics in Developmental Biology* (Vol. Volume 73, pp. 43-84): Academic Press.
- Goldberg, C. J., Dowling, F. E., Hall, J. E., & Emans, J. B. (1993). A statistical comparison between natural history of idiopathic scoliosis and brace treatment in skeletally immature adolescent girls. *Spine (Phila Pa 1976)*, *18*(7), 902-908.

- Gorman, K. F., Julien, C., & Moreau, A. (2012). The genetic epidemiology of idiopathic scoliosis. *Eur Spine J, 21*(10), 1905-1919. doi: 10.1007/s00586-012-2389-6
- Green, N. E. (1986). Part-time Bracing of Adolescent Idiopathic Scoliosis. *Journal of Bone and Joint Surgery*, 68-A(5), 738-742.
- Grivas, T. B., & Savvidou, O. D. (2007). Melatonin the "light of night" in human biology and adolescent idiopathic scoliosis. *Scoliosis*, 2(6).
- Guo, J., Lanske, B., Liu, B. Y., Divieti, P., Kronenberg, H. M., & Bringhurst, F. R. (2001). Signal-selectivity of parathyroid hormone (PTH)/PTH-related peptide receptor-mediated regulation of differentiation in conditionally immortalized growth-plate chondrocytes. *Endocrinology*, 142(3), 1260-1268.
- Haglund, L., Ouellet, J., & Roughley, P. (2009). Variation of Chondroadherin Abundance and Fragmentation in the Human Scoliotic Disc. *Spine (Phila Pa 1976), 34*(14), 1513-1518.
- Hahn, M., Vogel, M., Pompesius-Kempa, M., & Delling, G. (1992). Trabecular Bone Pattern Factor- A New Parameter for Simple Quantification of Bone Microarchitecture. *Bone*, 13, 327-330.
- Hartmann, C., & Tabin, C. J. (2000). Dual roles of Wnt signaling during chondrogenesis in the chicken limb. *Development*, 127(14), 3141-3159.
- Henderson, J. E., Naski, M. C., Aarts, M. M., Wang, D., Cheng, L., Goltzman, D., & Ornitz, D. M. (2000). Expression of FGFR3 with the G380R Achondroplasia Mutation Inhibits Proliferation and Maturation of CDK2 Chondrocyte Cells. *Journal of Bone and Mineral Research*, 15(1), 155-165.
- Henriksen, K., Bollerslev, J., Everts, V., & Karsdal, M. A. (2011). Osteoclast Activity and Subtypes as a Function of Physiology and Pathology—Implications for Future Treatments of Osteoporosis. *Endocrine Reviews*, *32*(1), 31-63. doi: 10.1210/er.2010-0006
- Hildebrand, T., Laib, A., Muller, R., Dequeker, J., & Ruegsegger, P. (1999). Direct three-dimensional morphometric analysis of human cancellous bone: microstructural data from spine, femur, iliac crest, and calcaneus. *J Bone Miner Res*, *14*(7), 1167-1174. doi: 10.1359/jbmr.1999.14.7.1167
- Hildebrand, T., & Ruegsegger, P. (1997). Quantification of Bone Microarchitecture with the Stucture Model Index. *Computer Methods in Biomechanics and Biomedical Engineering*, *1*, 15-25.
- Hilibrand, A. S., Blakemore, L. C., Loder, R., Greenfield, M. L., Farley, F. A., Hensinger, R. N., & Hariharan, M. (1996). The Role of Melatonin in the Pathogenesis of Adolescent Idiopathic Scoliosis. *Spine (Phila Pa 1976), 21*(10), 1140-1146.
- Ho, E. K. W., Upadalyay, S. S., Chan, F. L., Hsu, L. C., & Leong, J. C. (1993). New Methods of Measuring Vertebral Rotation from Computed Tomographic Scans. *Spine (Phila Pa 1976), 18*, 1173-1177.
- Hou, Y., Le Bihan, M. C., Vega-Avelaira, D., & Coulton, G. R. (2006). Proteomic changes in hearts of kyphoscoliosis (ky) mutant mice in the absence of structural pathology: implication for the analysis of early human heart disease. *Proteomics*, 6(10), 3096-3108. doi: 10.1002/pmic.200500475
- Hunt, J. C., & Pugh, D. G. (1961). Skeletal Lesions in Neurofibromatosis. *Radiology*, 76(1), 1-20. doi: 10.1148/76.1.1

- Hurley, M. M., Tetradis, S., Huang, Y. F., Hock, J., Kream, B. E., Raisz, L. G., & Sabbieti, M. G. (1999). Parathyroid hormone regulates the expression of fibroblast growth factor-2 mRNA and fibroblast growth factor receptor mRNA in osteoblastic cells. *J Bone Miner Res*, 14(5), 776-783. doi: 10.1359/jbmr.1999.14.5.776
- Janssen, M. M., de Wilde, R. F., Kouwenhoven, J. W., & Castelein, R. M. (2011). Experimental animal models in scoliosis research: a review of the literature. *Spine J, 11*(4), 347-358. doi: 10.1016/j.spinee.2011.03.010
- Janssen, M. M., Kouwenhoven, J. W., Schlosser, T. P., Viergever, M. A., Bartels, L. W., Castelein, R. M., & Vincken, K. L. (2011). Analysis of preexistant vertebral rotation in the normal infantile, juvenile, and adolescent spine. *Spine (Phila Pa 1976)*, *36*(7), E486-491.
- Justice, C. M., Miller, N. H., Marosy, B., Zhang, J., & Wilson, A. F. (2003). Familial idiopathic scoliosis: evidence of an X-linked susceptibility locus. *Spine (Phila Pa 1976)*, 28(6), 589-594. doi: 10.1097/01.brs.0000049940.39801.e6
- Kallemeier, P. M., Buttermann, G. R., Beaubien, B. P., Chen, X., Polga, D. J., Lew, W. D., & Wood, K. B. (2006). Validation, reliability, and complications of a tethering scoliosis model in the rabbit. *Eur Spine J, 15*(4), 449-456. doi: 10.1007/s00586-005-1032-1
- Kane, W. J. (1977). Scoliosis Prevalence: A Call for a Statement of Terms. *Clinical Orthopaedics and Related Research*(126), 43-46.
- Karol, L. A., Johnston, C., Mladenov, K., Schochet, P., Walters, P., & Browne, R. H. (2008). Pulmonary Function Following Early Thoracic Fusion in Non-Neuromuscular Scoliosis. *Journal of Bone and Joint Surgery*, 90-A(6), 1272-1281.
- Karsenty, G., & Wagner, E. F. (2002). Reaching a Genetic and Molecular Understanding of Skeletal Development. *Developmental Cell*, 2(4), 389-406. doi: 10.1016/s1534-5807(02)00157-0
- Kesling, K. L., & Reinker, K. A. (1997). Scoliosis in twins. A meta-analysis of the literature and report of six cases. *Spine (Phila Pa 1976)*, 22(17), 2009-2014; discussion 2015.
- Kim, H.-J., Kim, J.-H., Bae, S.-C., Choi, J.-Y., & Ryoo, H.-M. (2003). The Protein Kinase C Pathway Plays a Central Role in the Fibroblast Growth Factor-stimulated Expression and Transactivation Activity of Runx2. *Journal of Biological Chemistry*, 278(1), 319-326. doi: 10.1074/jbc.M203750200
- Klinker, F. (2011). Generalized Linear Mixed Models for Ratemaking: A Means of Introducing Credibility into a Generalized Linear Model Setting. *Casualty Actuarial Society E-Forum, Winter Volume 2*, 1-25.
- Kobayashi, T., & Kronenberg, H. (2005). Minireview: Transcriptional Regulation in Development of Bone. *Endocrinology*, *146*(3), 1012-1017. doi: 10.1210/en.2004-1343
- Komori, T. (2006). Regulation of osteoblast differentiation by transcription factors. *Journal of Cellular Biochemistry*, 99(5), 1233-1239. doi: 10.1002/jcb.20958
- Kronenberg, H. M. (2003). Developmental Regulation of the Growth Plate. *Nature*, 423, 332-336.

- L'Hôte, C. G. M., & Knowles, M. A. (2005). Cell responses to FGFR3 signalling: growth, differentiation and apoptosis. *Experimental Cell Research*, 304(2), 417-431. doi: 10.1016/j.yexcr.2004.11.012
- Laffosse, J. M., Accadbled, F., Bonnevialle, N., Gomez-Brouchet, A., de Gauzy, J. S., & Swider, P. (2010). Remodelling of vertebral endplate subchondral bone in scoliosis: a micro-CT analysis in a porcine model. *Clin Biomech (Bristol, Avon)*, 25(7), 636-641. doi: 10.1016/j.clinbiomech.2010.04.011
- Lam, G. C., Hill, D. L., Le, L. H., Raso, J. V., & Lou, E. H. (2008). Vertebral rotation measurement: a summary and comparison of common radiographic and CT methods. *Scoliosis*, *3*, 16. doi: 10.1186/1748-7161-3-16
- Langenskiold, A., & Michelsson, J.-E. (1961). Experimental Progressive Scoliosis in the Rabbit. *Journal of Bone and Joint Surgery*, 43-B(1), 116-120.
- Lee, K., Lanske, B., Karaplis, A. C., Deeds, J. D., Kohno, H., Nissenson, R. A., . . . Segre, G. V. (1996). Parathyroid hormone-related peptide delays terminal differentiation of chondrocytes during endochondral bone development. *Endocrinology*, *137*(11), 5109-5118. doi: 10.1210/en.137.11.5109
- Lee, K.-S., Kim, H.-J., Li, Q.-L., Chi, X.-Z., Ueta, C., Komori, T., . . . Bae, S.-C. (2000). Runx2 Is a Common Target of Transforming Growth Factor β1 and Bone Morphogenetic Protein 2, and Cooperation between Runx2 and Smad5 Induces Osteoblast-Specific Gene Expression in the Pluripotent Mesenchymal Precursor Cell Line C2C12. *Molecular and Cellular Biology, 20*(23), 8783-8792. doi: 10.1128/mcb.20.23.8783-8792.2000
- Lee, M.-H., Kim, Y.-J., Kim, H.-J., Park, H.-D., Kang, A.-R., Kyung, H.-M., . . . Ryoo, H.-M. (2003). BMP-2-induced Runx2 Expression Is Mediated by Dlx5, and TGF-β 1 Opposes the BMP-2-induced Osteoblast Differentiation by Suppression of Dlx5 Expression. *Journal of Biological Chemistry*, *278*(36), 34387-34394. doi: 10.1074/jbc.M211386200
- Lee, M. H., Kwon, T. G., Park, H. S., Wozney, J. M., & Ryoo, H. M. (2003). BMP-2-induced Osterix expression is mediated by Dlx5 but is independent of Runx2. *Biochem Biophys Res Commun*, 309(3), 689-694.
- Lee, P. L., Johnson, D. E., Cousens, L. S., Fried, V. A., & Williams, L. T. (1989).

  Purification and Complementary DNA Cloning of a Receptor for Basic Fibroblast Growth Factor. *Science*, 245(4913), 57-60.
- Lenke, L. G., Betz, R. R., Harms, J., Bridwell, K. H., Clements, D. H., Lowe, T. G., & Blanke, K. (2001). Adolescent Idiopathic Scoliosis: A New Classification to Determine Extent of Spinal Arthrodesis. *Journal of Bone and Joint Surgery*, 83-A(8), 1169-1181.
- Lenssinck, M.-L. B., Frijlink, A. C., Berger, M. Y., Bierma-Zeinstra, S. M., Verkerk, K., & Verhagen, A. P. (2005). Effect of Bracing And Other Conservative Interventions in Treatment of Idiopathic Scoliosis in Adolescents. *Physical Therapy*, 85(12), 1329-1339.
- Liu, Z., Xu, J., Colvin, J. S., & Ornitz, D. M. (2002). Coordination of chondrogenesis and osteogenesis by fibroblast growth factor 18. *Genes Dev, 16*(7), 859-869. doi: 10.1101/gad.965602
- Lonstein, J. E. (1994). Adolescent Idiopathic Scoliosis. The Lancet, 344, 1407-1412.

- Machida, M., Dubousset, J., Inamura, Y., Iwaya, T., Yamada, T., & Kimura, J. (1993). An Experimental Study in Chickens for the Pathogenesis of Idiopathic Scoliosis. *Spine (Phila Pa 1976), 18*(12), 1609-1615.
- Machida, M., Murai, I., Miyashita, Y., Dubousset, J., Yamada, T., & Kimura, J. (1999). Pathogenesis of Idiopathic Scoliosis: Experimental Study in Rats. *Spine (Phila Pa 1976)*, 24(19), 1985-1989.
- Machida, M., Saito, M., Dubousset, J., Yamada, T., Kimura, J., & Shibasaki, K. (2005). Pathological mechanism of idiopathic scoliosis: experimental scoliosis in pinealectomized rats. *Eur Spine J, 14*(9), 843-848. doi: 10.1007/s00586-004-0806-1
- Malfair, D., Flemming, A. K., Dvorak, M. F., Munk, P. L., Vertinsky, A. T., Heran, M. K., & Graeb, D. A. (2010). Radiographic evaluation of scoliosis: review. *AJR Am J Roentgenol*, 194(3 Suppl), S8-22. doi: 10.2214/AJR.07.7145
- Mansukhani, A., Bellosta, P., Sahni, M., & Basilico, C. (2000). Signaling by fibroblast growth factors (FGF) and fibroblast growth factor receptor 2 (FGFR2)-activating mutations blocks mineralization and induces apoptosis in osteoblasts. *J Cell Biol*, 149(6), 1297-1308.
- Marie, P. (2003). Fibroblast growth factor signaling controlling osteoblast differentiation. *Gene*, *316*, 23-32. doi: 10.1016/s0378-1119(03)00748-0
- Marie, P. J. (2008). Transcription factors controlling osteoblastogenesis. *Arch Biochem Biophys*, 473(2), 98-105. doi: 10.1016/j.abb.2008.02.030
- Maruyama, T., & Takeshita, K. (2008). Surgical treatment of scoliosis: a review of techniques currently applied. *Scoliosis*, *3*(1), 6.
- Mason, R. M., & Palfrey, A. J. (1984). Intervertebral Disc Degeneration in Adult Mice with Hereditary Kyphoscoliosis. *Journal of Orthopaedic Research*, 2, 333-338.
- Mayo, N. E., Goldberg, M. S., Poitras, B., Scott, S., & Hanley, J. (1994). The Ste-Justine Adolescent Idiopathic Scoliosis Cohort Study Part III: Back Pain. *Spine (Phila Pa 1976)*, 19(14), 1973-1981.
- McMaster, M. J., & Ohtsuka, K. (1982). The Natural History of Congenital Scoliosis. *Journal of Bone and Joint Surgery, 64-A*(8), 1128-1147.
- Miki, T., Bottaro, D. P., Fleming, T. P., Smith, C. L., Burgess, W. H., Chan, A. M.-L., & Aaronson, S. A. (1992). Determination of ligand-binding specificity by alternative splicing: Two distinct growth factor receptors encoded by a single gene. *Proc Natl Acad Sci U S A*, 89, 246-250.
- Miller, N. H. (1999). Cause and natural history of adolescent idiopathic scoliosis. *Orthop Clin North Am*, 30(3), 343-352, vii.
- Miller, N. H., Justice, C. M., Marosy, B., Doheny, K. F., Pugh, E., Zhang, J., . . . Wilson, A. F. (2005). Identification of Candidate Regions for Familial Idiopathic Scoliosis. *Spine (Phila Pa 1976)*, 30(10), 1181-1187 1110.1097/1101.brs.0000162282.0000146160.0000162280a.
- Minina, E., Kreschel, C., Naski, M. C., Ornitz, D. M., & Vortkamp, A. (2002). Interaction of FGF, Ihh/Pthlh, and BMP Signaling Integrates Chondrocyte Proliferation and Hypertrophic Differentiation. *Developmental Cell*, *3*(3), 439-449.
- Miyama, K., Yamada, G., Yamamoto, T. S., Takagi, C., Miyado, K., Sakai, M., . . . Shibuya, H. (1999). A BMP-inducible gene, dlx5, regulates osteoblast

- differentiation and mesoderm induction. *Dev Biol, 208*(1), 123-133. doi: 10.1006/dbio.1998.9197
- Mundlos, S., & Olsen, B. R. (1997). Heritable diseases of the skeleton. Part I: Molecular insights into skeletal development-transcription factors and signaling pathways. *FASEB Journal*, 11, 125-132.
- Murata, Y., Takahashi, K., Hanaoka, E., Utsumi, T., Yamagata, M., & Moriya, H. (2002). Changes in Scoliotic Curvature and Lordotic Angle During the Early Phase of Degenerative Lumbar Scoliosis. *Spine (Phila Pa 1976)*, *27*(20), 2268-2273.
- Nachemson, A. (1968). A Long Term Follow-up Study of Non-Treated Scoliosis. *Acta Orthopaedica*, 39(4), 466-476. doi: doi:10.3109/17453676808989664
- Nachemson, A. L., & Peterson, L.-E. (1995). Effectiveness of Treatment with a Brace in Girls Who Have Adolescent Idiopathic Scoliosis. *Journal of Bone and Joint Surgery*, 77-A(6), 815-822.
- Nakashima, K., Zhou, X., Kunkel, G., Zhang, Z., Deng, J. M., Behringer, R. R., & Crombrugghe, B. d. (2002). The Novel Zinc Finger-Containing Transcription Factor Osterix Is Required for Osteoblast Differentiation and Bone Formation. *Cell*, 108, 17-29.
- Naski, M. C., Colvin, J. S., Coffin, J. D., & Ornitz, D. M. (1998). Repression of hedgehog signaling and BMP4 expression in growth plate cartilage by fibroblast growth factor receptor 3. *Development*, *125*(24), 4977-4988.
- Naski, M. C., Wang, Q., Xu, J., & Ornitz, D. M. (1996). Graded activation of fibroblast growth factor receptor 3 by mutations causing achondroplasia and thanatophoric dysplasia. *Nature Genetics*, 13, 233-237.
- Nette, F., Dolynchuk, K., Wang, X., Daniel, A., Demianczuk, C., Moreau, M., . . . Bagnall, K. (2002). The effects of exposure to intense, 24 h light on the development of scoliosis in young chickens. *Stud Health Technol Inform*, 91, 1-6.
- Newton, P. O., Farnsworth, C. L., Faro, F. D., Mahar, A. T., Odell, T. R., Mohamad, F., . . . Amiel, D. (2008). Spinal growth modulation with an anterolateral flexible tether in an immature bovine model: disc health and motion preservation. *Spine (Phila Pa 1976)*, 33(7), 724-733. doi: 10.1097/BRS.0b013e31816950a0
- Newton, P. O., Faro, F. D., Farnsworth, C. L., Shapiro, G. S., Mohamad, F., Parent, S., & Fricka, K. (2005). Multilevel spinal growth modulation with an anterolateral flexible tether in an immature bovine model. *Spine (Phila Pa 1976), 30*(23), 2608-2613.
- Newton, P. O., Fricka, K. B., Lee, S. S., Farnsworth, C. L., Cox, T. G., & Mahar, A. T. (2002). Asymmetrical flexible tethering of spine growth in an immature bovine model. *Spine (Phila Pa 1976)*, *27*(7), 689-693.
- Newton, P. O., Upasani, V. V., Farnsworth, C. L., Oka, R., Chambers, R. C., Dwek, J., . . . Mahar, A. T. (2008). Spinal growth modulation with use of a tether in an immature porcine model. *J Bone Joint Surg Am*, 90(12), 2695-2706. doi: 10.2106/jbjs.g.01424
- Noonan, K. J., Weinstein, S. L., Jacobson, W. C., & Dolan, L. A. (1996). Use of the Milwaukee Brace for Progressive Idiopathic Scoliosis. *Journal of Bone and Joint Surgery*, 78-A(4), 557-567.

- O'Kelly, C., Wang, X., Raso, J., Moreau, M., Mahood, J., Zhao, J., & Bagnall, K. (1999). The production of scoliosis after pinealectomy in young chickens, rats, and hamsters. *Spine (Phila Pa 1976)*, 24(1), 35-43.
- Ohbayashi, N., Shibayama, M., Kurotaki, Y., Imanishi, M., Fujimori, T., Itoh, N., & Takada, S. (2002). FGF18 is required for normal cell proliferation and differentiation during osteogenesis and chondrogenesis. *Genes Dev, 16*(7), 870-879. doi: 10.1101/gad.965702
- Okoumassoun, L., Averill-Bates, D., Denizeau, F., & Henderson, J. E. (2007). Parathyroid hormone related protein (PTHrP) inhibits TNFalpha-induced apoptosis by blocking the extrinsic and intrinsic pathways. *J Cell Physiol*, 210(2), 507-516. doi: 10.1002/jcp.20892
- Okoumassoun, L. E., Russo, C., Denizeau, F., Averill-Bates, D., & Henderson, J. E. (2007). Parathyroid hormone-related protein (PTHrP) inhibits mitochondrial-dependent apoptosis through CK2. *J Cell Physiol*, *212*(3), 591-599. doi: 10.1002/jcp.21055
- Olsen, B. R., Reginato, A. M., & Wang, W. (2000). Bone Development. *Annual Review of Cell and Developmental Biology*, 16, 191-220.
- Olsen, S. K. (2006). Structural and Biochemical Analysis of the Molecular Determinants of FGF-FGFR Specificity. (Doctor of Philosophy), New York University.
- Ornitz, D. M., & Itoh, N. (2001). Fibroblast growth factors. *Genome Biology*, 2(3), 3005.3001-3005.3012.
- Oyama, J., Murai, I., Kanazawa, K., & Machida, M. (2006). Bipedal Ambulation Induces Experimental Scoliosis in C57BL/6J Mice with Reduced Plasma and Pineal Melatonin Levels. *Journal of Pineal Research*, 40, 219-224.
- Parkinson, I. H., Forbes, D., Sutton-Smith, P., & Fazzalari, N. L. (2010). Model-Independent 3D Descriptors of Vertebral Cancellous Bone Architecture. *Journal of Osteoporosis*, 2010. doi: 10.4061/2010/641578
- Patel, A., Schwab, F., Lafage, R., Lafage, V., & Farcy, J. P. (2011). Does removing the spinal tether in a porcine scoliosis model result in persistent deformity? A pilot study. *Clin Orthop Relat Res, 469*(5), 1368-1374. doi: 10.1007/s11999-010-1750-5
- Patel, A., Schwab, F., Lafage, V., Obeidat, M. M., & Farcy, J. P. (2010). Computed tomographic validation of the porcine model for thoracic scoliosis. *Spine (Phila Pa 1976)*, 35(1), 18-25. doi: 10.1097/BRS.0b013e3181b79169
- Patel, A., Schwab, F., Lafage, V., Patel, A., Obeidat, M. M., & Farcy, J.-P. (2009). Computed Tomographic Validation of the Porcine Model for Thoracic Scoliosis. *Spine (Phila Pa 1976), 35*(1), 18-25.
- Pehrsson, K., Larsson, S., & Nachemson, A. (1991). Lung Function in Adult Idiopathic Scoliosis: A 20 Year Follow Up. *Thorax*, 46, 474-478.
- Peters, K., Ornitz, D., Werner, S., & Williams, L. (1993). Unique Expression Pattern of the FGF Receptor 3 Gene during Mouse Organogenesis. *Dev Biol*, 155, 423-430.
- Ponseti, I. V., & Friedman, H. (1950). Prognosis in Idiopathic Scoliosis. *Journal of Bone and Joint Surgery*, 32-A(2), 381-395.
- Poussa, M., Schlenzka, D., & Ritsila, V. (1991). Scoliosis in growing rabbits induced with an extension splint. *Acta Orthop Scand*, 62(2), 136-138.

- Reames, D. L., Smith, J. S., Fu, K.-M. G., Polly, D. W. J., Ames, C. P., Berven, S. H., . . . Shaffrey, C. I. (2011). Complications in the Surgical Treatment of 19,360 Cases of Pediatric Scoliosis. *Spine (Phila Pa 1976)*, 36(18), 1484-1491.
- Reinhold, M. I., & Naski, M. C. (2007). Direct Interactions of Runx2 and Canonical Wnt Signaling Induce FGF18. *J. Biol. Chem.*, 282(6), 3653-3663. doi: 10.1074/jbc.M608995200
- Roach, J. W. (1999). Adolescent idiopathic scoliosis. *Orthop Clin North Am*, 30(3), 353-365, vii-viii.
- Rogala, E. J., Drummond, D. S., & Gurr, J. (1978). Scoliosis: Incidence and Natural History. *Journal of Bone and Joint Surgery*, 60-A(2), 173-176.
- Salehi, L. B., Mangino, M., De Serio, S., De Cicco, D., Capon, F., Semprini, S., . . . Dallapiccola, B. (2002). Assignment of a locus for autosomal dominant idiopathic scoliosis (IS) to human chromosome 17p11. *Hum Genet, 111*(4-5), 401-404. doi: 10.1007/s00439-002-0785-4
- Sanders, J. O., Browne, R. H., McConnell, S. J., Margraf, S. A., Cooney, T. E., & Finegold, D. N. (2007). Matury Assessment and Curve Progression in Girls with Idiopathic Scoliosis. *Journal of Bone and Joint Surgery*, 89-A(1), 64-73.
- Sarwark, J. F., Dabney, K. W., Salzman, S. K., Wakabayashi, T., Kitadai, H. K., Beauchamp, J. T., . . . Bunnell, W. P. (1988). Experimental scoliosis in the rat. I. Methodology, anatomic features and neurologic characterization. *Spine (Phila Pa 1976)*, *13*(5), 466-471.
- Schlessinger, J. (2000). Cell Signaling by Receptor Tyrosine Kinases. *Cell*, 103, 211-225. Schwab, F., Patel, A., Lafage, V., & Farcy, J.-P. (2009). A Porcine Model for Progressive Thoracic Scoliosis. *Spine (Phila Pa 1976)*, 34(11), E397-E404.
- Schwartzmann, J. R., & Miles, M. (1945). Experimental Production of Scoliosis in Rats and Mice. *Journal of Bone and Joint Surgery*, *27*(1), 59-69.
- Shea, K. G., Ford, T., Bloebaum, R. D., D'Astous, J., & King, H. (2004). A Comparison of the Microarchitectural Bone Adaptations of the Concave and Convex Thoracic Spinal Facets in Idiopathic Scoliosis. *Journal of Bone & Joint Surgery, American Volume*, 86(5), 1000-1006.
- Shukunami, C., Shigeno, C., Atsumi, T., Ishizeki, K., Suzuki, F., & Hiraki, Y. (1996). Chondrogenic Differentiation of Clonal Mouse Embryonic Cell Line ATDC5 In Vitro: Differentiation-dependent Gene Expression of Parathyroid Hormone (PTH)/PTH-related Peptide Receptor. *Journal of Cell Biology*, *133*(2), 457-468.
- Smith, R. M., & Dickson, R. A. (1987). Experimental Structural Scoliosis. *Journal of Bone and Joint Surgery*, 69-B(4), 576-581.
- Somerville, E. (1952). Rotational lordosis: the development of single curve. *Journal of Bone and Joint Surgery, 34-B*, 421-427.
- SPSS. (2005). Linear Mixed-Effects Modeling in SPSS: An Introduction to the MIXED Procedure (pp. 1-29): SPSS.
- Stokes, I., Burwell, R. G., & Dangerfield, P. (2006). Biomechanical spinal growth modulation and progressive adolescent scoliosis a test of the 'vicious cycle' pathogenetic hypothesis: Summary of an electronic focus group debate of the IBSE. *Scoliosis*, *1*(1), 16.

- Su, W.-C. S., Kitagawa, M., Xue, N., Xie, B., Garofalo, S., Cho, J., . . . Fu, X.-Y. (1997). Activation of Statl by mutant fibroblast growth-factor receptor in thanatophoric dysplasia type II dwarfism. *Nature*, *386*(6622), 288-292.
- Taylor, J. Statistics 203: Introduction to Regression and Analysis of Variance (pp. 1-15). Stanford.
- Thillard, M.-J. (1959). Deformations de la colonne vertebrale consequtives a l'epiphysectomie chez le poussin. *Extrait des Comptes Rendus de l'Association des Anatomistes*, 46, 22-26.
- Thirunavukkarasu, K., Halladay, D. L., Miles, R. R., Yang, X., Galvin, R. J., Chandrasekhar, S., . . . Onyia, J. E. (2000). The osteoblast-specific transcription factor Cbfa1 contributes to the expression of osteoprotegerin, a potent inhibitor of osteoclast differentiation and function. *J Biol Chem*, 275(33), 25163-25172. doi: 10.1074/jbc.M000322200
- Thomas, S., & Dave, P. K. (1985). Experimental Scoliosis in Monkeys. *Acta Orthopaedica Scandinavica*, 56, 43-46.
- Toydemir, R. M., Brassington, A. E., Bayral-Toydemir, P., Krakowiak, P., Jorde, L. B., Whitby, F. G., . . . Bamshad, M. J. (2006). A Novel Mutation in FGFR3 Causes Camptodactyly, Tall Stature, and Hearing Loss (CATSHL) Syndrome. *American Journal of Human Genetics*, 79, 935-941.
- Upasani, V. V., Farnsworth, C. L., Chambers, R. C., Bastrom, T. P., Williams, G. M., Sah, R. L., . . . Newton, P. O. (2011). Intervertebral disc health preservation after six months of spinal growth modulation. *J Bone Joint Surg Am*, *93*(15), 1408-1416. doi: 10.2106/jbjs.j.00247
- Valverde-Franco, G., Binette, J. S., Li, W., Wang, H., Chai, S., Laflamme, F., . . . Henderson, J. E. (2006). Defects in articular cartilage metabolism and early arthritis in fibroblast growth factor receptor 3 deficient mice. *Hum Mol Genet*, 15(11), 1783-1792. doi: 10.1093/hmg/ddl100
- Valverde-Franco, G., Liu, H., Davidson, D., Chai, S., Valderrama-Carvajal, H., Goltzman, D., . . . Henderson, J. E. (2004). Defective bone mineralization and osteopenia in young adult FGFR3-/- mice. *Hum Mol Genet, 13*(3), 271-284. doi: 10.1093/hmg/ddh034
- Vortkamp, A., Lee, K., Lanske, B., Segre, G. V., Kronenberg, H. M., & Tabin, C. J. (1996). Regulation of Rate of Cartilage Differentiation by Indian Hedgehog and PTH-Related Protein. *Science*, 273(5275), 613-622.
- Wang, Y., Spatz, M. K., Kannan, K., Hayk, H., Avivi, A., Gorivodsky, M., . . . Givol, D. (1999). A mouse model for achondroplasia produced by targeting fibroblast growth factor receptor 3. *Dev Biol*, *96*, 4455-4460.
- Weinstein, S. L. (1999). Natural History (of scoliosis). *Spine (Phila Pa 1976)*, 24(24), 2592-2600.
- Weinstein, S. L., Dolan, L. A., Cheng, J. C. Y., Danielsson, A., & Morcuende, J. A. (2008). Adolescent idiopathic scoliosis. *The Lancet*, *371*(9623), 1527-1537. doi: 10.1016/s0140-6736(08)60658-3
- Weinstein, S. L., Dolan, L. A., Wright, J. G., & Dobbs, M. B. (2013). Effects of Bracing in Adolescents with Idiopathic Scoliosis. *New England Journal of Medicine*, 369, 1512-1521.

- Weinstein, S. L., Dolan, Lori A., Spratt, Kevin F., Peterson, Kirk K., Spoonamore, Mark J., Ponseti, Ignacio V. (2003). Health and Function of Patients with Untreated Idiopathic Scoliosis. *Journal of the American Medical Association*, 289(5), 559-567.
- Weinstein, S. L., & Ponseti, I. V. (1983). Curve Progression in Idiopathic Scoliosis. *Journal of Bone and Joint Surgery*, 65-A(4), 447-455.
- Weinstein, S. L., Zavala, D. C., & Ponseti, I. V. (1981). Idiopathic Scoliosis: Long-Term Follow-Up and Prognosis in Untreated Patients. *Journal of Bone and Joint Surgery*, 63-A(5), 702-711.
- Weiss, H. R., Negrini, S., Rigo, M., Kotwicki, T., Hawes, M. C., Grivas, T. B., . . . Landauer, F. (2006). Indications for conservative management of scoliosis (guidelines). *Scoliosis*, 1, 5. doi: 10.1186/1748-7161-1-5
- Wise, C. A., Barnes, R., Gillum, J., Herring, J. A., Bowcock, A. M., & Lovett, M. (2000). Localization of susceptibility to familial idiopathic scoliosis. *Spine (Phila Pa 1976)*, 25(18), 2372-2380.
- Wu, H. L., Ding, W. Y., Shen, Y., Zhang, Y. Z., Guo, J. K., Sun, Y. P., & Cao, L. Z. (2012). Prevalence of vertebral endplate modic changes in degenerative lumbar scoliosis and its associated factors analysis. *Spine (Phila Pa 1976), 37*(23), 1958-1964. doi: 10.1097/BRS.0b013e31825bfb85
- Xiao, L., Naganawa, T., Obugunde, E., Gronowicz, G., Ornitz, D. M., Coffin, J. D., & Hurley, M. M. (2004). Stat1 Controls Postnatal Bone Formation by Regulating Fibroblast Growth Factor Signaling in Osteoblasts. *Journal of Biological Chemistry*, 279, 27743-27752.
- Yaffee, R. A. Mixed Analysis of Variance Models with SPSS (pp. 1-82). New York University.
- Yamanaka, Y., Tanaka, H., Koike, M., Nishimura, R., & Seino, Y. (2003). PTHrP Rescues ATDC5 Cells From Apoptosis Induced by FGF Receptor 3 Mutation. *Journal of Bone and Mineral Research*, 18(8), 1395-1403. doi: 10.1359/jbmr.2003.18.8.1395
- Yayon, A., Klagsbrun, M., Esko, J. D., Leder, P., & Ornitz, D. M. (1991). Cell Surface, Heparin-like Molecules Are Required for Binding of Basic Fibroblast Growth Factor to Its High Affinity Receptor. *Cell*, *64*, 841-848.
- Yu, K., & Ornitz, D. M. (2007). The FGF ligand–receptor signaling system in chondrogenesis, osteogenesis and vascularization of the endochondral skeleton. *International Congress Series*, 1302(0), 67-78. doi: 10.1016/j.ics.2006.09.021
- Zhang, H., & Sucato, D. J. (2008). Unilateral pedicle screw epiphysiodesis of the neurocentral synchondrosis. Production of idiopathic-like scoliosis in an immature animal model. *J Bone Joint Surg Am*, 90(11), 2460-2469. doi: 10.2106/jbjs.g.01493
- Zhang, H., & Sucato, D. J. (2011). Neurocentral synchondrosis screws to create and correct experimental deformity: a pilot study. *Clin Orthop Relat Res*, 469(5), 1383-1390. doi: 10.1007/s11999-010-1587-y
- Zhang, Y.-G., Zheng, G.-Q., Zhang, X.-S., & Wang, Y. (2009). Scoliosis Model Created by Pedicle Screw Tethering in Immature Goats. *Spine (Phila Pa 1976)*, *34*(21), 2305-2310.

- Zhang, Y. G., Zheng, G. Q., Zhang, X. S., & Wang, Y. (2009). Scoliosis model created by pedicle screw tethering in immature goats: the feasibility, reliability, and complications. *Spine (Phila Pa 1976)*, *34*(21), 2305-2310. doi: 10.1097/BRS.0b013e3181b1fdd0
- Zhou, Y., Zhu, W., Guo, Z., Zhao, Y., Song, Z., & Xiao, J. (2007). Effects of maternal nuclear genome on the timing of puberty in mice offspring. *Journal of Endocrinology*(193), 405-412.